Article:
Aad, G., Aakvaag, E., Abbott, B. et al. (2026) Constraints on effective field theories via quadruple-differential angular decay rates from t-channel single-top-quark production at √s = 13 TeV with the ATLAS detector. Journal of High Energy Physics, 2026 (7). 107. ISSN: 1126-6708

https://doi.org/10.1007/jhep07(2026)107

Published for SISSA by Springer

Received: *October 28, 2025*
Accepted: *May 15, 2026*
Published: *July 13, 2026*

Constraints on effective field theories via quadruple-differential angular decay rates from t-channel single-top-quark production at $\sqrt{s} = 13$ TeV with the ATLAS detector

The ATLAS collaboration

Full author list at the end of the paper

E-mail: atlas.publications@cern.ch

Abstract: Events with t-channel single top quarks are used to probe effective field theory operators in $\sqrt{s} = 13$ TeV proton–proton collision data corresponding to 140 fb^{-1} recorded by the ATLAS detector at the Large Hadron Collider. To extract a maximum amount of information from these events, the joint fourfold probability distribution for four kinematic angles is simultaneously analysed. A method leveraging Fourier techniques to handle the challenges arising from this approach is employed. The relevant effective field theory operators are those sensitive to top-quark decay and t-channel production vertices. Their Wilson coefficients are tightly constrained, with results compatible with Standard Model predictions.

Keywords: Hadron-Hadron Scattering, Top Physics

ArXiv ePrint: 2510.23372

https://doi.org/10.1007/JHEP07(2026)107

JHEP07(2026)107

Contents

1 Introduction **1**

2 Choice of Wilson coefficients **4**

3 ATLAS detector **6**

4 Data and simulated event samples **6**

5 Object definitions **9**

6 Reconstruction and event selection **12**

7 Sources of systematic uncertainty **14**

8 EFT analysis strategy **17**
- 8.1 Choice of basis functions 18
- 8.2 Morphing 19
- 8.3 Fit strategy 20

9 Results **23**

10 Conclusion **32**

The ATLAS collaboration **42**

1 Introduction

An interesting avenue in searching for possible interactions beyond the Standard Model (BSM) is looking for non-zero Wilson coefficients (WCs) of effective field theories (EFTs), and in particular those that couple to the top quark. Owing to its heavy mass, $m_t \approx 172.5\,\text{GeV}$ [1], and short lifetime, $1/\Gamma_t \sim \mathcal{O}(10^{-25})$ s [2], the top quark decays before hadronising, mainly through the weak process $t \to Wb$ [2]. This makes the measurement of its production and decay kinematics a unique probe of BSM physics.

In the bottom-up approach, an effective theory is an approximation to physics at a higher energy scale. A prominent example is the Standard Model effective field theory (SMEFT) [3]. In the SMEFT, the Standard Model (SM) is treated as the EFT of an unknown BSM theory at a higher scale, where the scale of the SM is characterised by the electroweak (EW) scale given by the vacuum expectation value v. Even though the BSM theory is unknown, its effects can still be parameterised by higher-dimensional operators in a power expansion. Therefore, the effective SM Lagrangian can be written as an expansion

$$\mathcal{L}_{\text{eff}} = \mathcal{L}_{\text{SM}}^{(4)} + \frac{1}{\Lambda}\sum_i c_i^{(5)}\mathcal{O}_i^{(5)} + \frac{1}{\Lambda^2}\sum_i c_i^{(6)}\mathcal{O}_i^{(6)} + \mathcal{O}\left(\frac{1}{\Lambda^3}\right) + \ldots,$$

where the c_i are the WCs [4] of the operators $\mathcal{O}_i$, containing all degrees of freedom below the scale Λ, which is the energy scale of the BSM physics. The scale Λ is the cut-off scale at which the power expansion breaks down and the BSM theory cannot be explained by the effective theory anymore. At this energy scale, the heavy particles that were parameterised out in the EFT approach can instead be produced directly ('on-shell'), and their dynamics must be explicitly included in the theory. The number in parentheses is the energy dimension of the respective operators. Usually, $\mathcal{O}^{(5)}$ terms are not considered because they violate baryon-number conservation.

BSM physics at higher scales could manifest itself at lower energies through its effective interactions, leading to detectable deviations from SM predictions [5]. There are a large number of top-quark-related dimension-six operators that can be constructed from the SM degrees of freedom [6]. A complete, non-redundant basis expressed in the Warsaw basis was given in ref. [7] and consists of 59 independent operators, not counting flavour indices and Hermitian conjugates. Among the 59 operators, this analysis focuses solely on the five operators contributing to the t-channel single-top-quark production process or the $t \to Wb$ decay, out of which three have complex WCs.

In proton–proton (pp) collisions at the Large Hadron Collider (LHC) [8], the t-channel has the largest rate among all single-top-quark production channels [9, 10]. Moreover, it is the only channel that produces a polarised top quark, providing unique access to the imaginary sector of the Lagrangian through analyses of differential angular decay rates. Figure 1 shows a representative Feynman diagram for t-channel single-top-quark production, occurring at leading order (LO) in the four-flavour factorisation scheme (4FS), but at next-to-leading order (NLO) in the five-flavour scheme (5FS) [11–13]. In this diagram, a light-flavour quark q (i.e. u-, c-, $\overline{d}$-, or $\overline{s}$-quark) from one of the colliding protons interacts with a gluon (splitting into a $b\overline{b}$ pair) by exchanging a space-like virtual W boson, producing a top quark t and a recoiling light-flavour quark q', the so-called spectator quark. The second b-quark from gluon scattering is expected to have a softer transverse momentum (p_{T}) spectrum and a broader pseudorapidity (η) distribution than the b-quark produced in the top-quark decay. It is generally either not detected in the experiment or does not pass the event selection. The final state includes one light-flavour spectator jet, one b-jet, one lepton and missing transverse momentum from the neutrino.

The differential distribution of the top-quark decay, $t \to Wb \to \ell\nu b$, can be fully determined by four angles [14]. The first two angles (θ, ϕ) are the spherical coordinates of the outgoing W-boson momentum direction in the top-quark rest frame, defined in a Cartesian coordinate system (x, y, z). The frame is chosen by first selecting the proton beam whose p_z matches that of the outgoing spectator jet, aligned with the incoming proton beam. Then, following ref. [15], three orthogonal directions are defined. The $\hat{z}$ direction is the direction of the momentum of the spectator jet, $\vec{p}_s$, in the top-quark rest frame. The $\hat{y}$ direction is taken to lie along $\hat{z} \times \hat{p}_q$, where $\vec{p}_q$ is the direction of the incoming proton, in the top-quark reference frame. The $\hat{x}$-direction is then chosen so as to make a right-handed coordinate system. The remaining two angles (θ^*, ϕ^*) are the spherical coordinates of the charged lepton's momentum in the W-boson rest frame, in the coordinate system (x', y', z') obtained by a "standard" boost from the previous frame, such that the $\hat{z}'$ axis is the direction

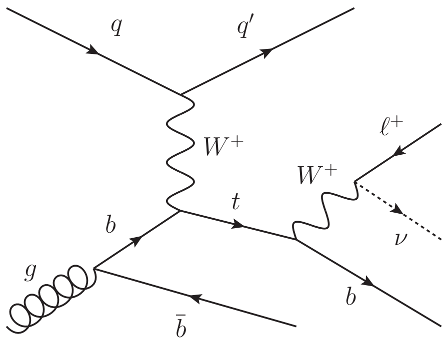

Figure 1. Representative LO Feynman diagram for t-channel single-top-quark production and decay in the 4FS. Here q represents a u/c or $\overline{d}/\overline{s}$ quark, and q' represents a d/s or $\overline{u}/\overline{c}$ quark. The initial b-quark typically arises from a gluon splitting into a $b\overline{b}$ pair.

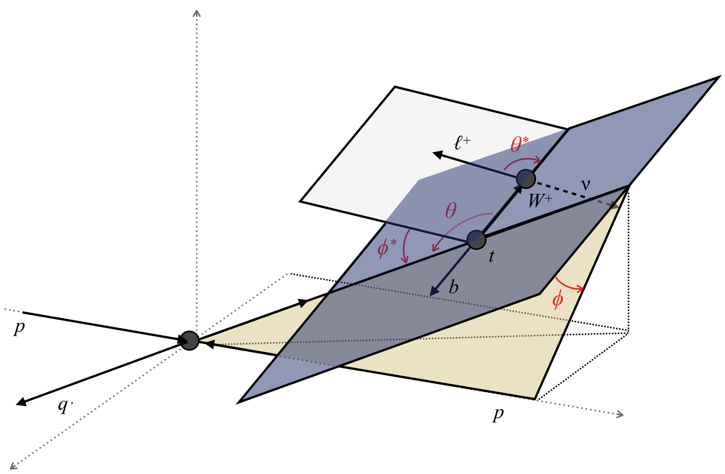

Figure 2. Illustration of the definition of the four angles $(\theta, \phi, \theta^*, \phi^*)$ in the $t \to Wb \to \ell\nu b$ decay chain. The incoming protons, the spectator, top and b quarks, the W boson, and the lepton and neutrino are denoted by p, q', t, b, W, ℓ, and ν, respectively. The angles θ and ϕ specify the direction of the W-boson (or spectator-quark) momentum in the top-quark rest frame, while θ^* and ϕ^* specify the direction of the charged lepton momentum in the W-boson rest frame.

(θ, ϕ) of the W-boson momentum and the $\hat{y}' = \hat{z}' \times \hat{p}_s$ axis lies in the $x-y$ plane. In this system, ϕ is the angle between the production plane and the top-quark decay frame, while ϕ^* is the angle between the top-quark decay plane and the W-boson decay frame. The four angles are illustrated in figure 2.

Many previous measurements by ATLAS [10, 16–18] and CMS [19–23] provide constraints on the WCs examined in this paper. In addition, other measurements [24–27] by ATLAS constrain BSM contributions to the tWb vertex, albeit in the language of anomalous couplings rather than EFT coefficients. Constraints on the real parts of the three complex WCs examined in this paper have also been obtained from an ATLAS measurement of W-boson helicity in top-quark decay [28], although there were not enough independent observables available to constrain all of the WCs simultaneously.

This paper is structured as follows. The WCs chosen for study in this analysis are introduced in section 2. A brief description of the ATLAS detector is given in section 3. Details about the data samples, the Monte Carlo (MC) simulation event samples, and the background estimation are provided in section 4. Then the object definitions, reconstruction, and the event selection are discussed in section 5 and section 6, respectively. Section 7 describes the systematic uncertainties arising in this analysis. Section 8 presents the analysis strategy, including the Fourier techniques employed to extract observables from the dataset, the manner in which they are related to the WCs, and the construction of the profile-likelihood. Finally, the results are discussed in section 9 and the conclusions are given in section 10.

2 Choice of Wilson coefficients

Written in the physical basis, where the Higgs field of the Warsaw basis is set to its vacuum expectation value [29], four of the operators contribute to the tWb Lagrangian as

$$\begin{aligned}
\mathcal{O}^{3}_{\varphi Q} &\supset -\frac{gv^2}{\sqrt{2}}\bar{b}_{\mathrm{L}}\gamma^{\mu}t_{\mathrm{L}}W^{-}_{\mu}\,,\\
\mathcal{O}_{\varphi tb} &\supset \left[\frac{gv^2}{2\sqrt{2}}\bar{b}_{\mathrm{R}}\gamma^{\mu}t_{\mathrm{R}}W^{-}_{\mu}\right]^{\dagger},\\
\mathcal{O}_{tW} &\supset 2v\bar{b}_{\mathrm{L}}i\sigma^{\mu\nu}q_{\nu}t_{\mathrm{R}}W^{-}_{\mu}\,,\\
\mathcal{O}_{bW} &\supset \left[2v\bar{b}_{\mathrm{R}}i\sigma^{\mu\nu}q_{\nu}t_{\mathrm{L}}W^{-}_{\mu}\right]^{\dagger},
\end{aligned}$$

where γ denotes the Dirac matrices, σ the generators of the Clifford basis, and q_{ν} the four-momentum transferred in the t-channel process.

Each of the operators contributes to the tWb vertex with a different Lorentz structure: $\mathcal{O}^{3}_{\varphi Q}$ has a Lorentz structure similar to the SM and therefore modifies the left-handed vector coupling (V_{L}) present in the SM, while $\mathcal{O}_{\varphi tb}$ induces a right-handed vector coupling and $\mathcal{O}_{bW}$ and $\mathcal{O}_{tW}$ contribute as left-handed and right-handed tensor couplings, respectively. Furthermore, $\mathcal{O}_{\varphi tb}$, $\mathcal{O}_{bW}$, and $\mathcal{O}_{tW}$ are non-Hermitian operators and therefore their WCs are complex. A non-vanishing imaginary part then leads to CP violation [30].

The remaining two operators contributing to the top-quark physics studied in this analysis are two four-quark operators, which modify the top-quark production in the t-channel. The relevant four-quark operators have the left–left (LL) and right–right (RR) chiral structure

$$\begin{aligned}
\mathcal{O}^{3,1}_{Qq} &= \left(\bar{Q}\gamma_{\mu}\tau^{I}Q\right)\left(\bar{q}_{i}\gamma^{\mu}\tau^{I}q_{i}\right),\\
\mathcal{O}^{3,8}_{Qq} &= \left(\bar{Q}\gamma_{\mu}T^{A}\tau^{I}Q\right)\left(\bar{q}_{i}\gamma^{\mu}T^{A}\tau^{I}q_{i}\right),
\end{aligned}$$

where $Q = (t_{\mathrm{L}}, b_{\mathrm{L}})$, while q refers to left-handed doublets in the first two generations. The first operator is an SU(2) triplet and colour singlet and the second one is an SU(2) triplet and colour octet. From these two, only the first operator interferes with the SM amplitude, since W-boson exchange is also a colour singlet. The colour-octet operator has already been constrained quite tightly using processes where it does interfere with the SM amplitude [17, 20, 31, 32]. Therefore, it is assumed that the colour-singlet operator dominates, and this analysis is restricted to studying the operator $\mathcal{O}^{3,1}_{Qq}$. For convenience, the WC of $\mathcal{O}^{3,1}_{Qq}$, $c^{3,1}_{Qq}$, is referred to as c_{Qq} in this paper.

As seen above, the dimension-six operators contributing to the top-quark interactions considered in this analysis are

$$\mathcal{O}^{3}_{\varphi Q}, \qquad \mathcal{O}_{\varphi tb}, \qquad \mathcal{O}_{bW}, \qquad \mathcal{O}_{tW}, \qquad \mathcal{O}^{3,1}_{Qq}.$$

The corresponding EFT coefficients $c_{\varphi Q}$ and c_{Qq} are real, while $c_{\varphi tb}$, c_{bW}, and c_{tW} are complex, giving a total of eight free parameters. However, the measurement of the angular distributions can only constrain a subspace of the eight-dimensional complex parameter space. At LO, there are four distinct amplitudes for top-quark decay. Two of them correspond to decays to a left-handed b-quark and for $m_b = 0$, only receive contributions from the SM, $c_{\varphi Q}$ and c_{tW}. The others correspond to decays to a right-handed b-quark and only receive contributions from $c_{\varphi tb}$ and c_{bW}. Thus, one can in principle determine the relative phase between $c_{\varphi tb}$ and c_{bW}, but one cannot determine the phase relative to the SM for either. For convenience, the analysis takes $c_{\varphi tb}$ to be real and positive, and interprets $\mathrm{Arg}\,(c_{bW})$ as implying a phase relative to that of $c_{\varphi tb}$. This leaves two imaginary parameters that, in principle, can be constrained by analysing the angular variables. In total, seven free parameters [14] remain to be measured: $C_{\varphi Q}$, C_{tW}, C^{I}_{tW}, C_{bW}, C^{I}_{bW}, $C_{\varphi tb}$, and C_{Qq}, with:[1]

$$\begin{aligned} V_{\mathrm{L}} &= V_{tb}\left(1+\frac{v^2}{\Lambda^2}C_{\varphi Q}\right), \\ c_{tW} &= C_{tW} + iC^{I}_{tW}, \\ c_{bW} &= C_{bW} + iC^{I}_{bW}, \\ c_{\varphi tb} &= C_{\varphi tb}, \\ c_{Q,q} &= C_{Qq}, \end{aligned}$$

where V_{L} is the left-handed vector coupling in the anomalous-coupling notation [33] and V_{tb} is the quark-mixing matrix element (ME) in the Cabibbo–Kobayashi–Maskawa (CKM) matrix [2]. The superscript ^{I} on the WCs C denotes their imaginary part.

Fixing $c_{\varphi tb}$ to be real and positive is done purely for practical purposes and does not constrain $c_{\varphi tb}$ to have positive or even real values. Multiplying $c_{\varphi tb}$ by an arbitrary phase does not change the posterior probability distributions of the fit as long as c_{bW} is multiplied by the same phase.

Finally, it is noted that $\mathcal{O}^{3}_{\varphi Q}$ has the same Lorentz structure as the SM top-quark decay, and therefore only affects the overall cross-section, and has no effect on the angular distributions. Thus, measuring normalised angular distributions only constrains the ratios of coefficients C_{tW}/V_{L}, $C^{I}_{tW}/V_{\mathrm{L}}$, etc., while measuring the total rate allows one to set constraints on the absolute values of the coefficients. In this analysis, the strength of measuring both the normalised angular distribution and the cross-section is used to obtain the best sensitivity among all the targeted WCs.

[1] In this work, lowercase c is used for complex-valued WCs, while uppercase C is reserved for parameters that are strictly real.

3 ATLAS detector

The ATLAS experiment [34] at the LHC is a multipurpose particle detector with a forward–backward symmetric cylindrical geometry and nearly 4π coverage in solid angle.[2] It consists of an inner tracking detector surrounded by a thin superconducting solenoid providing a 2 T axial magnetic field, electromagnetic and hadronic calorimeters, and a muon spectrometer. The inner tracking detector covers the pseudorapidity range $|\eta| < 2.5$. It consists of silicon pixel and microstrip detectors, and a transition radiation tracker (TRT). Lead/liquid-argon (LAr) sampling calorimeters provide electromagnetic (EM) energy measurements with high granularity within the region $|\eta| < 3.2$. A steel/scintillator-tile hadronic calorimeter covers the central pseudorapidity range ($|\eta| < 1.7$). The endcap and forward regions are instrumented with LAr calorimeters for EM and hadronic energy measurements up to $|\eta| = 4.9$. The muon spectrometer surrounds the calorimeters and is based on three large superconducting air-core toroidal magnets with eight coils each. The field integral of the toroids ranges between 2.0 and 6.0 T m across most of the detector. The muon spectrometer includes a system of precision tracking chambers up to $|\eta| = 2.7$ and fast detectors for triggering up to $|\eta| = 2.4$. The luminosity is measured mainly by the LUCID-2 [35] detector, which is located close to the beam pipe. A two-level trigger system is used to select events [36]. The first-level trigger is implemented in hardware and uses a subset of the detector information to accept events at a rate below 100 kHz. This is followed by a software-based trigger that reduces the accepted event rate to about 1.25 kHz on average depending on the data-taking conditions. A software suite [37] is used in data simulation, in the reconstruction and analysis of real and simulated data, in detector operations, and in the trigger and data acquisition systems of the experiment.

4 Data and simulated event samples

This analysis uses data from pp collisions at $\sqrt{s} = 13$ TeV collected with the ATLAS detector at the LHC during 2015–2018. Stringent detector and data quality requirements were applied [38], resulting in a data sample corresponding to a total integrated luminosity of 140 fb^{-1} [35]. The events were selected by single-lepton (electron or muon) triggers [39, 40], imposing low thresholds on the transverse energy (E_{T}) of electrons and the p_{T} of muons, in addition to isolation requirements, or imposing a looser identification criterion and higher thresholds with no isolation requirement. The lowest thresholds were varied from 20 to 26 GeV depending on the lepton flavour and the data-taking period.

Samples of simulated events were produced using different MC event generators, including parton shower (PS) and hadronisation models for both the signal and background processes. The effect of multiple interactions in the same and neighbouring bunch crossings (pile-up) was modelled by overlaying the hard-scattering event with simulated inelastic pp collisions

[2] ATLAS uses a right-handed coordinate system with its origin at the nominal interaction point (IP) in the centre of the detector and the z-axis along the beam pipe. The x-axis points from the IP to the centre of the LHC ring, and the y-axis points upwards. Polar coordinates (r, ϕ) are used in the transverse plane, ϕ being the azimuthal angle around the z-axis. The pseudorapidity is defined in terms of the polar angle θ as $\eta = -\ln\tan(\theta/2)$ and is equal to the rapidity $y = (1/2)\ln[(E + p_z)/(E - p_z)]$ in the relativistic limit. Angular distance is measured in units of $\Delta R \equiv \sqrt{(\Delta y)^2 + (\Delta\phi)^2}$.

Process	Generator	ME order	PS	PDF set	PS tune
t-channel	POWHEG BOX [45–48]	NLO	PYTHIA 8	NNPDF3.0NLO	A14 [49]
	MADGRAPH [50]	LO	PYTHIA 8	NNPDF3.0NLO	A14
$t\bar{t}$	POWHEG BOX	NLO	PYTHIA 8	NNPDF3.0NLO	A14
	MADGRAPH	LO	PYTHIA 8	NNPDF3.0NLO	A14
$V+\text{jets}$	SHERPA 2.2.11 [44]	MEPS@NLO	SHERPA	NNPDF3.0NNLO	default
Associated tW	POWHEG BOX	NLO	PYTHIA 8	NNPDF3.0NLO	A14
s-channel	POWHEG BOX	NLO	PYTHIA 8	NNPDF3.0NLO	A14
VV, $qqVV$	SHERPA 2.2.2	MEPS@NLO	SHERPA	NNPDF3.0NNLO	default
VVV	SHERPA 2.2.2	MEPS@NLO	SHERPA	NNPDF3.0NNLO	default
$t\bar{t}H$	POWHEG BOX	NLO	PYTHIA 8	NNPDF3.0NLO	A14
$t\bar{t}W$	SHERPA 2.2.10	NLO QCD+EW	SHERPA	NNPDF3.0NNLO	default
$t\bar{t}Z$	MADGRAPH5_AMC@NLO [50]	NLO	PYTHIA 8	NNPDF3.0NLO	A14
tZ	MADGRAPH5_AMC@NLO	NLO	PYTHIA 8	NNPDF3.0NLO	A14
tWZ	MADGRAPH5_AMC@NLO	NLO DR1	PYTHIA 8	NNPDF3.0NLO	A14
$t\bar{t}t$	MADGRAPH5_AMC@NLO	QCD NLO	PYTHIA 8	NNPDF2.3LO	A14
$t\bar{t}t\bar{t}$	MADGRAPH5_AMC@NLO	QCD NLO	PYTHIA 8	NNPDF3.1NLO	A14
ggH, qqH	POWHEG BOX	QCD NLO	PYTHIA 8	CT10 [51]	AZNLO [52]
WH, ZH	PYTHIA 8	QCD NLO	PYTHIA 8	NNPDF2.3LO	A14

Table 1. The configurations used to generate events for signal (t-channel) and background processes. "ME order" refers to the order of the matrix-element calculation. The simulation samples used to model EFT effects are shown in grey. A dedicated set of tuned PS parameters [44], developed by the SHERPA authors and referred to as the "default" tune, was used for simulation samples generated with SHERPA.

generated with PYTHIA 8.186 [41] using the NNPDF2.3LO set of parton distribution functions (PDFs) [42] and the A3 set of parameters (tune) [43]. Events were reweighted such that the distribution of the average number of interactions per bunch crossing matches that observed in data. Table 1 presents a summary of all configurations used to generate events for signal (t-channel) and background processes.

The effects of variations associated with different sources of modelling systematic uncertainty were evaluated by comparing alternative simulation samples with the nominal ones. These alternative samples were generated either through internal reweighting or with dedicated event generators. Each variation was introduced independently unless explicitly stated otherwise, ensuring a consistent assessment of its individual impact on the analysis. Further details about these samples are provided in section 7.

Single-top-quark production in the t-channel was modelled using the POWHEG BOX v2 [46–48, 53] generator, which provides ME calculations at NLO accuracy in the strong coupling constant α_s in the 4FS with the corresponding NNPDF3.0NLO [54] set of PDFs. The functional form of the renormalisation (μ_r) and factorisation (μ_f) scales was set to $\sqrt{m_b^2 + p_{T,b}^2}$ following the recommendations of refs. [53, 55]. Top quarks were decayed at LO using MADSPIN [56, 57] to preserve all spin correlations. For PS and hadronisation, the events were interfaced with PYTHIA 8.230 [58], which used the A14 tune [49] and the NNPDF2.3LO PDF set [42].

The predicted cross-sections for single-top-quark and single-top-antiquark production in the t-channel in pp collisions at a centre-of-mass energy of 13 TeV are $\sigma(tq) = 134.2^{+2.6}_{-1.7}$ pb and $\sigma(\bar{t}q) = 80.0^{+1.8}_{-1.4}$ pb, respectively. The cross-sections were calculated with the MCFM program [59] at next-to-next-to-leading order (NNLO) in quantum chromodynamics (QCD). The quoted uncertainties include the uncertainties due to choosing μ_{r} and μ_{f} scale values, the uncertainty in the PDFs, and the uncertainty in the value of the strong coupling constant α_{s}. The uncertainty due to the scales was determined by raising and lowering μ_{r} and μ_{f} independently by a factor of two, whilst never allowing them to differ by more than a factor of two. The combined PDF and α_{s} uncertainties were determined at the 68% confidence level (CL) according to the Hessian representation of the PDF4LHC21 PDF set [60].

The production of $t\bar{t}$ events was modelled at NLO in QCD in the 5FS using POWHEG BOX v2 [45–48] with the NNPDF3.0NLO PDF set. The `POWHEG:hdamp` parameter was set to $1.5 \times m_t$ [61].[3] Events were interfaced with PYTHIA 8.230, which used the A14 tune and the NNPDF2.3LO PDF set [42]. The simulation samples were normalised to the cross-section of 834^{+29}_{-37} pb predicted at NNLO in QCD, including the resummation of next-to-next-to-leading logarithmic (NNLL) soft-gluon terms calculated using TOP++ 2.0 [62–68]. The combined PDF and α_{s} uncertainties were determined at the 68% CL according to the Hessian representation of the PDF4LHC21 PDF set.

To model the EFT effects, LO SM events were produced with MADGRAPH 2.8.1 [50] with the NNPDF3.0NLO PDF set interfaced with PYTHIA 8.244, which used the A14 tune and the NNPDF2.3LO PDF set. The events were subsequently reweighted at LO by rescaling each event by the ratio of EFT to SM MEs [69], computed using the `dim6top` UFO model [70]. In this setup, the `dim6top` model is used with EFT insertions allowed at both the production and decay vertex of the top quark. This setup therefore retains all contributions up to quadratic order in the WCs in the cross-section, arising from the squared ME. In this approach, events with different parton multiplicities in the MADGRAPH simulation sample are each reweighted using the tree-level ME evaluated at the corresponding final-state multiplicity; this reweighting is applied solely within the LO MADGRAPH simulation sample and does not involve the NLO POWHEG simulation. Higher-order QCD corrections are accounted for by an additive yield correction defined as the difference between the NLO POWHEG and LO MADGRAPH predictions at the SM point, treated as a constant k-factor independent of the WC values. Consequently, the modelling includes the interference between SM and EFT amplitudes, as well as all interference terms between EFT contributions arising in the production and decay of the top quark. A six-dimensional grid, formed by C_{tW}, C^{I}_{tW}, C_{bW}, C^{I}_{bW}, $C_{\varphi tb}$, and C_{Qq}, was generated for both the t-channel signal sample and the $t\bar{t}$ background sample. Here, $C_{\varphi Q}$ is not included in the grids, since it only changes the overall cross-section, which can be parameterised by a scale factor, as introduced in section 2. The points of this grid were designed to cover the 95% confidence intervals of the previous analysis results [16, 27]. An analytically derived top-quark width correction was incorporated into the reweighting to account for variations in the top-quark's width Γ_t induced by changes in the WCs [71], since this correction cannot be handled by the MADGRAPH 2.8.1 reweighting function. This procedure ensures a consistent treatment of EFT effects in both production and decay, including the dependence of the top-quark width on the WCs, thereby ensuring

[3]The `POWHEG:hdamp` parameter controls the p_{T} of the first additional emission beyond LO in the PS and therefore regulates the high-p_{T} emission against which the $t\bar{t}$ system recoils.

that the total width scales correctly with the modified couplings. The approach follows the same formalism as presented in ref. [16], where the dependence of the cross-section on the WCs is explicitly constructed. Overall, the signal model consistently includes all SM, linear EFT, and quadratic EFT contributions, together with their mutual interferences, for the full process including both production and decay.

The production of single-boson ($V+$jets) events was simulated using SHERPA 2.2.11 [44]. The MEs were calculated at NLO (LO) accuracy in QCD for up to two (for three or four) partons (0,1,2j@NLO + 3,4j@LO) using the COMIX library [72], with the virtual QCD loop corrections supplied by the OPENLOOPS library [73–75]. The ME calculations were matched and merged with the default SHERPA PS [76], based on Catani–Seymour dipole factorisation and the cluster hadronisation model [77]. The NNPDF3.0NNLO PDF set was used together with a dedicated set of SHERPA-tuned PS parameters, and the simulation samples were normalised to NNLO cross-section predictions [78].

Single top quarks from s-channel and tW associated production were generated with POWHEG BOX v2 in the 5FS at NLO in QCD with the NNPDF3.0NLO PDF set, with μ_f and μ_r set to $\sqrt{m_b^2+p_{\mathrm{T},b}^2}$, following the recommendation of refs. [55, 79], respectively. For the latter process, the Diagram Removal 1 (DR1) scheme was employed to handle the interference between tW and $t\bar{t}$ [61]. The EFT effects in the tW process are neglected, since its impact on the total event yield is small compared to the dominant t-channel and $t\bar{t}$ processes, as demonstrated in the yield tables and figures in the following sections.

The VV and VVV processes were simulated by SHERPA 2.2.2 [44] with off-shell effects and Higgs contributions at NLO (LO accurate for up to three additional parton emissions). The MEs were matched to PS with MEPS@NLO [80–83] with the set of tuned parameters developed by the SHERPA authors. The samples include events from loop-induced and EW production.

Top-quark associated and Higgs-boson backgrounds were simulated at NLO in QCD using various generators with matched PS. They include $t\bar{t}H$, $t\bar{t}W$, $t\bar{t}Z$, tZq, tWZ, ttt, $t\bar{t}t\bar{t}$, and Higgs-related processes (ggH, qqH, WH, ZH).

In all simulated signal and background samples, the top-quark mass was set to $m_t = 172.5\,\mathrm{GeV}$. The strong coupling constant was set to $\alpha_\mathrm{s} = 0.118$. These values were also used in the computation of production cross-sections for processes involving the top quark. The bottom and charm hadron decays were simulated with EVTGEN [84] for non-SHERPA-generated event samples.

5 Object definitions

Interaction vertices from the pp collisions are reconstructed from at least two tracks with $p_\mathrm{T} > 500\,\mathrm{MeV}$ that are consistent with originating from the beam collision region in the x–y plane. If more than one primary vertex candidate is found in the event, the candidate for which the associated tracks form the largest sum of squared p_T is selected as the hard-scatter primary vertex [85].

Electron candidates are reconstructed from energy clusters in the electromagnetic calorimeter matched to a track in the inner tracking detector (ID) [86]. They are required to satisfy $p_\mathrm{T} > 10\,\mathrm{GeV}$ and $|\eta_\mathrm{cluster}| < 2.47$, excluding the transition region between the barrel and

	Loose electron	Loose muon
Identification	`loose`	`medium`
Acceptance	$p_{\mathrm{T}} > 10\,\mathrm{GeV}$, $\lvert\eta^{\mathrm{cluster}}\rvert < 2.47$	$p_{\mathrm{T}} > 10\,\mathrm{GeV}$, $\lvert\eta\rvert < 2.5$
	except $1.37 < \lvert\eta^{\mathrm{cluster}}\rvert < 1.52$	
Impact parameter	$\lvert d_0/\sigma(d_0)\rvert < 5.0$	$\lvert d_0/\sigma(d_0)\rvert < 3.0$
	$\lvert z_0 \sin(\theta)\rvert < 0.5\,\mathrm{mm}$	$\lvert z_0 \sin(\theta)\rvert < 0.5\,\mathrm{mm}$
	Tight electron	**Tight muon**
Identification	`tight`	`medium`
Isolation	required	required
Extra selections	Electron charge-misassignment veto	
	Electron conversion candidate veto	

Table 2. Summary of the electron and muon object definitions. The selection requirements for Tight electrons/muons are applied in addition to the preselected (Loose) objects used for the overlap removal.

endcap calorimeters ($1.37 < \lvert\eta_{\mathrm{cluster}}\rvert < 1.52$). The `loose` and `tight` electron identification working points are used to identify Loose and Tight electrons respectively [86], based on a likelihood discriminant employing calorimeter, tracking, and combined variables that provide separation between electrons and jets, and electrons and photons.

Muon candidates are reconstructed from tracks measured in the ID matched to tracks measured in the muon spectrometer [87, 88]. The resulting muon candidates are re-fitted using the complete track information from both detector systems. They are required to satisfy $p_{\mathrm{T}} > 10\,\mathrm{GeV}$ and $\lvert\eta\rvert < 2.5$. The `medium` muon identification working point [88] is used.

Electron (muon) candidates are matched to the primary vertex by requiring that the significance of their transverse impact parameter, d_0, satisfies $\lvert d_0/\sigma(d_0)\rvert < 5.0\,(3.0)$, where $\sigma(d_0)$ is the measured uncertainty in d_0, and by requiring that their longitudinal impact parameter, z_0, satisfies $\lvert z_0 \sin(\theta)\rvert < 0.5\,\mathrm{mm}$ [86, 87].[4] Furthermore, lepton isolation is required for both electron and muon candidates [87, 89]. Tight leptons with incorrect charge assignment, or originating from heavy-flavour hadron decays, misidentified jets, or photon conversions (collectively referred to as "non-prompt leptons") are suppressed using a BDT discriminant, based on calorimeter, tracking, isolation, and lifetime-related quantities [87, 89], which allows prompt muons (barrel/endcap electrons) to be selected with an efficiency of about 60% (60%/70%) at $p_{\mathrm{T}} \sim 20\,\mathrm{GeV}$ and reaching a plateau of approximately 95% (95%/90%) at $p_{\mathrm{T}} \sim 40$ (40/65) GeV, while achieving a rejection factor of about 20 against leptons from b-hadron decays.

Table 2 summarises the definitions of the reconstructed electron and muon candidates.

The constituents for jet reconstruction are identified by combining measurements from both the ID and the calorimeter using a particle flow (PFlow) algorithm [90]. Jet candidates are reconstructed from these PFlow objects using the anti-k_t algorithm [91, 92] with a radius parameter of $R = 0.4$. They are calibrated using simulation with corrections obtained by

[4] The transverse impact parameter, d_0, is defined in the x–y plane as the distance of closest approach of the track to the beamline. The longitudinal impact parameter, z_0, is defined as the distance in z between the primary vertex and the point on the track used to evaluate d_0.

using in situ techniques in data [93]. Only jet candidates with $p_{\mathrm{T}} > 30\,\mathrm{GeV}$ and within $|\eta| < 4.5$ are selected. To reduce the effect of pileup, each jet with $p_{\mathrm{T}} < 60\,\mathrm{GeV}$ and $|\eta| < 2.4$ must satisfy the `Tight` working point of the jet vertex tagger (JVT) [94] criteria. Moreover, jets with $2.5 < |\eta| < 4.5$ (hereafter called "forward jets") and $p_{\mathrm{T}} < 120\,\mathrm{GeV}$ must satisfy the `Tight` working point of the forward jet vertex tagger (fJVT) [95] criteria. A set of quality criteria is also applied to reject events containing at least one jet arising from non-collision sources or detector noise [96].

Jets containing b-hadrons are identified (b-tagged) via the `DL1r` [97] algorithm. It uses a deep feed-forward neural network based on the distinctive features of b-hadron decays, primarily the impact parameters of tracks and the displaced vertices reconstructed in the ID. Additional input to this network is provided by discriminating variables constructed by a recurrent neural network (RNN) [97], which exploits the spatial and kinematic correlations between tracks originating from the same b-hadron. A multivariate b-tagging discriminant value is calculated for each jet. In this measurement, a jet is considered b-tagged if it passes the working point corresponding to 60% average expected efficiency to tag a b-quark jet, with a light-flavour-jet rejection factor of about 2500, and a charm-jet rejection factor of about 40. Correction factors, derived from dedicated calibration samples enriched in b-jets, c-jets, or light-flavour jets, are applied to the simulated event samples [98–100].

The reconstruction of hadronically decaying τ-lepton candidates (τ_{had}) is seeded by jets reconstructed via the anti-k_t algorithm, using calibrated energy clusters as inputs, with a radius parameter of $R = 0.4$ [101, 102]. Jets seeding τ_{had} candidates are additionally required to have $p_{\mathrm{T}} > 10\,\mathrm{GeV}$ and $|\eta| < 2.5$. To separate the τ_{had} candidates initiated by hadronic τ-lepton decays from jets initiated by quarks or gluons, an RNN [102] identification method was trained on information from reconstructed charged-particle tracks and clusters of energy in the calorimeter matched to τ_{had} candidates, as well as on high-level discriminating variables. A separate multivariate discriminant based on a BDT [101, 103] is also used to reject backgrounds arising from electrons mimicking a τ_{had}. This discriminant (`eBDT`) is built using information from the calorimeter and the ID. Transition radiation information from the TRT system plays a key role in the performance of this discriminant. Baseline τ_{had} are required to have one or three associated tracks, electric charge of ± 1, $p_{\mathrm{T}} > 20\,\mathrm{GeV}$ and $|\eta| < 2.5$, excluding the barrel–endcap transition region. Each τ_{had} must satisfy the `Medium` RNN identification requirement, with efficiencies of 75% for 1-prong decays and 60% for 3-prong decays, and the `Loose eBDT` requirement, with an efficiency of 95% [101, 103].

Ambiguities between independently reconstructed electrons, muons, jets and τ_{had} can arise. A sequential "overlap removal" procedure is performed to resolve these ambiguities and thus avoid double counting of candidates. This procedure is applied to leptons satisfying the Loose criteria described in table 2. If two electrons are separated by $\Delta R < 0.1$, only the one with the higher p_{T} is kept. If an electron and a muon overlap within $\Delta R < 0.1$, the muon is removed if it is reconstructed only from an ID track and calorimeter energy deposits consistent with a minimum-ionising particle, otherwise the electron is removed. If an electron and a selected jet are found within $\Delta R < 0.2$, the jet is removed. Any electron subsequently found less than $\Delta R = 0.4$ from a jet is removed. A jet–muon separation is required at $\Delta R < 0.4$ if a muon is found within a jet using the ghost-matching technique [91]. If the overlapping jet contains less than three tracks with $p_{\mathrm{T}} > 500\,\mathrm{MeV}$, the jet is removed, otherwise the muon is rejected. Any τ_{had} found less than $\Delta R = 0.2$ from an electron is removed. Any τ_{had} found less than $\Delta R = 0.2$ from any type of muon with $p_{\mathrm{T}} > 2\,\mathrm{GeV}$ is removed, except those with $p_{\mathrm{T}} > 50\,\mathrm{GeV}$ which are only removed if overlapping with a combined-type muon. Finally, if a jet is found less than $\Delta R = 0.2$ from a τ_{had}, the jet is removed.

The missing transverse momentum $\vec{p_{\mathrm{T}}}^{\mathrm{miss}}$ (with magnitude $E_{\mathrm{T}}^{\mathrm{miss}}$) is defined as the negative vector sum of the transverse momenta of all identified and calibrated objects and remaining unclustered energy, the latter (composing the "soft term") being estimated from low-p_{T} tracks associated with the primary vertex but not with any lepton or jet candidate [104]. The $E_{\mathrm{T}}^{\mathrm{miss}}$ is taken as a measurement of the undetectable particles, and is affected by energy losses due to detector inefficiencies and acceptance, and by energy resolution.

6 Reconstruction and event selection

The on-shell W boson originating from the decay of the top quark is reconstructed from the momenta of the lepton (electron or muon) and the neutrino by imposing four-momentum conservation. Since the neutrino escapes undetected, the x and y components of the reconstructed $\vec{p_{\mathrm{T}}}^{\mathrm{miss}}$ are assumed to correspond to the p_{T} of the neutrino. The unmeasured longitudinal component of the neutrino momentum, p_z^{ν}, is computed by imposing a W-boson mass constraint[5] on the lepton–neutrino system. If the resulting quadratic equation yields two real solutions for p_z^{ν}, the solution closer to the reference top-quark mass $m_t = 172.5\,\mathrm{GeV}$ is taken. If the solutions are complex, the reconstructed $\vec{p_{\mathrm{T}}}^{\mathrm{miss}}$ is rescaled, preserving its direction, to obtain a unique real solution for p_z^{ν}. The top-quark candidate is then reconstructed by combining the four-momenta of the reconstructed W boson and the selected b-tagged jet.

To enhance the sensitivity to the relevant WCs, it is crucial to maximise the selected yield of t-channel single-top-quark events while minimising background contributions from other processes. To achieve this, one signal-enriched region (SR) and two control regions (CRs) are defined. These regions facilitate the simultaneous extraction of the WC values and the data-driven normalisation factors of the $t\bar{t}$ and $W+$jets backgrounds. In the analysis, both the SR and CRs are divided into four channels based on the lepton charge and the p_{T} of the reconstructed top quark, where channels with reconstructed top-quark p_{T} greater than 80 GeV are labelled as high-p_{T}, and those with lower p_{T} are labelled as low-p_{T}. Partitioning the data by lepton charge takes advantage of the charge asymmetry present in $W+$jets and t-channel single-top-quark production, in contrast to the charge-symmetric $t\bar{t}$ background. Likewise, separating events by top-quark p_{T} above and below the 80 GeV threshold, optimised using simulated signal samples, improves the sensitivity because certain EFT operators, most notably C_{Qq}, impact the high- and low-energy regions differently; for C_{Qq}, the ratio of the EFT prediction to the SM expectation exhibits a pronounced shape variation, with a sign change around 80 GeV, enhancing the expected constraint by about 20% in the full likelihood fit.

[5]The constraints used to reconstruct the neutrino momentum are set using the world-average values of the W-boson mass, $m_W = 80.399$ GeV from ref. [105], which correspond to the value employed in the generation of the MC simulation samples.

Events are first required to satisfy a set of preselection criteria, primarily designed to suppress backgrounds from jets misidentified as other objects. The preselection is defined as follows:

- Exactly one Tight charged lepton ℓ (electron or muon, as defined in table 2, originating from the decay of the W boson or from the subsequent decay of a leptonically decaying τ) with $p_{\mathrm{T}} > 30\,\mathrm{GeV}$, matched to the single-lepton trigger.
- Veto on any additional Loose charged leptons (defined in table 2) to reduce the dilepton backgrounds; events containing reconstructed hadronically decaying τ-leptons (τ_{had}) are also vetoed to further suppress processes involving a τ_{had}.
- Exactly two jets; for jets within the calorimeter's endcap–forward transition region ($2.75 < |\eta_j| < 3.5$, where η_j denotes the η of the jets), the threshold is increased to $35\,\mathrm{GeV}$.
- At least one of the jets must be b-tagged.
- $E_{\mathrm{T}}^{\mathrm{miss}} > 35\,\mathrm{GeV}$.

Two additional multijet background rejection criteria are applied [16]:

- Transverse mass of the lepton–$\vec{p}_{\mathrm{T}}^{\,\mathrm{miss}}$system must fulfill $m_{\mathrm{T}}(\ell\vec{p}_{\mathrm{T}}^{\,\mathrm{miss}}) > 60\,\mathrm{GeV}$.
- The lepton transverse momentum $p_{\mathrm{T}}(\ell)$ must satisfy

$$p_{\mathrm{T}}(\ell) > 50\,[1 - (\pi - |\Delta\phi(j_1, \ell)|)/(\pi - 1)]\ \mathrm{GeV}\,,$$

  where j_1 refers to the jet with leading p_{T} and $\Delta\phi$ is the azimuthal angle between the jet and lepton. This requirement rejects backgrounds, especially the QCD multijet process where two jets are produced back-to-back in the azimuthal plane and one of those is misreconstructed as a lepton.

Events that pass the single-lepton trigger but fail the preselection are enriched in non-prompt lepton ("fake") background contributions and are therefore used to validate the fake-lepton background estimation. These backgrounds arise from processes that produce either a jet misidentified as an electron, or a muon or electron originating from the semileptonic decay of a heavy-flavour quark. In this analysis, a matrix method [89] is employed to estimate such backgrounds in a data-driven way. The parameterised efficiencies of lepton misidentification are derived from a multijet-enriched control region requiring a single Loose lepton. The real- and fake-lepton efficiencies, parameterised in lepton p_{T} and $|\eta|$, are then applied event by event to data events with a Loose, but not Tight, lepton.

Events that satisfy the preselection criteria are classified into three mutually exclusive regions: an SR, a W+jets-enriched CR (CR-W), and a $t\bar{t}$-enriched CR (CR-$t\bar{t}$). Events in the SR and CR-W are required to have exactly one b-tagged jet, with the second jet failing the b-tagging working point. The CR-W region is defined by events that match this b-tagging configuration but fail at least one of the additional SR selection requirements. Events in CR-$t\bar{t}$ are required to contain two jets that both satisfy the b-tagging criteria.

JHEP07(2026)107

An event is classified as being in the SR if it satisfies the preselection and the following additional requirements:

- Invariant mass of the lepton and b-jet: $m_{\ell b} < 153\,\text{GeV}$; top-quark mass proxy reconstructed from the lepton, missing transverse momentum $\vec{p_{\text{T}}}^{\text{miss}}$and b-jet four-vectors: $m_t^{\text{reco}} = m_{\ell \vec{p_{\text{T}}}^{\text{miss}} b} \in [120.6, 234.6]$ GeV. These criteria help to select events consistent with a top-quark mass around 172.5 GeV.

- Trapezoidal requirement defined as:

$$\left(\eta_j < a_1 \eta_{\ell \vec{p_{\text{T}}}^{\text{miss}} b} + b_1\right) \cap \left(\eta_j > a_1 \eta_{\ell \vec{p_{\text{T}}}^{\text{miss}} b} - b_1\right) \cap$$
$$\left[\left(\eta_j > a_2 \eta_{\ell \vec{p_{\text{T}}}^{\text{miss}} b} + b_2\right) \cup \left(\eta_j < a_2 \eta_{\ell \vec{p_{\text{T}}}^{\text{miss}} b} - b_2\right)\right],$$

  where the parameters $a_{1,2}$ and $b_{1,2}$ are optimised by applying the $m_{\ell b}$ requirement and finding the maximum signal-to-background ratio, S/B. The chosen values are $a_1 = 3$, $b_1 = 10.5$, $a_2 = 0.25$, and $b_2 = 2.5$. This requirement helps to distinguish the signal process from the W+jets background.

- Invariant mass of the full system: $m_{j\ell \vec{p_{\text{T}}}^{\text{miss}} b} > 320\,\text{GeV}$. In t-channel single-top-quark events, the angles between these objects are typically large, leading to a high invariant mass, whereas the backgrounds peak at a lower mass value.

- Scalar sum of the p_{T} of all the reconstructed objects in the final state (lepton, jets and $\vec{p_{\text{T}}}^{\text{miss}}$): $H_{\text{T}} > 190\,\text{GeV}$. This ensures the presence of significant hadronic activity.

- To reject events with semileptonic decayed b-jets, the events are selected by performing a kinematic fit with the reconstructed masses of the W boson and the top quark constrained to their measured values [2] in the kinematic likelihood (KL) fit framework [106].[6]

Table 3 summarises the yields for each channel in the SR, detailing contributions from different MC process components as well as the data.

7 Sources of systematic uncertainty

Various sources of systematic uncertainty are evaluated for their effect on the signal and background rates and the shape of the angular distributions. In the following, the procedures used to evaluate these sources of systematic uncertainty are discussed. The systematic uncertainties considered are of two main types: experimental uncertainties and theory modelling uncertainties. All systematic uncertainties are modelled uniformly across the full set of simulation and reconstruction procedures for ATLAS data-taking during the LHC Run 2 scenario. The effect due to the limited size of the simulated event samples is also taken into account when evaluating the total uncertainty.

[6]Breit–Wigner distributions are used to construct the kinematic likelihood function. For the W boson, the Breit–Wigner distribution of the $\ell\nu$ system has a mean value of $m_W = 80.399\,\text{GeV}$ [105] and a width of $\Gamma_W = 2.1\,\text{GeV}$. For the top quark, the Breit–Wigner distribution of the $W\ b$ system has a mean value of $m_t = 172.5\,\text{GeV}$ and a width of $\Gamma_t = 1.5\,\text{GeV}$.

JHEP07(2026)107

Process	**SR t low-p_T**	**SR t high-p_T**	**SR $\bar{t}$ low-p_T**	**SR $\bar{t}$ high-p_T**
t-channel	$23\,900 \pm 1400$	$15\,400 \pm 1300$	$13\,900 \pm 800$	7260 ± 600
s-channel	80 ± 7	20 ± 2	80 ± 5	30 ± 2
tW	570 ± 20	210 ± 10	570 ± 20	198 ± 10
$t\bar{t}$	3350 ± 450	1730 ± 240	3380 ± 540	1780 ± 230
$W+$jets	6500 ± 700	1680 ± 200	5300 ± 800	1150 ± 150
$Z+$jets, VV	600 ± 130	170 ± 32	550 ± 120	160 ± 35
Others	300 ± 110	80 ± 40	400 ± 160	110 ± 40
Total expected	$35\,300 \pm 1600$	$19\,300 \pm 1300$	$24\,100 \pm 1200$	$10\,690 \pm 700$
Data	35 817	18 573	24 639	10 536
$\boldsymbol{S/B}$	2.10 ± 0.20	3.95 ± 0.50	1.36 ± 0.15	2.12 ± 0.25
Data / Prediction	1.02 ± 0.05	0.96 ± 0.07	1.02 ± 0.05	0.99 ± 0.06

Table 3. The pre-fit event yields in the four SRs: t low-p_T, t high-p_T, $\bar{t}$ low-p_T, and $\bar{t}$ high-p_T. The event yield predictions are obtained from simulated samples normalised to theoretical cross-sections, except for the multijet contribution which is derived from a data-driven method. Uncertainties quoted include both statistical and systematic components. Individual predictions are rounded to the relevant digit with the 'Total expected' obtained from the sum of the full-precision individual predictions and subsequently rounded. The last two rows show the signal-to-background (S/B) and the data-to-prediction ratios in each region, computed using full-precision individual predictions.

The uncertainty in the integrated luminosity is $\pm 0.83\%$ [107] and is applied to the signal and all simulated background processes that are scaled by the luminosity as one overall rate uncertainty in the fit. To account for the difference between the pile-up distributions in data and MC simulations, an uncertainty related to the scale factor used to adjust the MC pile-up to the data pile-up profile is applied. This uncertainty is obtained by scaling the value of average number of interactions per bunch-crossing $\langle\mu\rangle$ in data by factors of 1.01 and 0.93 instead of the nominal scale factor of 0.97 [108].

To determine the jet energy scale (JES) and its associated uncertainty, information from test-beam data, LHC collision data and simulation are used as described in ref. [93]. The JES uncertainty is decomposed into a set of 31 uncorrelated components, with contributions from pile-up, jet flavour composition, single-particle response, effects of jets not contained within the calorimeter, theory modelling, and statistical uncertainties. The jet energy resolution (JER) is measured separately for data and MC simulation, using in situ techniques [93]. Its uncertainty is represented by 13 components accounting for jet-p_T- and jet-η-dependent differences between simulation and data. The uncertainty associated with the JVT is obtained by increasing and decreasing the scale factor used to correct the JVT efficiency in simulation within its uncertainties [95]. The uncertainties associated with the fJVT are related to data–MC efficiency scale factors in the same manner as the JVT uncertainty.

The efficiency of the b-tagging algorithm is measured for each jet flavour using control samples in data and in simulation. From these measurements, correction factors are derived to correct the tagging rates in the simulation. For b-jets, the correction factors and their uncertainties are estimated from data using dileptonic $t\bar{t}$ events [97, 98]. For c-jets, they

JHEP07(2026)107

are derived from jets arising from W boson decays in $t\bar{t}$ events [99]. For light-flavour jets, the correction factors are derived from $Z+$jets events [100]. Uncertainties from sources affecting the b-tagging efficiencies of b-jets, c-jets and light-jets are evaluated as a function of jet p_{T}, including bin-to-bin correlations.

For electrons and muons, the reconstruction, identification, isolation, and trigger performance can differ slightly between data and MC simulation. Scale factors, estimated using the tag-and-probe method [86–88], are applied to simulated events to correct for these differences. The lepton momentum scales and resolutions are assessed using leptonic decays of Z bosons and J/ψ mesons. Corrections to the lepton momentum scale and resolution are applied to data and simulation respectively, and include uncertainties in the lepton trigger efficiencies. The associated systematic uncertainties are then propagated to the distributions used in this analysis. Since events containing reconstructed hadronically decaying τ-leptons are vetoed, a τ_{had} energy scale systematic uncertainty [101] is also included.

The systematic uncertainties related to the modelling of the $E_{\mathrm{T}}^{\mathrm{miss}}$ in the simulation are estimated by propagating the uncertainties in the energy and momentum scales of electrons, muons and jets, as well as the uncertainties in the resolution and scale of the soft term [109]. For the data-driven fake-lepton background estimate, real-lepton and fake-lepton efficiency differences between the MC-driven and data-driven methods are taken as an additional source of systematic uncertainty.[7] Systematic uncertainties associated with the signal and background MC modelling are estimated by comparing event samples from different generators and by varying parameter values in the event generation.

The uncertainty due to the choice of hadronisation model and the other non-perturbative aspects of the PS is evaluated by comparing samples generated with different hadronisation models or set-ups. The uncertainty in the PS is estimated for all top-quark processes by comparing samples from Powheg Box interfaced to Pythia 8 with samples from Powheg Box interfaced to Herwig 7.1.3. To estimate the matching scheme uncertainties in t-channel single-top-quark and $t\bar{t}$ production, a sample was produced with Powheg Box v2 and Pythia using a `POWHEG:pThard` setting of 1, instead of 0 as in the nominal sample. This setting regulates the definition of the vetoed region of the Pythia 8 showering [110]. The effect of choosing a different `Powheg:hdamp` parameter value in $t\bar{t}$ simulation is assessed with alternative samples generated with $h_{\mathrm{damp}} = 3.0 \times m_t$. To assess the uncertainty arising from the choice of recoil scheme in the modelling of QCD radiation from b-quarks in top-quark decays, an alternative $t\bar{t}$ sample is generated with Powheg Box v2 interfaced to Pythia, in which the `POWHEG:recoilToTop` option replaces the nominal `POWHEG:recoilToColor` configuration used for the baseline $t\bar{t}$ simulation setup [111]. The effect of the top-quark mass uncertainty is estimated as the difference resulting from samples with a 0.5 GeV top-quark mass variation, for t-channel and $t\bar{t}$ productions. All the other modelling uncertainties are uncorrelated between the t-channel and $t\bar{t}$ processes, except for the top-quark mass uncertainty. For associated tW production, an additional sample using the diagram subtraction (DS) scheme was produced to evaluate the $t\bar{t}$ interference uncertainties.

[7]The MC-driven method employs the same matrix method as the data-driven method but replaces the data with simulated samples and recomputes the fake-lepton efficiency. The real-lepton efficiency remains the same for both methods.

JHEP07(2026)107

The uncertainty due to missing higher-order QCD corrections in the ME computation is estimated for all processes involving top quarks by independently varying the μ_r and μ_f scales by factors of 0.5 and 2.0 with respect to their chosen value. Additionally, for the t-channel and $t\bar{t}$ processes, uncertainties due to initial-state radiation modelled by the PS are assessed by varying the `Var3c` eigentune variation of the A14 tune [112]. Furthermore, the impact of final-state radiation is evaluated by varying the μ_r scale for PS emissions by factors of 0.5 and 2.0, using reweighted events. For all processes, PDF uncertainties are evaluated using the PDF4LHC15 uncertainty set which consists of 30 eigenvector variations from multiple NLO PDF sets [113].

The event yields associated with the simulated signal and background processes are estimated using the selection acceptances and the theoretically predicted cross-sections reported in Section 4. The uncertainties in these cross-sections are taken into account. However, for those processes whose normalisation is extracted from the data-driven fits, the effect is negligible. To evaluate the impact of the flavour composition uncertainty in the $W+$jets simulation templates, an upward and downward variation of 10% is applied to the relative rate of $W+b$-jets vs $W+c$-jets. No variation is considered for $W+$light-flavour jets production since its contribution is negligible. An uncertainty of 20% is assigned to the $Z+$jets cross-section. For $t\bar{t}$ events, an additional uncertainty in the modelling of the top-quark p_T distribution is evaluated by taking the full difference between applying and not applying the correction needed to match the predictions accurate to NNLO in QCD and NLO in EW theory [114].

Statistical fluctuations in the MC-simulated event samples contribute to the overall systematic uncertainty. These uncertainties arise from the finite number of simulated background and signal events.

8 EFT analysis strategy

A standard method for modelling EFT effects in differential distributions involves the use of templates; however, this becomes impractical for a fourfold distribution. The method used here instead performs a Fourier analysis of the quadruple-differential angular decay rate of t-channel single-top-quark production at detector level, using a set of orthogonal basis functions. The resulting Fourier coefficients provide a complete characterisation of the shape of the quadruple-differential angular decay distribution. They are computed through a simple averaging procedure, which simultaneously provides their uncertainties and correlations. Along with the event yields, these coefficients, their uncertainties, and their correlations serve as inputs to a χ^2 fit to the WCs. An advantage of this approach lies in its ability to simultaneously capture many features of the shape and normalisation of the differential cross-section, including those that are more frequently studied in dedicated analyses, such as cross-section or polarisation analyses.

This analysis procedure is described in more detail in the following sections. Section 8.1 explains the procedure used to transform the quadruple-differential angular decay rates into a limited number of coefficients for an orthogonal basis of so-called M-function. Section 8.2 describes how to obtain the EFT dependency of the M-function coefficients. Section 8.3 introduces the statistical tool used to obtain the final limits.

8.1 Choice of basis functions

The orthogonal functions employed in this analysis are called M-functions and are defined as

$$M^{j_1 j_2}_{m' m}(\phi,\theta,\phi^*,\theta^*) = \frac{1}{4\pi}(2j_1+1)^{1/2}(2j_2+1)^{1/2} D^{j_1}_{m' m}(\phi,\theta,0) D^{j_2}_{m,0}(\phi^*,\theta^*,0) \tag{8.1}$$

where $D^{j_1}_{m' m}$ and $D^{j_2}_{m,0}$ are the Wigner D-functions [115].

$$D^{j}_{m' m}(\alpha,\beta,\gamma) \equiv \langle jm' | e^{-i\alpha J_z} e^{-i\beta J_y} e^{-i\gamma J_z} | jm \rangle \,.$$

The M-function obeys the orthonormality condition

$$\iint M^{j_1 j_2}_{m_1 m_2}(\phi,\theta,\phi^*,\theta^*)^* M^{j'_1 j'_2}_{m'_1 m'_2}(\phi,\theta,\phi^*,\theta^*) d\Omega d\Omega^* = \delta_{j_1,j'_1}\delta_{j_2,j'_2}\delta_{m_1,m'_1}\delta_{m_2,m'_2} \,.$$

This choice of basis functions is motivated by the form of the quadruple-differential top-quark decay distribution [116]. Using the helicity formalism of ref. [117], the amplitude for the top-quark decay $t \to Wb \to \ell\nu b$ can be written, in the narrow-width approximation, as

$$A_{\mu\lambda_2\lambda_3\lambda_4} = \sum_{\lambda_1} a_{\lambda_1\lambda_2} b_{\lambda_3\lambda_4} D^{1/2\,*}_{\mu\nu}(\phi,\theta,0)\, D^{1\,*}_{\lambda_1\lambda}(\phi^*,\theta^*,0)\,, \tag{8.2}$$

where λ_1, λ_2, λ_3 and λ_4 are defined to be the helicities of the W boson, b-quark, charged lepton and neutrino, respectively, μ is the third spin component of the top quark, $\nu = \lambda_1 - \lambda_2$, $\lambda = \lambda_3 - \lambda_4$, and $a_{\lambda_1\lambda_2}$ and $b_{\lambda_3\lambda_4}$ are constants. For the top-quark decay, angular momentum conservation implies that there are only four non-zero reduced amplitudes (or just "amplitudes" for short): $a_{1,\frac{1}{2}}$, $a_{0,\frac{1}{2}}$, $a_{0,-\frac{1}{2}}$ and $a_{-1,-\frac{1}{2}}$. The reduced amplitudes are simply complex constants unlike the $A_{\mu\lambda_2\lambda_3\lambda_4}$ of eq. (8.2), which carry the angular dependence. The SM interaction of the W boson with charged leptons implies $\lambda_3 = \pm 1/2$ and $\lambda_4 = \mp 1/2$ for $W^\pm$ decays, assuming massless charged leptons. Therefore, $\lambda = 1$ for top quarks, $\lambda = -1$ for top anti-quarks, and in each case there is only one non-zero b constant, which can be factored out and plays no further role in the distributions. With this choice of basis functions, only 23 coefficients fully describe the top-quark decay.

Thus, the differential cross-section at parton level can be fully determined by 23 coefficients $c^{j_1 j_2}_{m' m}$ defined in eq. (8.3), having $j_1 \leq 1$ and $j_2 \leq 2$ [116]:

$$\frac{1}{\Gamma}\frac{d\Gamma}{d\Omega d\Omega^*} = \sum_{j_1 j_2 m' m} c^{j_1 j_2}_{m' m} M^{j_1 j_2}_{m' m}(\phi,\theta,\phi^*,\theta^*)\,, \tag{8.3}$$

where Γ is the decay rate.

Through a Fourier transform, the M-function coefficients can be determined by projecting the differential distribution $\rho(\phi,\theta,\phi^*,\theta^*) \equiv (1/\Gamma) d\Gamma/d\Omega d\Omega^*$ onto the M-function basis:

$$c^{j_1 j_2}_{m' m} = \int d\Omega d\Omega^* \rho(\phi,\theta,\phi^*,\theta^*) M^{j_1 j_2}_{m' m}(\phi,\theta,\phi^*,\theta^*)^* \,.$$

The right-hand side of this equation is not only interpreted as a coefficient, but also represents the average of the quantity $M^{j_1 j_2}_{m' m}(\phi,\theta,\phi^*,\theta^*)^*$ over a dataset distributed according to $\rho(\phi,\theta,\phi^*,\theta^*)$. Therefore, the practical approach to determining $c^{j_1 j_2}_{m' m}$ for any given dataset is to first substitute $(\phi_i, \theta_i, \phi_i^*, \theta_i^*)$ into eq. (8.1) for each individual event i, and then take the average over the entire dataset. This averaging procedure serves as the foundation of this analysis. Hence, the procedure used to obtain these coefficients for both data and MC simulation is to calculate

$$c^{j_1 j_2}_{m' m} = \frac{\sum_{i=1}^{N} w_i M^{j_1 j_2}_{m' m} (\phi_i, \theta_i, \phi_i^*, \theta_i^*)}{\sum_{i=1}^{N} w_i}, \tag{8.4}$$

where the sum is over the event sample, and w_i is the MC weight of the i^{th} event, and for data events $w_i = 1$. The weighted averages yield 23 mean values designated as $\vec{c}^{(s)}$ of channel (s) for real and, when relevant, imaginary parts of M-function values over the dataset.

The averaging procedure used in eq. (8.4) is also applied to products of real and imaginary parts of M-functions to obtain the average of their products over the dataset. Subtracting the product of the averages from the average of the products yeilds the sample covariance, then dividing by the sum of weights (or number of events, in data), gives the covariance of the two observables, or the variance if the two observables are identical. These are elements of the statistical covariance matrix $\mathbb{C}^{(s)}$ which is used below in the construction of the likelihood function.

Detector effects, including resolution, acceptance, and efficiency, strongly affect the angular distributions and hence the M-function coefficients. As well as modifying the 23 M-function coefficients, these effects introduce coefficients with $j_1 > 1$ and/or $j_2 > 2$.[8] This analysis is restricted to considering angular components with $j_1 \leq 1$ and $j_2 \leq 2$, at reconstruction level, since the coefficients with $j_1 > 1$ and/or $j_2 > 2$ are mainly shaped by the detector effects, whereas the chosen M-function coefficients are mainly shaped by the EFT operators. The dependence of these M-function coefficients on the WCs is computed at reconstruction level using MadGraph+Pythia MC events as described in section 4.

Both the signal and the $t\bar{t}$ background are modelled using MC simulation, and the corresponding M-function coefficients are obtained after the background is suppressed by the event selection defined in section 6. The background coefficients are then added linearly to the signal M-function coefficients, since Fourier analysis is a linear operation, to construct a model for the data. The signal component of the model, as well as the $t\bar{t}$ background component, are allowed to vary with the WCs, as described in section 8.2.

8.2 Morphing

To model the response of the M-function coefficients to variations of the WCs, a morphing technique is used. The numerator of the right-hand expression in eq. (8.4) is taken to give the unnormalised M-function coefficients. They are proportional to the cross-section of the process, and are each a polynomial function of the WCs. This parameterisation is mathematically equivalent to the explicit morphing functions used in previous measurements with a smaller number of operators (e.g. ref. [16]), but is generalised here to simultaneously accommodate the larger set of WCs considered. For the WCs C_{tW}, C^I_{tW}, C_{bW}, C^I_{bW} and $C_{\varphi tb}$, the corresponding operators contribute to both the t-channel production of a single top

[8] Angular momentum conservation ensures that, at the generator level, the M-function coefficients vanish whenever $j_1 > 1$ and $j_2 > 2$.

quark and its decay. Therefore, the observables that are proportional to the cross-section depend on these WCs to at most fourth-order, as the amplitude is at most quadratic in the WCs and the cross-section is obtained from its square.

On the other hand, their dependence on C_{Qq}, which only affects the production of single-top-quark events, will be at most second-order.

The unnormalised M-function coefficients, for different EFT assumptions, are computed from reconstructed LO MadGraph+Pythia events. For C_{Qq}, a three-point Lagrange interpolation is used to parameterise the M-function; for the other WCs, a five-point Lagrange interpolation is employed. The correlations among all the WCs are incorporated in the results via the interference terms when using this procedure. Consequently, the final morphing function for each M-function coefficient is expressed as a 203-term polynomial in C_{tW}, C^I_{tW}, C_{bW}, C^I_{bW}, $C_{\varphi tb}$, and C_{Qq}. This is of the same form as the simpler 15-term polynomial used in ref. [16].

An overall LO-to-NLO correction term for the M-function coefficients is calculated by determining the difference between the LO MadGraph+Pythia SM event sample and the NLO Powheg Box+Pythia SM event sample:

$$\vec{c}_O^{\,\mathrm{NLO}}(\vec{C}) = \vec{c}_O^{\,\mathrm{LO}}(\vec{C}) + \left[\vec{c}_O^{\,\mathrm{NLO}}(\vec{C}_{\mathrm{SM}}) - \vec{c}_O^{\,\mathrm{LO}}(\vec{C}_{\mathrm{SM}})\right].$$

The LO-to-NLO event-count correction is obtained as a scale factor equal to the ratio of the two event counts.

Finally, $C_{\varphi Q}$ is not morphed; instead, the dependency of $C_{\varphi Q}$ could be obtained from the t-channel scale factor $S_{t\text{-channel}}$ as described in eq. (8.5):

$$S_{t\text{-channel}} = |V_{\mathrm{L}}|^2 = \left(1 + \frac{v^2}{\Lambda^2} C_{\varphi Q}\right)^2. \tag{8.5}$$

8.3 Fit strategy

Data used in the statistical analysis consist of 23 M-function coefficients $\vec{c}^{(s)}$ for each of the four channels $s = 1, \ldots, 4$, distinguished by top-quark p_{T} and lepton charge as defined in section 6, which results in a total of 92 coefficients. In addition, the event counts in each channel's SR, $W+$jets CR and $t\bar{t}$ CR are used, which gives 12 additional inputs. A statistical covariance matrix in the coefficients is determined by the M-function analysis along with their values as described in section 8.1. Because of the manner in which the M-functions are obtained, i.e. eq. (8.1), the central limit theorem guarantees Gaussian uncertainties, and a simple χ^2 fit is used. Parameters of the fit include the WCs C_{tW}, C^I_{tW}, $C_{\varphi tb}$, C_{bW}, C^I_{bW}, and C_{Qq}, collectively referred to as the parameter of interest (POI) vector $\vec{C}$, as well as normalisation factors for the t-channel single-top-quark process (namely $C_{\varphi Q}$ as defined in eq. (8.5)) and the $W+$jets and $t\bar{t}$ processes, collectively denoted by the vector $\vec{S}$.

The systematic uncertainty is taken into account by computing a covariance matrix for the systematic uncertainty sources:

$$\mathbb{C}^{\mathrm{syst.}} = \sum_{\mathrm{syst.\ sources}} \Delta\vec{v} \otimes \Delta\vec{v}^{T}, \tag{8.6}$$

Source of uncertainty	C_{tW}	C_{tW}^{I}	$C_{\varphi tb}$	C_{bW}	C_{bW}^{I}	C_{Qq}	$C_{\varphi Q}$
Jet energy scale	$-0.03, +0.03$	$-0.01, +0.01$	$-0.6, +0.4$	$-0.3, +0.3$	$-0.3, +0.3$	$-0.02, +0.05$	$-0.10, +0.09$
Pile-up	$-0.01, -$	$-$	$-0.1, +0.2$	$-, +0.1$	$-0.1, -$	$-, +0.01$	$-0.08, +0.06$
b-tagging	$-0.02, +0.03$	$-0.01, +0.01$	$-0.6, +0.6$	$-0.1, +0.2$	$-0.1, +0.1$	$-0.02, +0.02$	$-0.13, +0.13$
Jet energy resolution	$-0.02, +0.02$	$-0.01, +0.01$	$-0.8, +0.7$	$-0.1, +0.1$	$-0.1, +0.1$	$-0.02, +0.03$	$-0.08, +0.09$
PDF	$-0.02, +0.02$	$-0.01, +0.01$	$-0.7, +0.6$	$-0.1, +0.1$	$-0.1, +0.1$	$-0.03, +0.04$	$-0.08, +0.09$
Muon	$-0.03, +0.02$	$-$	$-0.4, +0.3$	$-0.1, +0.1$	$-0.1, +0.1$	$-0.01, +0.03$	$-0.07, +0.06$
$E_{\mathrm{T}}^{\mathrm{miss}}$	$-0.02, +0.02$	$-$	$-0.5, +0.4$	$-0.1, +0.1$	$-0.2, +0.2$	$-0.01, +0.02$	$-0.06, +0.05$
e/γ	$-0.01, +0.01$	$-$	$-0.2, +0.1$	$-0.1, +0.1$	$-0.1, +0.1$	$-, +0.01$	$-0.06, +0.07$
Jet vertex tagging	$-0.01, +0.01$	$-$	$-0.1, +0.2$	$-, +0.1$	$-$	$-0.02, +0.03$	$-0.17, +0.18$
Lumi. & cross-section	$-0.01, -$	$-$	$-0.1, +0.1$	$-0.1, +0.1$	$-0.1, +0.1$	$-0.01, -$	$-0.07, +0.07$
τ_{had} energy scale	$-$	$-$	$-$	$-$	$-$	$-$	$-$
Non-prompt leptons	$-0.01, -$	$-$	$-, +0.2$	$-, +0.1$	$-0.1, +0.1$	$-0.01, -$	$-0.01, +0.01$
t-channel modelling	$-0.01, +0.01$	$-$	$-0.3, +0.1$	$-$	$-$	$-0.04, +0.04$	$-0.15, +0.15$
$t\bar{t}$ modelling	$-0.03, +0.02$	$-0.01, -$	$-0.5, +0.4$	$-0.1, +0.1$	$-0.1, +0.1$	$-0.01, +0.03$	$-0.04, +0.08$
W+jets modelling	$-0.01, +0.02$	$-0.01, +0.01$	$-0.8, +0.6$	$-0.1, +0.1$	$-, +0.1$	$-0.01, +0.02$	$-0.06, +0.08$
MC sample sizes	$-0.03, +0.03$	$-0.03, +0.03$	$-0.9, +0.8$	$-0.2, +0.2$	$-0.2, +0.2$	$-0.03, +0.05$	$-0.14, +0.14$
Data sample size	$-0.06, +0.05$	$-0.04, +0.04$	$-3.1, +1.7$	$-0.5, +0.7$	$-0.5, +0.5$	$-0.05, +0.08$	$-0.13, +0.15$
Total systematic	$-0.07, +0.07$	$-0.02, +0.02$	$-1.8, +1.5$	$-0.4, +0.5$	$-0.5, +0.5$	$-0.07, +0.10$	$-0.35, +0.36$
Total	$-0.10, +0.09$	$-0.06, +0.06$	$-3.9, +2.6$	$-0.8, +0.9$	$-0.7, +0.7$	$-0.09, +0.14$	$-0.41, +0.43$

Table 4. Summary of the expected systematic and statistical uncertainty breakdown for the 1σ confidence interval of each WC from the one-dimensional likelihood scans. The limited data and MC simulation sample sizes are sources of statistical uncertainty. The symbol '$-$' indicates that the uncertainty is negligible.

where $\Delta\vec{v}$ is the vector of the expected 1σ uncertainties from the sources of systematic uncertainty described in section 7. Due to the central limit theorem, the likelihood function combining the M-function coefficients and the event counts is a multivariable Gaussian function. The $\chi^2 = -2\ln\mathcal{L}$ is given by

$$\chi^2(\vec{C},\vec{S}) = \sum_{(s)}\Bigg\{\left(\vec{c}^{(s)} - \vec{c}^{(s),\mathrm{model}}(\vec{C},\vec{S})\right)^T \left(\mathbb{C}^{(s)}\right)^{-1} \left(\vec{c}^{(s)} - \vec{c}^{(s),\mathrm{model}}(\vec{C},\vec{S})\right) \\ + \sum_{j\in\{\mathrm{SR,\,CR\text{-}W,\,CR\text{-}t\bar{t}}\}} \frac{\left(N^{(s,j),\mathrm{model}}(\vec{C},\vec{S}) - N^{(s,j)}\right)^2}{N^{(s,j)}}\Bigg\}, \tag{8.7}$$

where $\vec{c}^{(s)}$ is the vector of 23 M-function coefficients in channel s, $N^{(s,j)}$ is the event count in channel s and SR or CR j, and the covariance matrix $\mathbb{C}^{(s)}$ is a linear sum of statistical covariance $\mathbb{C}^{\mathrm{stat.}}_{\mathrm{data}}$ from the data, statistical covariance $\mathbb{C}^{\mathrm{stat.}}_{\mathrm{MC}}$ from the MC events, and systematic covariance $\mathbb{C}^{\mathrm{syst.}}$ as defined in eq. (8.6). The superscript "model" indicates values predicted from the fitting model. The fit has $92 + 12$ inputs $- 9$ parameters $= 95$ degrees of freedom. Systematic uncertainties can be treated either individually or collectively by computing the systematic covariance matrix of eq. (8.6) from a restricted set of sources of uncertainty, and introducing the resulting matrix into the χ^2 of eq. (8.7). The fit is tested with pseudoexperiments over a wide range of input physics and nuisance parameters consistent with the expected precision of the measurement.

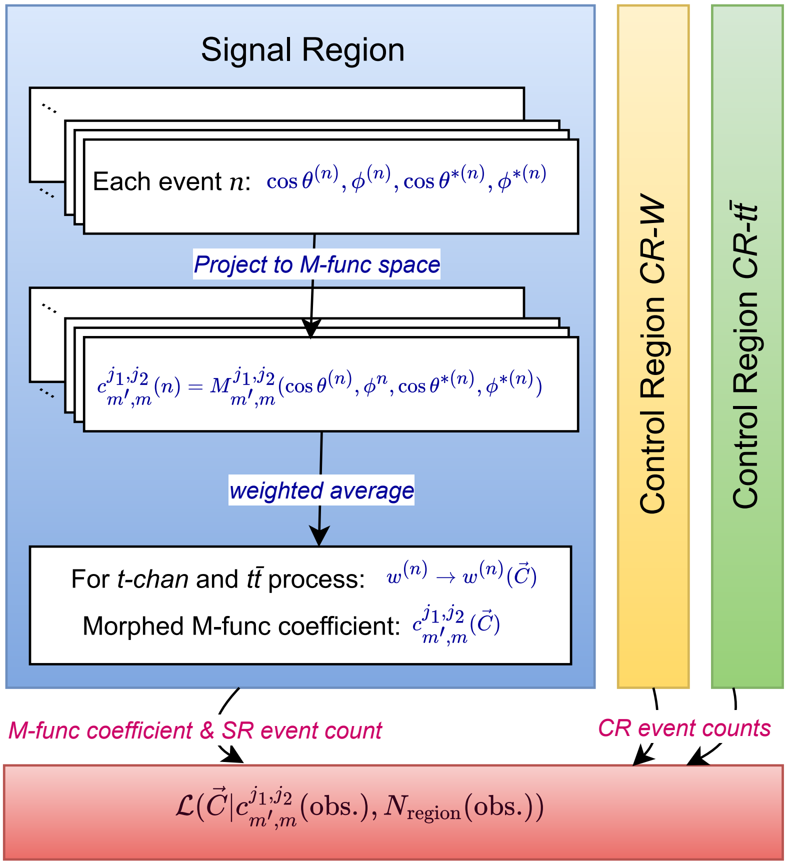

Figure 3. Schematic overview of the analysis workflow, from individual events selected in SR and CRs to the final likelihood function used for limit settings.

The effect of each systematic uncertainty on the WCs is evaluated by removing that systematic uncertainty from eq. (8.6) and comparing the $-\ln\mathcal{L}$ scan with that for the nominal fit. Similarly, the impact of the MC statistical uncertainty is obtained by comparing the $-\ln\mathcal{L}$ scans with and without inclusion of $\mathbb{C}^{\text{stat.}}_{\text{MC}}$. Table 4 summarises the sources of both the systematic and statistical uncertainties for the 1σ confidence interval for each of the POIs. Although the total systematic uncertainty is comparable to the statistical uncertainty of the data except for $C_{\varphi Q}$, no single source of systematic uncertainty significantly outweighs the overall MC statistical uncertainty, which is distributed among the dominant simulated processes, with the t-channel contribution slightly larger than those from the $\mathrm{t\bar{t}}$ and W+jets samples, which are of comparable size.

Finally, the overall analysis workflow is illustrated in figure 3. For the SR, the four decay angles are reconstructed event by event and inserted into eq. (8.1) to compute the coefficients of the orthonormal M-function basis. These per-event coefficients are then combined via a (weighted) average over all SR events (as defined in eq. (8.1)) to form the final M-function observables. The dependence of the (averaged) coefficients on the WC vector, $\vec{C}$, in both the t-channel single-top-quark and $t\bar{t}$ processes is obtained from MC simulation and modelled using the morphing technique described in section 8.2. This approach fully captures the

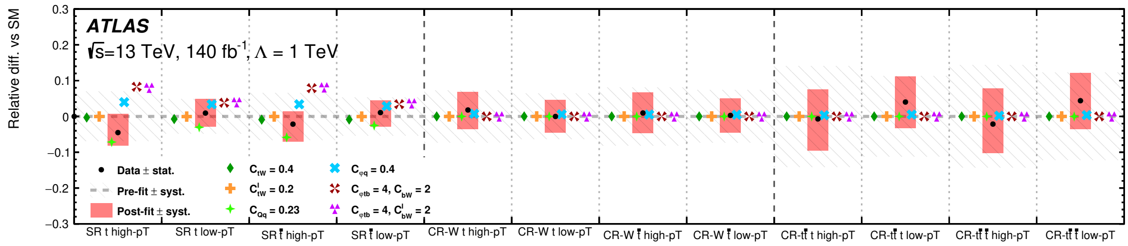

Figure 4. The relative differences between the observed and SM predicted event counts in the SRs and CRs, for both the observed data and the fitted EFT model. The black points represent observed data, with the data statistical uncertainties as uncertainty bars. The grey dashed area indicates the total systematic uncertainties, while the red boxes are centred at positions determined by the best-fit values of the WCs, with heights determined by systematic uncertainties constrained by the fit. The coloured scattered markers correspond to expected values when making various WC assumptions.

impact of the WCs on the quadruple-differential phase space without the need to bin a four-dimensional distribution. A Gaussian likelihood $\mathcal{L}$, built from the averaged M-function coefficients and the event counts in the SR and CRs, is then maximised to extract the best-fit WC values.

9 Results

Summing over the four channels, the final observables are the 3×4 event counts in the SR and two CRs, along with the 23×4 M-function coefficients in the SR. Figure 4 shows the relative differences between the observed event counts and the SM predictions. Figure 5 shows the absolute deviations of the M-function coefficients from the SM prediction, for both the observed data and the fitted EFT model in each channel's SR. The black points represent the data, while the scattered markers correspond to the expected values when making various WC assumptions. The grey band, centred at zero, represents the SM expectation; its width indicates the pre-fit systematic uncertainties. The centre of each red box is determined by the best-fit value from the EFT fit; its height is set by the post-fit uncertainties, which include the effect of correlations. The plots demonstrate the effect of the data upon the fitted model.

As expected, due to the large number of observables compared to the number of unconstrained parameters, the uncertainties of the observables are reduced by the fit.

The SM prediction is in reasonable overall agreement with the 104 observables, with a $\chi^2 = -2 \ln \mathcal{L} = 105.2$, indicating a p-value at 44.9%, although agreement is poorer for some high-p_{T} SR observables. At the best-fit point of the EFT fit with nine parameters, the likelihood has a $\chi^2 = 87.4$ for 95 degrees of freedom (p-value of 70.0%). Both hypotheses are consistent with the data.

The best-fit values of the WCs are substituted into the morphing functions of the t-channel and $t\bar{t}$ cross-sections to obtain the post-fit angular distributions, in order to demonstrate that the overall agreement between data and MC is preserved after the fit. The post-fit SR distributions of the four angles $\cos\theta$, $\cos\theta^*$, ϕ, and ϕ^* are shown in figure 6. They are all in good agreement with the data, with χ^2 values ranging from 5 to 18 for 20 bins.

JHEP07(2026)107

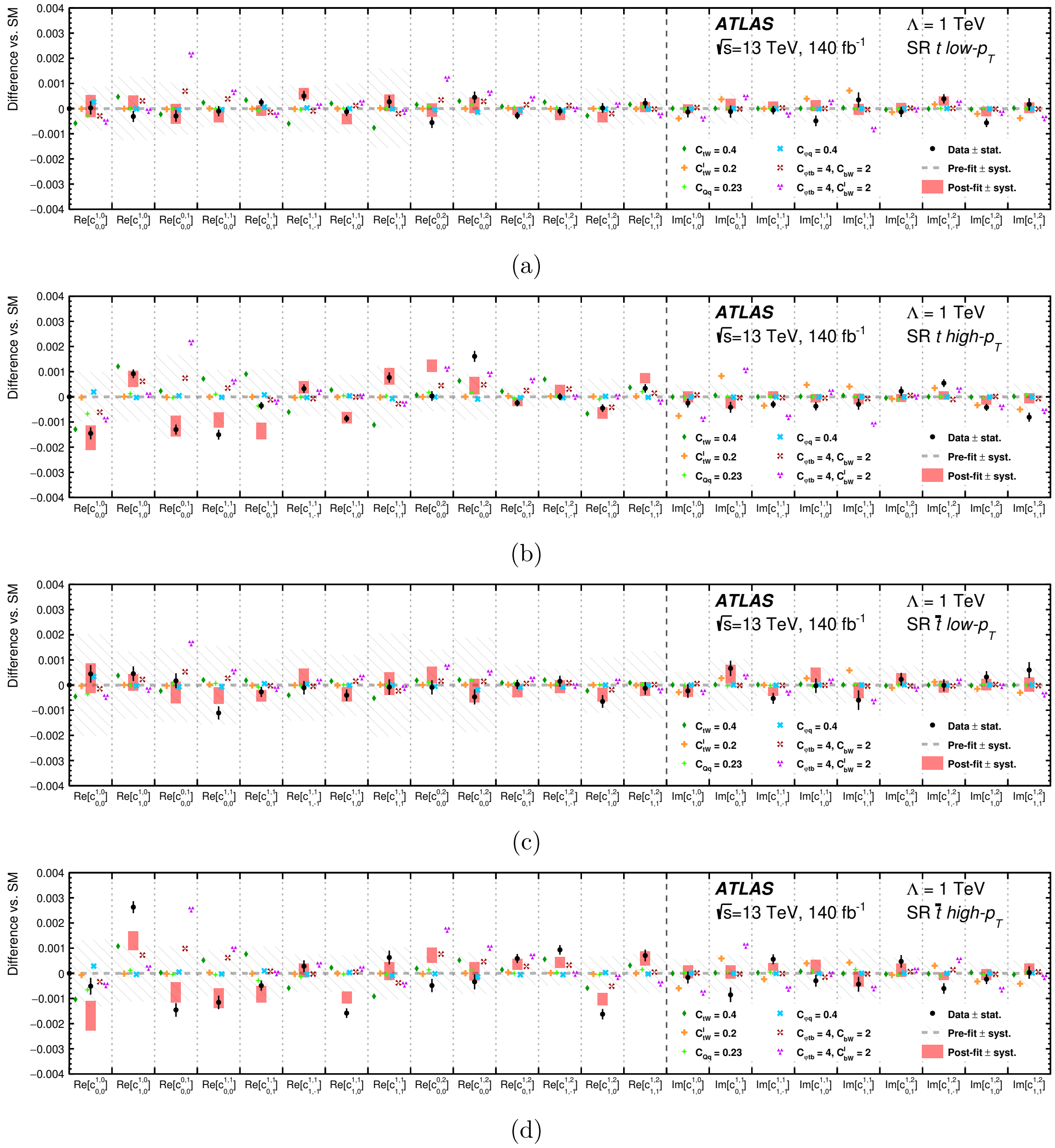

Figure 5. The absolute deviations of the M-function coefficients, as defined in eq. (8.4), from the SM prediction, for both the observed data and the fitted EFT model, in the SR of the (a) low-p_{T} ($< 80\,\mathrm{GeV}$) top-quark channel, (b) high-p_{T} ($\geq 80\,\mathrm{GeV}$) top-quark channel, (c) low-p_{T} top-antiquark channel, and (d) high-p_{T} top-antiquark channel, respectively. The black points represent observed data, with the data statistical uncertainties as uncertainty bars. The grey dashed area indicates the total systematic uncertainties, while the red boxes are centred at positions determined by the best-fit values of the WCs, with heights determined by systematic uncertainties constrained by the fit. The coloured scattered markers correspond to expected values when making various WC assumptions.

JHEP07(2026)107

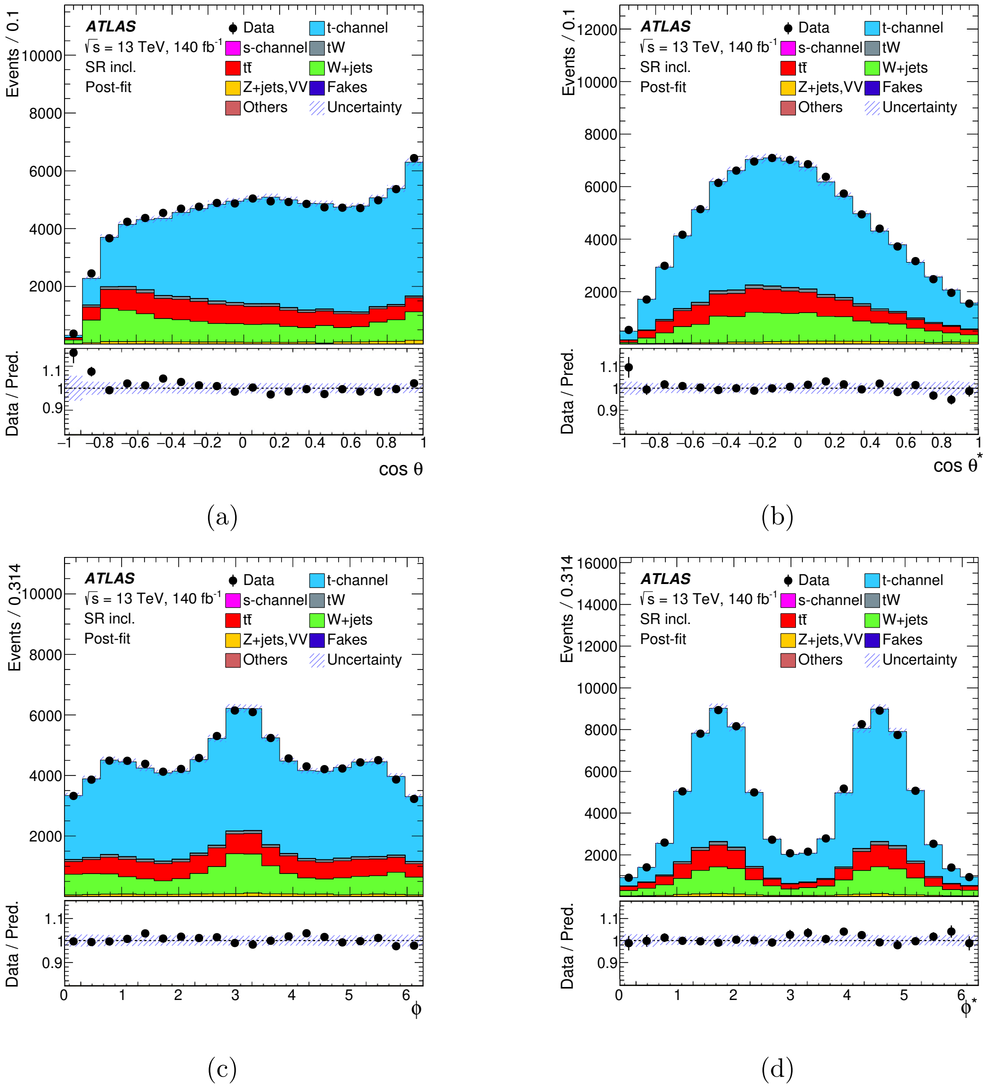

Figure 6. Post-fit distributions of the four angles, namely (a) $\cos\theta$, (b) $\cos\theta^*$, (c) ϕ, and (d) ϕ^* in the inclusive SR. The fitted predicted distributions are compared with the observed data, depicted as black points with statistical uncertainties. The uncertainty bands reflect the statistical and systematic uncertainties, taking into account the post-fit constraints from the profile likelihood fit. Correlations among all parameters obtained from the fit are accounted for in the calculation of the uncertainty bands. The lower plot for each angular distribution shows the ratio of the observed data to the fitted prediction in each bin, offering a quantitative measure of how well the two agree.

Scale factor	Fully profiled fit		Reduced fit	
	Best-fit value	**68% CL interval**	**Best-fit value**	**68% CL interval**
$S^{W+\text{jets}}$	0.92	±0.07	0.91	±0.06
$S^{t\bar{t}}$	1.09	±0.08	1.10	±0.08

Table 5. The best-fit results for the scale-factor vector $\vec{S}$ with the corresponding 68% CL intervals.

JHEP07(2026)107

Wilson coefficient [TeV^{-2}]	Reduced fit Central value	68% CL interval	95% CL interval
C_{tW}/Λ^2	0.12	$[+0.04, +0.20]$	$[-0.03, +0.28]$
C^I_{tW}/Λ^2	0.02	$[-0.03, +0.06]$	$[-0.08, +0.11]$
C_{Qq}/Λ^2	0.21	$[+0.13, +0.27]$	$[+0.05, +0.32]$
$C_{\varphi Q}/\Lambda^2$	0.54	$[+0.19, +0.88]$	$[-0.16, +1.21]$

Table 6. The best-fit values obtained by the reduced fit scheme, and the 68% and 95% CL intervals. In this fitting scheme, only the WCs C_{tW}, C^I_{tW}, C_{Qq} and $C_{\varphi Q}$ that have a linear effect on the M-function coefficients are free floating.

Three different fitting schemes are considered for a one-dimensional likelihood scan:

- **Fully profiled fit**: each POI is scanned while profiling the other six POIs.
- **Reduced fit**: WCs that are dominated by quadratic dependencies ($C_{\varphi tb}$, C_{bW}, C^I_{bW}) are fixed at SM values in this scheme. This fit allows one to obtain well-defined point estimates and a covariance matrix for the remaining parameters.
- **Individual fit**: all other POIs fixed at the SM values when scanning a POI.

The fitted scale factors of the two major background processes $t\bar{t}$ and $W+$jets are summarised in table 5.

One-dimensional likelihood scans for these fitting schemes are shown in figure 7 for the EFT coefficients that have a linear effect on the M-function coefficients, and in figure 8 for those that have a quadratic effect. The non-zero value of the b-quark mass used in the generation of the EFT grid points used for the morphing leads to a slight linear dependence, so the resulting likelihood scans are not expected to be completely symmetric about the SM point.

The limits on each WC for each fitting scheme introduced above are summarised in table 6 and table 7. For the reduced fit, the covariance matrix of the four WCs C_{tW}, C^I_{tW}, C_{Qq} and $C_{\varphi Q}$ is given in figure 9.

Two-dimensional likelihood scans for the fully profiled fitting scheme are shown in figure 10 and figure 11. The 68% and 95% CL regions are obtained by using the conventional $-2\Delta\ln\mathcal{L}$ thresholds for two degrees of freedom [2]. It is known that one can construct a linear combination of $\mathcal{O}_{\varphi tb}$ and $\mathcal{O}_{bW}$ that has no sensitivity to the fraction of top quarks that decay to right-handed W bosons [14]. Additional observables in this analysis somewhat break that degeneracy, but a strong correlation still remains. Negligible correlation between C_{tW} and C^I_{tW} is observed. There is, however, some correlation between the fitted results for C_{Qq} and $C_{\varphi Q}$ or C_{tW}.

The constraints on all seven WCs are summarised in figure 12. Competitive constraints are placed on all of these parameters, the most restrictive being those on the real and imaginary parts of c_{tW}. The sensitivity to the various WCs arises from different aspects of the data:

- The imaginary components of c_{tW} and the product of $c_{\varphi tb}$ and c_{bW} are constrained by the imaginary parts of the M-function coefficients, while the constraints on the real parts of c_{tW}, c_{bW}, and $c_{\varphi tb}$ are determined by the real parts of the M-function coefficients.

JHEP07(2026)107

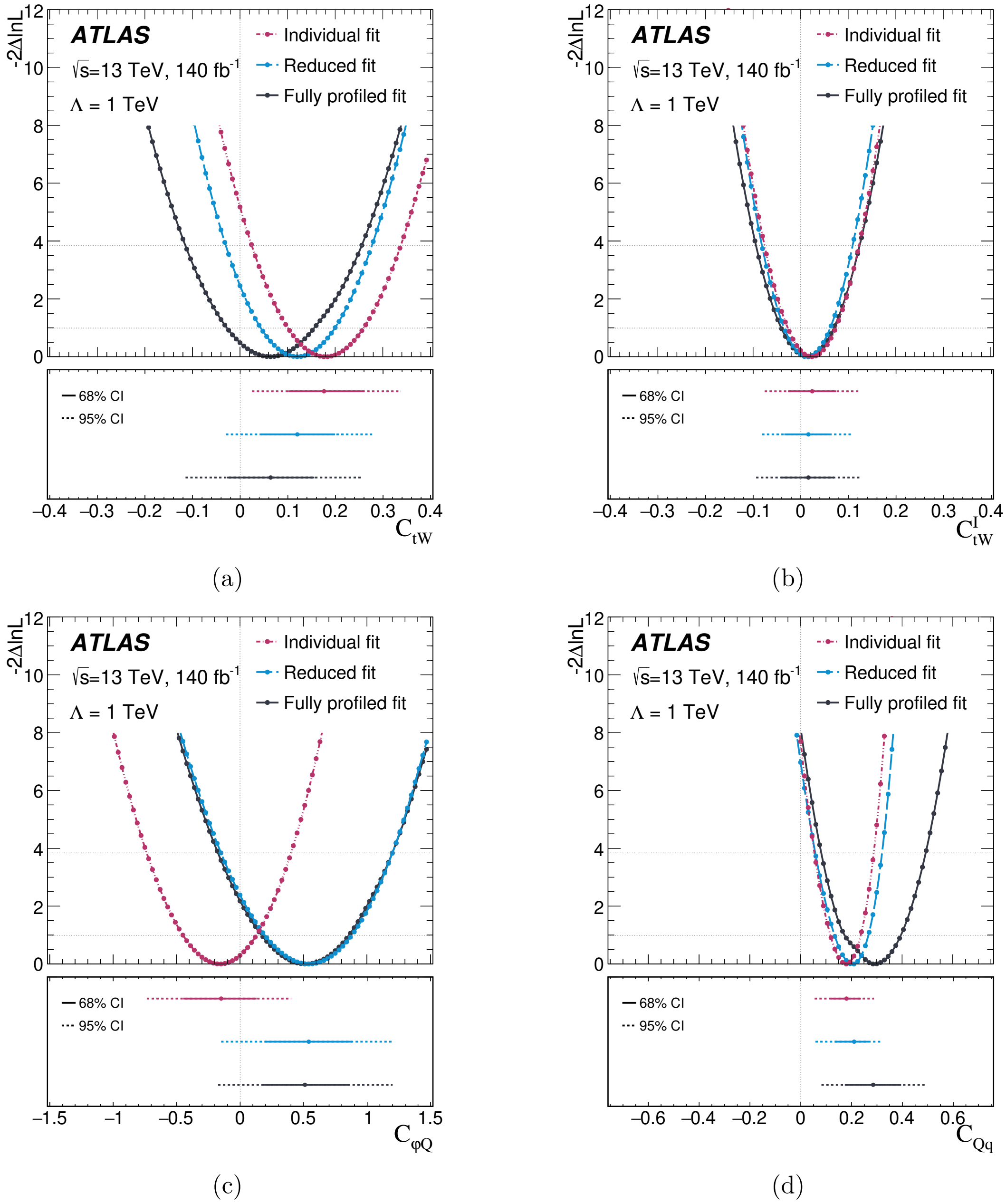

Figure 7. The likelihood scans for the parameters (a) C_{tW}, (b) C^{I}_{tW}, (c) $C_{\varphi Q}$, and (d) C_{Qq}, comparing the fully profiled fit scheme (black curve), the reduced fit scheme (dashed blue curve) and the individual fit scheme (dash-dotted red curve). The 68% and 95% CL intervals (CI) for each parameter in each scheme are shown in the bottom plots.

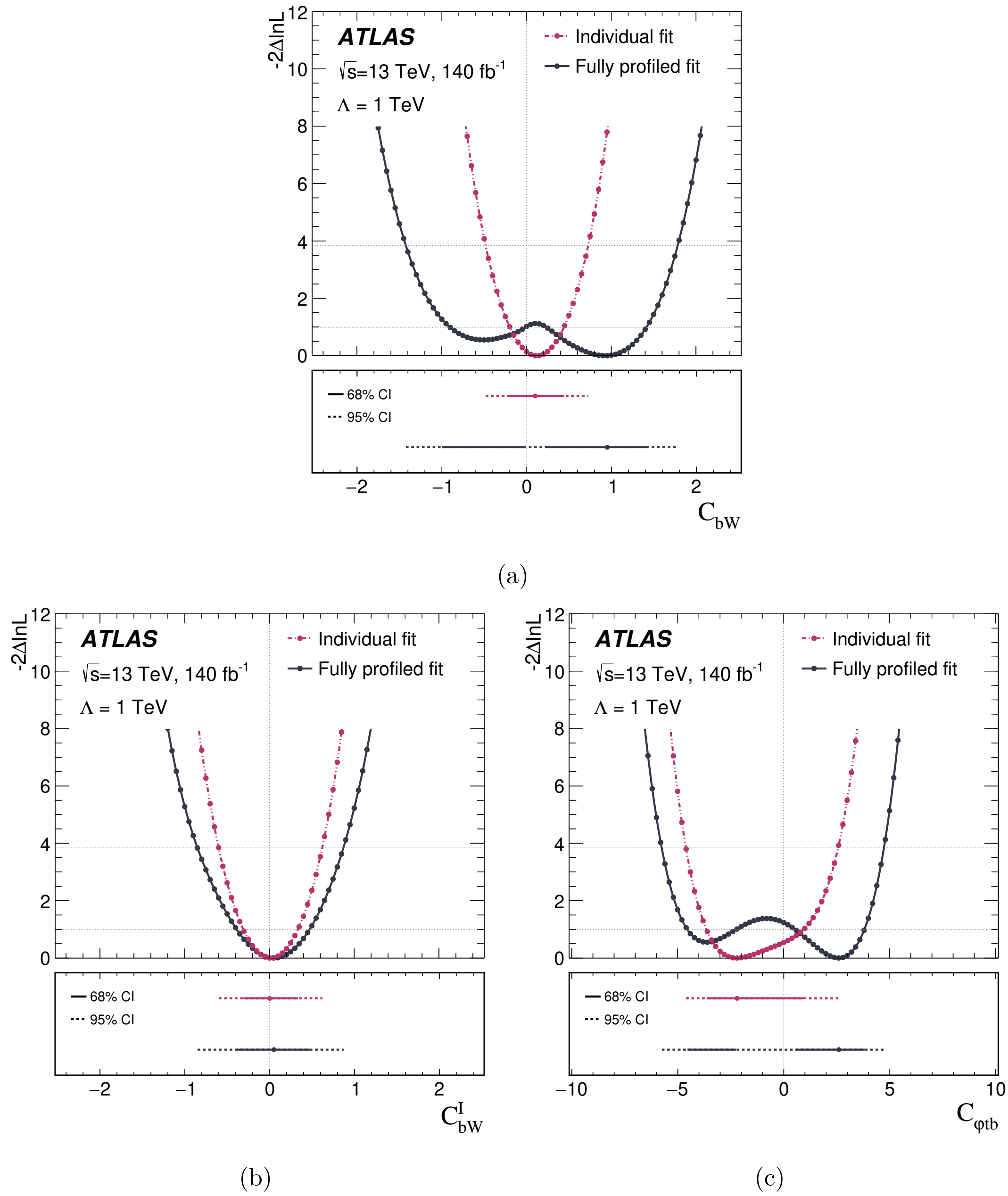

Figure 8. The likelihood scans for the parameters (a) C_{bW}, (b) C_{bW}^{I} and (c) $C_{\varphi tb}$, comparing the fully profiled fit scheme (black curve) with the individual fit scheme (dash-dotted red curve). The 68% and 95% CL intervals (CI) for each parameter in each scheme are shown in the bottom plots.

JHEP07(2026)107

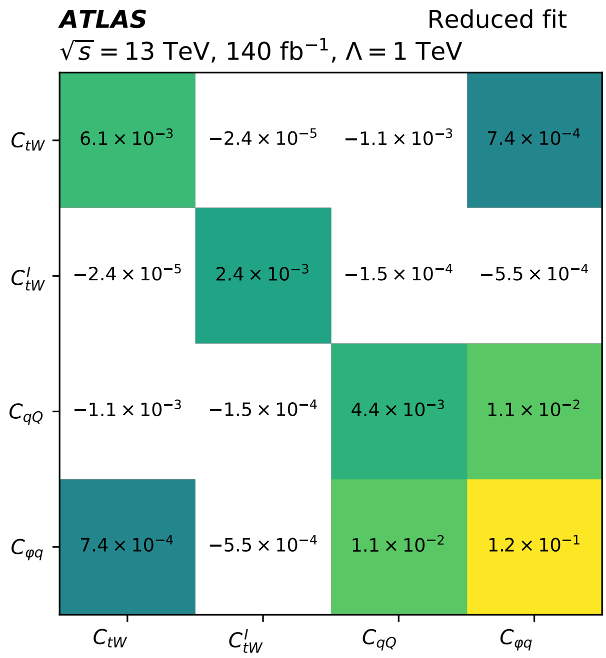

Figure 9. Covariance matrix for the reduced fit, assuming $\Lambda = 1$ TeV.

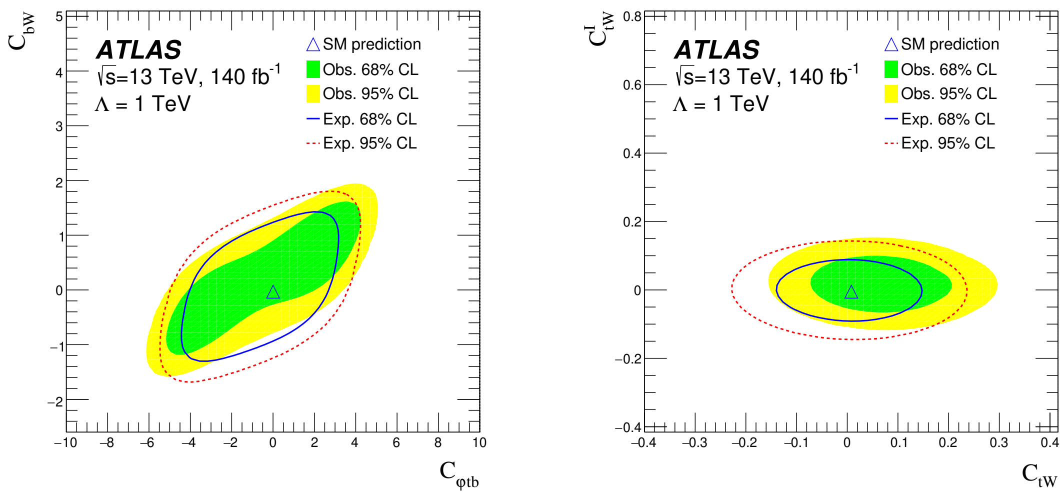

(a) (b)

Figure 10. Likelihood scan of (a) $C_{\varphi tb}$ and C_{bW}, and (b) C_{tW} and C^{I}_{tW}, with all other parameters profiled. The expected SM point is marked with a blue triangle. The observed (expected) 68% and 95% CL regions are shown as inner green (blue) and outer yellow (red) regions (lines), respectively.

JHEP07(2026)107

Wilson coefficient [TeV^{-2}]	Fully profiled fit 68% CL interval	Fully profiled fit 95% CL interval	Individual fit 68% CL interval	Individual fit 95% CL interval
C_{tW}/Λ^2	$[-0.03, +0.17]$	$[-0.12, +0.26]$	$[+0.10, +0.26]$	$[+0.02, +0.34]$
C^I_{tW}/Λ^2	$[-0.04, +0.07]$	$[-0.10, +0.13]$	$[-0.03, +0.07]$	$[-0.08, +0.12]$
$C_{\varphi tb}/\Lambda^2$	$[-4.6, -2.3] \cup [+0.5, +3.8]$	$[-5.8, +4.8]$	$[-3.6, +1.0]$	$[-4.6, +2.6]$
C_{bW}/Λ^2	$[-1.0, 0.0] \cup [+0.2, +1.4]$	$[-1.4, +1.8]$	$[-0.2, +0.4]$	$[-0.5, +0.7]$
C^I_{bW}/Λ^2	$[-0.4, +0.5]$	$[-0.9, +0.9]$	$[-0.3, +0.3]$	$[-0.6, +0.6]$
C_{Qq}/Λ^2	$[+0.17, +0.37]$	$[+0.08, +0.50]$	$[+0.12, +0.24]$	$[+0.05, +0.29]$
$C_{\varphi Q}/\Lambda^2$	$[+0.17, +0.86]$	$[-0.19, +1.2]$	$[-0.45, +0.13]$	$[-0.75, +0.41]$

Table 7. The WC intervals at 68% and 95% CL, obtained by a one-dimensional likelihood scan. The table compares two scenarios: a fully profiled fit in which all non-scanned WCs are profiled simultaneously, and an individual fit in which all other coefficients are kept fixed at their SM value (zero).

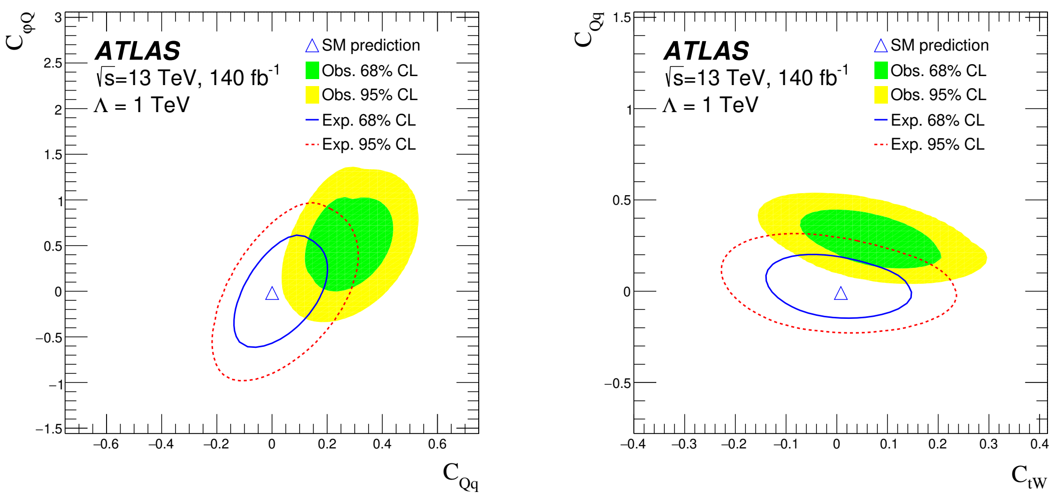

Figure 11. Likelihood scan of (a) C_{Qq} and $C_{\varphi Q}$, and (b) C_{tW} and C_{Qq}, with all other parameters profiled. The expected SM point is marked with a blue triangle. The observed (expected) 68% and 95% CL regions are as inner green (blue) and outer yellow (red) regions (lines), respectively.

Since $\mathcal{O}_{bW}$ and $\mathcal{O}_{\varphi tb}$ do not produce large interference with the SM amplitude, the corresponding WCs are less constrained.

- $C_{\varphi Q}$ and C_{Qq} are constrained by the event counts in the two p_{T} regions; $C_{\varphi Q}$ affects the overall rate, whereas C_{Qq} impacts the high-p_{T} region more than the low-p_{T} region. Having multiple p_{T} regions allows one to separate the effects of these two WCs. A non-zero C_{Qq} also predicts a slight reduction in the polarisation of the produced top quarks, with more of an effect in the high-p_{T} region [118]. The fitted result of C_{Qq}, which corresponds to a 2.8σ deviation from the SM, is attributed to the small difference

JHEP07(2026)107

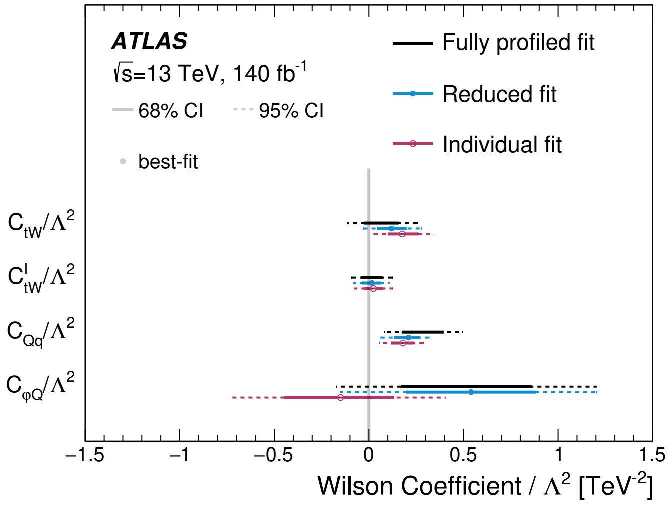

(a)

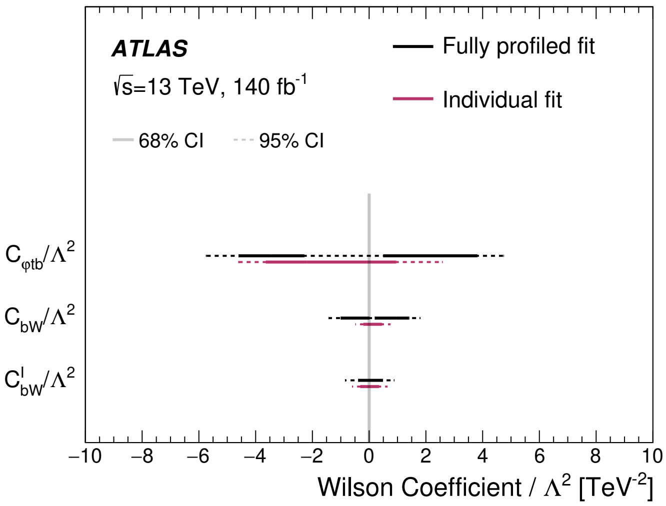

(b)

Figure 12. Summary of confidence intervals extracted from the likelihood fits described in section 9 for (a) C_{tW}, C^{I}_{tW}, C_{Qq}, $C_{\varphi Q}$ and (b) $C_{\varphi tb}$, C_{bW}, C^{I}_{bW}. The WC 68% CL (thick line) and 95% CL (dotted line) intervals are shown for each of the different fitting schemes.

between the number of events observed in the high-p_{T} signal region and the number predicted by the POWHEG BOX v2 simulation. More studies are needed to determine whether NNLO effects could provide better agreement with the data. Since both C_{Qq} and $C_{\varphi Q}$ affect the event counts, two bins in p_{T} are the minimum required to separate their effects. In the future, it would be beneficial to use more p_{T} bins to better determine C_{Qq}.

The best previously published constraint on C_{tW} comes from a measurement of the fraction of top-quark decays that produce each W-boson helicity state (F_0, F_{L}, F_{R}) in pp

JHEP07(2026)107

collisions at $\sqrt{s}$ =8 TeV, assuming that $C_{\varphi Q} = 0$ [28]. This analysis improves on that result by a factor of two, while removing the assumption that the other WCs are zero. The two-dimensional limit contours for $C_{\varphi tb}$ and C_{bW} improve on the results from the measurement of F_{R} in ref. [28] by providing constraints along the direction to which F_{R} is blind, while achieving comparable precision along the direction to which F_{R} is sensitive. This result also improves on the limits on C^{I}_{tW} from measurements of top-quark polarisation [16] by a factor of three. More recent measurements from CMS [22] also yield constraints on the WCs investigated here. The precision of those constraints is a factor of two better in $C_{\varphi tb}$ and C_{bW}, and complementary to those presented here; however, they do not provide any information on the imaginary components of these WCs. Reference [22] also provides tighter constraints on C_{Qq} by a factor of three and shows no significant tension with the SM. The constraints on C_{Qq} presented here are found to be compatible, within uncertainties, with ref. [22]. After the submission of this manuscript, a related study was reported in ref. [119]. Although that analysis was not optimised for the extraction of EFT parameters, it indicates that the inclusion of NNLO effects improves the agreement between SM predictions and the data. The measurement of the total t-channel single-top-quark cross-section [10] provides slightly better constraints on $C_{\varphi Q}$, but only under the assumption that all other WCs are zero. This paper leads to an improvement in the constraints on $C_{\varphi Q}$ by a factor of two.

It should be pointed out that while NLO and EW corrections [120–122] have been calculated for the structure functions, defined in ref. [123], to the M-function coefficients used in this analysis, NNLO corrections are currently available only for those associated with W-boson helicity fractions [124]. With additional data from LHC Run 3, together with an improved understanding of systematic uncertainties, the overall uncertainty could be reduced to a level comparable to the expected size of these NNLO corrections.

10 Conclusion

In summary, constraints are placed on dimension-six WCs at the tWb vertex, and on the four-quark coefficient C_{Qq}, using the 140 fb^{-1} dataset collected from $\sqrt{s} = 13$ TeV pp collisions by the ATLAS detector during Run 2 of the LHC. The strategy used in this study offers an approach for probing EFT WCs with high precision through Fourier-based angular analysis. The quadruple-differential decay spectrum of t-channel single-top-quark events is projected onto an orthonormal M-function basis, and the 23 leading normalised M-function coefficients for each of four different channels are fitted simultaneously with the event yields using a maximum-likelihood method. Although the systematic uncertainty is the dominant source of uncertainty overall, no individual source of systematic uncertainty significantly outweighs the total statistical uncertainty, which is primarily driven by the size of the data sample. All best-fit points are consistent with the SM expectation.

Acknowledgments

We thank CERN for the very successful operation of the LHC and its injectors, as well as the support staff at CERN and at our institutions worldwide without whom ATLAS could not be operated efficiently.

The crucial computing support from all WLCG partners is acknowledged gratefully, in particular from CERN, the ATLAS Tier-1 facilities at TRIUMF/SFU (Canada), NDGF (Denmark, Norway, Sweden), CC-IN2P3 (France), KIT/GridKA (Germany), INFN-CNAF (Italy), NL-T1 (Netherlands), PIC (Spain), RAL (U.K.) and BNL (U.S.A.), the Tier-2 facilities worldwide and large non-WLCG resource providers. Major contributors of computing resources are listed in ref. [125].

We gratefully acknowledge the support of ANPCyT, Argentina; YerPhI, Armenia; ARC, Australia; BMWFW and FWF, Austria; ANAS, Azerbaijan; CNPq and FAPESP, Brazil; NSERC, NRC and CFI, Canada; CERN; ANID, Chile; CAS, MOST and NSFC, China; Minciencias, Colombia; MEYS CR, Czech Republic; DNRF and DNSRC, Denmark; IN2P3-CNRS and CEA-DRF/IRFU, France; SRNSFG, Georgia; BMFTR, HGF and MPG, Germany; GSRI, Greece; RGC and Hong Kong SAR, China; ICHEP and Academy of Sciences and Humanities, Israel; INFN, Italy; MEXT and JSPS, Japan; CNRST, Morocco; NWO, Netherlands; RCN, Norway; MNiSW, Poland; FCT, Portugal; MNE/IFA, Romania; MSTDI, Serbia; MSSR, Slovakia; ARIS and MVZI, Slovenia; DSI/NRF, South Africa; MICIU/AEI, Spain; SRC and Wallenberg Foundation, Sweden; SERI, SNSF and Cantons of Bern and Geneva, Switzerland; NSTC, Taipei; TENMAK, Türkiye; STFC/UKRI, United Kingdom; DOE and NSF, United States of America.

Individual groups and members have received support from BCKDF, CANARIE, CRC and DRAC, Canada; CERN-CZ, FORTE and PRIMUS, Czech Republic; COST, ERC, ERDF, Horizon 2020, ICSC-NextGenerationEU and Marie Skłodowska-Curie Actions, European Union; Investissements d'Avenir Labex, Investissements d'Avenir Idex and ANR, France; DFG and AvH Foundation, Germany; Herakleitos, Thales and Aristeia programmes co-financed by EU-ESF and the Greek NSRF, Greece; BSF-NSF and MINERVA, Israel; NCN and NAWA, Poland; La Caixa Banking Foundation, CERCA Programme Generalitat de Catalunya and PROMETEO and GenT Programmes Generalitat Valenciana, Spain; Göran Gustafssons Stiftelse, Sweden; The Royal Society and Leverhulme Trust, United Kingdom; United States of America.

In addition, individual members wish to acknowledge support from CERN: European Organization for Nuclear Research (CERN DOCT); Chile: Agencia Nacional de Investigación y Desarrollo (ANID FONDECYT reg. 1230987, FONDECYT 1230812, FONDECYT 1240864, Fondecyt 3240661, Fondecyt Regular 1240721); China: Chinese Ministry of Science and Technology (MOST-2023YFA1605700, MOST-2023YFA1609300), National Natural Science Foundation of China (NSFC – 12175119, NSFC 12275265); Czech Republic: Czech Science Foundation (GACR – 24-11373S), Ministry of Education Youth and Sports (ERC-CZ-LL2327, FORTE CZ.02.01.01/00/22_008/0004632), PRIMUS Research Programme (PRIMUS/21/SCI/017); EU: H2020 European Research Council (ERC – 101002463); European Union: European Research Council (BARD No. 101116429, ERC – 948254, ERC 101089007), European Regional Development Fund (HE COFUND GA No.101081355, ERDF), European Union, Future Artificial Intelligence Research (FAIR-NextGenerationEU PE00000013), Italian Center for High Performance Computing, Big Data and Quantum Computing (ICSC, NextGenerationEU), Marie Sklodowska-Curie Actions (GAP-101168829); France: Agence Nationale de la Recherche (ANR-21-CE31-0013, ANR-21-CE31-0022, ANR-

JHEP07(2026)107

22-EDIR-0002, ANR-24-CE31-0504-01); Germany: Deutsche Forschungsgemeinschaft (DFG – 469666862, DFG – CR 312/5-2); China: Research Grants Council (GRF); Italy: Istituto Nazionale di Fisica Nucleare (ICSC, NextGenerationEU), Ministero dell'Università e della Ricerca (NextGenEU 153D23001490006 M4C2.1.1, NextGenEU I53D23000820006 M4C2.1.1, NextGenEU I53D23001490006 M4C2.1.1, SOE2024_0000023); Japan: Japan Society for the Promotion of Science (JSPS KAKENHI JP22H01227, JSPS KAKENHI JP22H04944, JSPS KAKENHI JP22KK0227, JSPS KAKENHI JP24K23939, JSPS KAKENHI JP24KK0251, JSPS KAKENHI JP25H00650, JSPS KAKENHI JP25H01291, JSPS KAKENHI JP25K01023); Norway: Research Council of Norway (RCN-314472); Poland: Ministry of Science and Higher Education (IDUB AGH, POB8, D4 no 9722), Polish National Science Centre (NCN 2021/42/E/ST2/00350, NCN OPUS 2023/51/B/ST2/02507, NCN OPUS nr 2022/47/B/ST2/03059, NCN UMO-2019/34/E/ST2/00393, UMO-2022/47/O/ST2/00148, UMO-2023/49/B/ST2/04085, UMO-2023/51/B/ST2/00920, UMO-2024/53/N/ST2/00869); Portugal: Foundation for Science and Technology (FCT); Spain: Agencia de Gestión de Ayudas Universitarias y de Investigación (AGAUR – 2023 BP 00141), Generalitat Valenciana (ASFAE/2022/008), Ministry of Science and Innovation (MCIN & NextGenEU PCI2022-135018-2, MICIN & FEDER PID2021-125273NB, RYC2019-028510-I, RYC2020-030254-I, RYC2021-031273-I, RYC2022-038164-I), Ministerio de Ciencia, Innovación y Universidades/Agencia Estatal de Investigación (PID2022-142604OB-C22); Sweden: Carl Trygger Foundation (Carl Trygger Foundation CTS 22:2312), Swedish Research Council (Swedish Research Council 2023-04654, VR 2021-03651, VR 2022-03845, VR 2022-04683, VR 2023-03403, VR 2024-05451), Knut and Alice Wallenberg Foundation (KAW 2018.0458, KAW 2022.0358, KAW 2023.0366); Switzerland: Swiss National Science Foundation (SNSF – PCEFP2_194658); United Kingdom: Royal Society (NIF-R1-231091); United States of America: U.S. Department of Energy (ECA DE-AC02-76SF00515), Neubauer Family Foundation.

Data Availability Statement. This article has no associated data or the data will not be deposited.

Code Availability Statement. This article has no associated code or the code will not be deposited.

References

[1] ATLAS and CMS collaborations, *Combination of Measurements of the Top Quark Mass from Data Collected by the ATLAS and CMS Experiments at* $\sqrt{s} = 7$ *and* 8 *TeV*, *Phys. Rev. Lett.* **132** (2024) 261902 [arXiv:2402.08713] [INSPIRE].

[2] Particle Data Group collaboration, *Review of particle physics*, *Phys. Rev. D* **110** (2024) 030001 [INSPIRE].

[3] I. Brivio and M. Trott, *The standard model as an effective field theory*, *Phys. Rept.* **793** (2019) 1 [arXiv:1706.08945] [INSPIRE].

[4] K.G. Wilson and W. Zimmermann, *Operator product expansions and composite field operators in the general framework of quantum field theory*, Commun. Math. Phys. **24** (1972) 87 [INSPIRE].

[5] S. Willenbrock and C. Zhang, *Effective Field Theory Beyond the Standard Model*, Ann. Rev. Nucl. Part. Sci. **64** (2014) 83 [arXiv:1401.0470] [INSPIRE].

[6] W. Buchmüller and D. Wyler, *Effective lagrangian analysis of new interactions and flavour conservation*, Nucl. Phys. B **268** (1986) 621 [INSPIRE].

[7] B. Grzadkowski, M. Iskrzyński, M. Misiak and J. Rosiek, *Dimension-Six Terms in the Standard Model Lagrangian*, JHEP **10** (2010) 085 [arXiv:1008.4884] [INSPIRE].

[8] L. Evans and P. Bryant, *LHC Machine*, 2008 *JINST* **3** S08001 [INSPIRE].

[9] CMS collaboration, *Measurement of the single top quark and antiquark production cross sections in the t channel and their ratio in proton-proton collisions at $\sqrt{s} = 13$ TeV*, Phys. Lett. B **800** (2020) 135042 [arXiv:1812.10514] [INSPIRE].

[10] ATLAS collaboration, *Measurement of t-channel production of single top quarks and antiquarks in pp collisions at 13 TeV using the full ATLAS Run 2 data sample*, JHEP **05** (2024) 305 [*Erratum ibid.* **06** (2024) 024] [arXiv:2403.02126] [INSPIRE].

[11] J.M. Campbell, R. Frederix, F. Maltoni and F. Tramontano, *Next-to-Leading-Order Predictions for t-Channel Single-Top Production at Hadron Colliders*, Phys. Rev. Lett. **102** (2009) 182003 [arXiv:0903.0005] [INSPIRE].

[12] F. Maltoni, G. Ridolfi and M. Ubiali, *b-initiated processes at the LHC: a reappraisal*, JHEP **07** (2012) 022 [*Erratum ibid.* **04** (2013) 095] [arXiv:1203.6393] [INSPIRE].

[13] E. Bothmann, F. Krauss and M. Schönherr, *Single top-quark production with SHERPA*, Eur. Phys. J. C **78** (2018) 220 [arXiv:1711.02568] [INSPIRE].

[14] J.A. Aguilar-Saavedra, J. Boudreau, C. Escobar and J. Mueller, *The fully differential top decay distribution*, Eur. Phys. J. C **77** (2017) 200 [arXiv:1702.03297] [INSPIRE].

[15] J.A. Aguilar-Saavedra and S. Amor Dos Santos, *New directions for top quark polarization in the t-channel process*, Phys. Rev. D **89** (2014) 114009 [arXiv:1404.1585] [INSPIRE].

[16] ATLAS collaboration, *Measurement of the polarisation of single top quarks and antiquarks produced in the t-channel at $\sqrt{s} = 13$ TeV and bounds on the tWb dipole operator from the ATLAS experiment*, JHEP **11** (2022) 040 [arXiv:2202.11382] [INSPIRE].

[17] ATLAS collaboration, *Inclusive and differential cross-section measurements of $t\bar{t}Z$ production in pp collisions at $\sqrt{s} = 13$ TeV with the ATLAS detector, including EFT and spin-correlation interpretations*, JHEP **07** (2024) 163 [arXiv:2312.04450] [INSPIRE].

[18] ATLAS collaboration, *Measurements of inclusive and differential cross-sections of $t\bar{t}\gamma$ production in pp collisions at $\sqrt{s} = 13$ TeV with the ATLAS detector*, JHEP **10** (2024) 191 [arXiv:2403.09452] [INSPIRE].

[19] CMS collaboration, *Search for new physics in top quark production in dilepton final states in proton–proton collisions at $\sqrt{s} = 13$ TeV*, Eur. Phys. J. C **79** (2019) 886 [arXiv:1903.11144] [INSPIRE].

[20] CMS collaboration, *Search for new physics in top quark production with additional leptons in proton–proton collisions at $\sqrt{s} = 13$ TeV using effective field theory*, JHEP **03** (2021) 095 [arXiv:2012.04120] [INSPIRE].

JHEP07(2026)107

[21] CMS collaboration, *Probing effective field theory operators in the associated production of top quarks with a Z boson in multilepton final states at* $\sqrt{s} = 13$ *TeV*, JHEP **12** (2021) 083 [arXiv:2107.13896] [INSPIRE].

[22] CMS collaboration, *Search for physics beyond the standard model in top quark production with additional leptons in the context of effective field theory*, JHEP **12** (2023) 068 [arXiv:2307.15761] [INSPIRE].

[23] CMS collaboration, *Search for new physics using effective field theory in 13 TeV pp collision events that contain a top quark pair and a boosted Z or Higgs boson*, Phys. Rev. D **108** (2023) 032008 [arXiv:2208.12837] [INSPIRE].

[24] ATLAS collaboration, *Search for anomalous couplings in the Wtb vertex from the measurement of double differential angular decay rates of single top quarks produced in the t-channel with the ATLAS detector*, JHEP **04** (2016) 023 [arXiv:1510.03764] [INSPIRE].

[25] ATLAS collaboration, *Probing the Wtb vertex structure in t-channel single-top-quark production and decay in pp collisions at* $\sqrt{s} = 8$ *TeV with the ATLAS detector*, JHEP **04** (2017) 124 [arXiv:1702.08309] [INSPIRE].

[26] ATLAS collaboration, *Measurements of top-quark pair differential cross-sections in the lepton+jets channel in pp collisions at* $\sqrt{s} = 8$ *TeV using the ATLAS detector*, Eur. Phys. J. C **76** (2016) 538 [arXiv:1511.04716] [INSPIRE].

[27] ATLAS collaboration, *Analysis of the Wtb vertex from the measurement of triple-differential angular decay rates of single top quarks produced in the t-channel at* $\sqrt{s} = 8$ *TeV with the ATLAS detector*, JHEP **12** (2017) 017 [arXiv:1707.05393] [INSPIRE].

[28] CMS and ATLAS collaborations, *Combination of the W boson polarization measurements in top quark decays using ATLAS and CMS data at* $\sqrt{s} = 8$ *TeV*, JHEP **08** (2020) 051 [arXiv:2005.03799] [INSPIRE].

[29] B. Grzadkowski and M. Misiak, *Anomalous Wtb coupling effects in the weak radiative B-meson decay*, Phys. Rev. D **78** (2008) 077501 [*Erratum ibid.* **84** (2011) 059903] [arXiv:0802.1413] [INSPIRE].

[30] J.A. Aguilar-Saavedra and J. Bernabeu, *W polarisation beyond helicity fractions in top quark decays*, Nucl. Phys. B **840** (2010) 349 [arXiv:1005.5382] [INSPIRE].

[31] ATLAS collaboration, *Differential* $t\bar{t}$ *cross-section measurements using boosted top quarks in the all-hadronic final state with* $139\,fb^{-1}$ *of ATLAS data*, JHEP **04** (2023) 080 [arXiv:2205.02817] [INSPIRE].

[32] ATLAS collaboration, *Evidence for the charge asymmetry in* $pp \to t\bar{t}$ *production at* $\sqrt{s} = 13$ *TeV with the ATLAS detector*, JHEP **08** (2023) 077 [arXiv:2208.12095] [INSPIRE].

[33] J.A. Aguilar-Saavedra et al., *Probing anomalous Wtb couplings in top pair decays*, Eur. Phys. J. C **50** (2007) 519 [hep-ph/0605190] [INSPIRE].

[34] ATLAS collaboration, *The ATLAS Experiment at the CERN Large Hadron Collider*, 2008 JINST **3** S08003 [INSPIRE].

[35] G. Avoni et al., *The new LUCID-2 detector for luminosity measurement and monitoring in ATLAS*, 2018 JINST **13** P07017 [INSPIRE].

[36] ATLAS collaboration, *Performance of the ATLAS trigger system in 2015*, Eur. Phys. J. C **77** (2017) 317 [arXiv:1611.09661] [INSPIRE].

[37] ATLAS collaboration, *Software and computing for Run 3 of the ATLAS experiment at the LHC*, *Eur. Phys. J. C* **85** (2025) 234 [arXiv:2404.06335] [INSPIRE].

[38] ATLAS collaboration, *ATLAS data quality operations and performance for 2015–2018 data-taking*, 2020 *JINST* **15** P04003 [arXiv:1911.04632] [INSPIRE].

[39] ATLAS collaboration, *Performance of electron and photon triggers in ATLAS during LHC Run 2*, *Eur. Phys. J. C* **80** (2020) 47 [arXiv:1909.00761] [INSPIRE].

[40] ATLAS collaboration, *Performance of the ATLAS muon triggers in Run 2*, 2020 *JINST* **15** P09015 [arXiv:2004.13447] [INSPIRE].

[41] T. Sjöstrand, S. Mrenna and P.Z. Skands, *A brief introduction to PYTHIA 8.1*, *Comput. Phys. Commun.* **178** (2008) 852 [arXiv:0710.3820] [INSPIRE].

[42] R.D. Ball et al., *Parton distributions with LHC data*, *Nucl. Phys. B* **867** (2013) 244 [arXiv:1207.1303] [INSPIRE].

[43] ATLAS collaboration, *The Pythia 8 A3 tune description of ATLAS minimum bias and inelastic measurements incorporating the Donnachie–Landshoff diffractive model*, ATL-PHYS-PUB-2016-017 [INSPIRE].

[44] SHERPA collaboration, *Event generation with Sherpa 2.2*, *SciPost Phys.* **7** (2019) 034 [arXiv:1905.09127] [INSPIRE].

[45] S. Frixione, P. Nason and G. Ridolfi, *A positive-weight next-to-leading-order Monte Carlo for heavy flavour hadroproduction*, *JHEP* **09** (2007) 126 [arXiv:0707.3088] [INSPIRE].

[46] P. Nason, *A new method for combining NLO QCD with shower Monte Carlo algorithms*, *JHEP* **11** (2004) 040 [hep-ph/0409146] [INSPIRE].

[47] S. Frixione, P. Nason and C. Oleari, *Matching NLO QCD computations with parton shower simulations: the POWHEG method*, *JHEP* **11** (2007) 070 [arXiv:0709.2092] [INSPIRE].

[48] S. Alioli, P. Nason, C. Oleari and E. Re, *A general framework for implementing NLO calculations in shower Monte Carlo programs: the POWHEG BOX*, *JHEP* **06** (2010) 043 [arXiv:1002.2581] [INSPIRE].

[49] ATLAS collaboration, *ATLAS Pythia 8 tunes to* 7 *TeV data*, ATL-PHYS-PUB-2014-021 [INSPIRE].

[50] J. Alwall et al., *The automated computation of tree-level and next-to-leading order differential cross sections, and their matching to parton shower simulations*, *JHEP* **07** (2014) 079 [arXiv:1405.0301] [INSPIRE].

[51] J. Pumplin et al., *New Generation of Parton Distributions with Uncertainties from Global QCD Analysis*, *JHEP* **07** (2002) 012 [hep-ph/0201195] [INSPIRE].

[52] ATLAS collaboration, *Measurement of the Z/γ^* boson transverse momentum distribution in pp collisions at $\sqrt{s} = 7$ TeV with the ATLAS detector*, *JHEP* **09** (2014) 145 [arXiv:1406.3660] [INSPIRE].

[53] R. Frederix, E. Re and P. Torrielli, *Single-top t-channel hadroproduction in the four-flavour scheme with POWHEG and aMC@NLO*, *JHEP* **09** (2012) 130 [arXiv:1207.5391] [INSPIRE].

[54] NNPDF collaboration, *Parton distributions for the LHC run II*, *JHEP* **04** (2015) 040 [arXiv:1410.8849] [INSPIRE].

[55] S. Alioli, P. Nason, C. Oleari and E. Re, *NLO single-top production matched with shower in POWHEG: s- and t-channel contributions*, *JHEP* **09** (2009) 111 [*Erratum ibid.* **02** (2010) 011] [arXiv:0907.4076] [INSPIRE].

JHEP07(2026)107

[56] S. Frixione, E. Laenen, P. Motylinski and B.R. Webber, *Angular correlations of lepton pairs from vector boson and top quark decays in Monte Carlo simulations*, JHEP **04** (2007) 081 [hep-ph/0702198] [INSPIRE].

[57] P. Artoisenet, R. Frederix, O. Mattelaer and R. Rietkerk, *Automatic spin-entangled decays of heavy resonances in Monte Carlo simulations*, JHEP **03** (2013) 015 [arXiv:1212.3460] [INSPIRE].

[58] T. Sjöstrand et al., *An introduction to PYTHIA 8.2*, Comput. Phys. Commun. **191** (2015) 159 [arXiv:1410.3012] [INSPIRE].

[59] J. Campbell, T. Neumann and Z. Sullivan, *Single-top-quark production in the t-channel at NNLO*, JHEP **02** (2021) 040 [arXiv:2012.01574] [INSPIRE].

[60] PDF4LHC Working Group collaboration, *The PDF4LHC21 combination of global PDF fits for the LHC Run III*, J. Phys. G **49** (2022) 080501 [arXiv:2203.05506] [INSPIRE].

[61] ATLAS collaboration, *Studies on top-quark Monte Carlo modelling for Top2016*, ATL-PHYS-PUB-2016-020 [INSPIRE].

[62] M. Beneke, P. Falgari, S. Klein and C. Schwinn, *Hadronic top-quark pair production with NNLL threshold resummation*, Nucl. Phys. B **855** (2012) 695 [arXiv:1109.1536] [INSPIRE].

[63] M. Cacciari et al., *Top-pair production at hadron colliders with next-to-next-to-leading logarithmic soft-gluon resummation*, Phys. Lett. B **710** (2012) 612 [arXiv:1111.5869] [INSPIRE].

[64] P. Bärnreuther, M. Czakon and A. Mitov, *Percent-Level-Precision Physics at the Tevatron: Next-to-Next-to-Leading Order QCD Corrections to $q\bar{q} \to t\bar{t} + X$*, Phys. Rev. Lett. **109** (2012) 132001 [arXiv:1204.5201] [INSPIRE].

[65] M. Czakon and A. Mitov, *NNLO corrections to top-pair production at hadron colliders: the all-fermionic scattering channels*, JHEP **12** (2012) 054 [arXiv:1207.0236] [INSPIRE].

[66] M. Czakon and A. Mitov, *NNLO corrections to top pair production at hadron colliders: the quark-gluon reaction*, JHEP **01** (2013) 080 [arXiv:1210.6832] [INSPIRE].

[67] M. Czakon, P. Fiedler and A. Mitov, *Total Top-Quark Pair-Production Cross Section at Hadron Colliders Through $\mathcal{O}(\alpha_S^4)$*, Phys. Rev. Lett. **110** (2013) 252004 [arXiv:1303.6254] [INSPIRE].

[68] M. Czakon and A. Mitov, *Top++: A program for the calculation of the top-pair cross-section at hadron colliders*, Comput. Phys. Commun. **185** (2014) 2930 [arXiv:1112.5675] [INSPIRE].

[69] J.S. Gainer et al., *Exploring Theory Space with Monte Carlo Reweighting*, JHEP **10** (2014) 078 [arXiv:1404.7129] [INSPIRE].

[70] D. Barducci et al., *Interpreting top-quark LHC measurements in the standard-model effective field theory*, arXiv:1802.07237 [INSPIRE].

[71] M. de Beurs, E. Laenen, M. Vreeswijk and E. Vryonidou, *Effective operators in t-channel single top production and decay*, Eur. Phys. J. C **78** (2018) 919 [arXiv:1807.03576] [INSPIRE].

[72] T. Gleisberg and S. Hoeche, *Comix, a new matrix element generator*, JHEP **12** (2008) 039 [arXiv:0808.3674] [INSPIRE].

[73] F. Buccioni et al., *OpenLoops 2*, Eur. Phys. J. C **79** (2019) 866 [arXiv:1907.13071] [INSPIRE].

[74] F. Cascioli, P. Maierhöfer and S. Pozzorini, *Scattering Amplitudes with Open Loops*, Phys. Rev. Lett. **108** (2012) 111601 [arXiv:1111.5206] [INSPIRE].

[75] A. Denner, S. Dittmaier and L. Hofer, *Collier: A fortran-based complex one-loop library in extended regularizations*, Comput. Phys. Commun. **212** (2017) 220 [arXiv:1604.06792] [INSPIRE].

[76] S. Schumann and F. Krauss, *A parton shower algorithm based on Catani–Seymour dipole factorisation*, JHEP **03** (2008) 038 [arXiv:0709.1027] [INSPIRE].

[77] J.-C. Winter, F. Krauss and G. Soff, *A modified cluster-hadronisation model*, Eur. Phys. J. C **36** (2004) 381 [hep-ph/0311085] [INSPIRE].

[78] C. Anastasiou, L.J. Dixon, K. Melnikov and F. Petriello, *High-precision QCD at hadron colliders: Electroweak gauge boson rapidity distributions at next-to-next-to leading order*, Phys. Rev. D **69** (2004) 094008 [hep-ph/0312266] [INSPIRE].

[79] E. Re, *Single-top Wt-channel production matched with parton showers using the POWHEG method*, Eur. Phys. J. C **71** (2011) 1547 [arXiv:1009.2450] [INSPIRE].

[80] S. Hoeche, F. Krauss, M. Schönherr and F. Siegert, *A critical appraisal of NLO+PS matching methods*, JHEP **09** (2012) 049 [arXiv:1111.1220] [INSPIRE].

[81] S. Hoeche, F. Krauss, M. Schönherr and F. Siegert, *QCD matrix elements + parton showers. The NLO case*, JHEP **04** (2013) 027 [arXiv:1207.5030] [INSPIRE].

[82] S. Catani, F. Krauss, R. Kuhn and B.R. Webber, *QCD Matrix Elements + Parton Showers*, JHEP **11** (2001) 063 [hep-ph/0109231] [INSPIRE].

[83] S. Hoeche, F. Krauss, S. Schumann and F. Siegert, *QCD matrix elements and truncated showers*, JHEP **05** (2009) 053 [arXiv:0903.1219] [INSPIRE].

[84] D.J. Lange, *The EvtGen particle decay simulation package*, Nucl. Instrum. Meth. A **462** (2001) 152 [INSPIRE].

[85] ATLAS collaboration, *Vertex Reconstruction Performance of the ATLAS Detector at $\sqrt{s} = 13$ TeV*, ATL-PHYS-PUB-2015-026 [INSPIRE].

[86] ATLAS collaboration, *Electron and photon performance measurements with the ATLAS detector using the 2015–2017 LHC proton–proton collision data*, 2019 JINST **14** P12006 [arXiv:1908.00005] [INSPIRE].

[87] ATLAS collaboration, *Muon reconstruction and identification efficiency in ATLAS using the full Run 2 pp collision data set at $\sqrt{s} = 13$ TeV*, Eur. Phys. J. C **81** (2021) 578 [arXiv:2012.00578] [INSPIRE].

[88] ATLAS collaboration, *Studies of the muon momentum calibration and performance of the ATLAS detector with pp collisions at $\sqrt{s} = 13$ TeV*, Eur. Phys. J. C **83** (2023) 686 [arXiv:2212.07338] [INSPIRE].

[89] ATLAS collaboration, *Tools for estimating fake/non-prompt lepton backgrounds with the ATLAS detector at the LHC*, 2023 JINST **18** T11004 [arXiv:2211.16178] [INSPIRE].

[90] ATLAS collaboration, *Jet reconstruction and performance using particle flow with the ATLAS Detector*, Eur. Phys. J. C **77** (2017) 466 [arXiv:1703.10485] [INSPIRE].

[91] M. Cacciari, G.P. Salam and G. Soyez, *The anti-k_t jet clustering algorithm*, JHEP **04** (2008) 063 [arXiv:0802.1189] [INSPIRE].

[92] M. Cacciari, G.P. Salam and G. Soyez, *FastJet user manual*, Eur. Phys. J. C **72** (2012) 1896 [arXiv:1111.6097] [INSPIRE].

[93] ATLAS collaboration, *Jet energy scale and resolution measured in proton–proton collisions at $\sqrt{s} = 13$ TeV with the ATLAS detector*, Eur. Phys. J. C **81** (2021) 689 [arXiv:2007.02645] [INSPIRE].

[94] ATLAS collaboration, *Performance of pile-up mitigation techniques for jets in pp collisions at $\sqrt{s} = 8$ TeV using the ATLAS detector*, Eur. Phys. J. C **76** (2016) 581 [arXiv:1510.03823] [INSPIRE].

[95] ATLAS collaboration, *Identification and rejection of pile-up jets at high pseudorapidity with the ATLAS detector*, Eur. Phys. J. C **77** (2017) 580 [*Erratum ibid.* **77** (2017) 712] [arXiv:1705.02211] [INSPIRE].

[96] ATLAS collaboration, *Selection of jets produced in 13 TeV proton–proton collisions with the ATLAS detector*, ATLAS-CONF-2015-029 [INSPIRE].

[97] ATLAS collaboration, *ATLAS flavour-tagging algorithms for the LHC Run 2 pp collision dataset*, Eur. Phys. J. C **83** (2023) 681 [arXiv:2211.16345] [INSPIRE].

[98] ATLAS collaboration, *ATLAS b-jet identification performance and efficiency measurement with $t\bar{t}$ events in pp collisions at $\sqrt{s} = 13$ TeV*, Eur. Phys. J. C **79** (2019) 970 [arXiv:1907.05120] [INSPIRE].

[99] ATLAS collaboration, *Measurement of the c-jet mistagging efficiency in $t\bar{t}$ events using pp collision data at $\sqrt{s} = 13$ TeV collected with the ATLAS detector*, Eur. Phys. J. C **82** (2022) 95 [arXiv:2109.10627] [INSPIRE].

[100] ATLAS collaboration, *Calibration of the light-flavour jet mistagging efficiency of the b-tagging algorithms with Z+jets events using 139 fb^{-1} of ATLAS proton–proton collision data at $\sqrt{s} = 13$ TeV*, Eur. Phys. J. C **83** (2023) 728 [arXiv:2301.06319] [INSPIRE].

[101] ATLAS collaboration, *Measurement of the tau lepton reconstruction and identification performance in the ATLAS experiment using pp collisions at $\sqrt{s} = 13$ TeV*, ATLAS-CONF-2017-029 [INSPIRE].

[102] ATLAS collaboration, *Identification of hadronic tau lepton decays using neural networks in the ATLAS experiment*, ATL-PHYS-PUB-2019-033 [INSPIRE].

[103] ATLAS collaboration, *Reconstruction, Identification, and Calibration of hadronically decaying tau leptons with the ATLAS detector for the LHC Run 3 and reprocessed Run 2 data*, ATL-PHYS-PUB-2022-044 [INSPIRE].

[104] ATLAS collaboration, *The performance of missing transverse momentum reconstruction and its significance with the ATLAS detector using 140 fb^{-1} of $\sqrt{s} = 13$ TeV pp collisions*, Eur. Phys. J. C **85** (2025) 606 [arXiv:2402.05858] [INSPIRE].

[105] Particle Data Group collaboration, *Review of particle physics*, J. Phys. G **37** (2010) 075021 [INSPIRE].

[106] J. Erdmann et al., *A likelihood-based reconstruction algorithm for top-quark pairs and the KLFitter framework*, Nucl. Instrum. Meth. A **748** (2014) 18 [arXiv:1312.5595] [INSPIRE].

[107] ATLAS collaboration, *Luminosity determination in pp collisions at $\sqrt{s} = 13$ TeV using the ATLAS detector at the LHC*, Eur. Phys. J. C **83** (2023) 982 [arXiv:2212.09379] [INSPIRE].

[108] ATLAS collaboration, *Measurement of the Inelastic Proton–Proton Cross Section at $\sqrt{s} = 13$ TeV with the ATLAS Detector at the LHC*, Phys. Rev. Lett. **117** (2016) 182002 [arXiv:1606.02625] [INSPIRE].

JHEP07(2026)107

[109] ATLAS collaboration, *Performance of missing transverse momentum reconstruction with the ATLAS detector using proton–proton collisions at $\sqrt{s} = 13$ TeV*, Eur. Phys. J. C **78** (2018) 903 [arXiv:1802.08168] [INSPIRE].

[110] S. Höche et al., *A Study of QCD Radiation in VBF Higgs Production with Vincia and Pythia*, SciPost Phys. **12** (2022) 010 [arXiv:2106.10987] [INSPIRE].

[111] H. Brooks and P. Skands, *Coherent showers in decays of colored resonances*, Phys. Rev. D **100** (2019) 076006 [arXiv:1907.08980] [INSPIRE].

[112] ATLAS collaboration, *Studies on top-quark Monte Carlo modelling with Sherpa and MG5_aMC@NLO*, ATL-PHYS-PUB-2017-007 [INSPIRE].

[113] J. Butterworth et al., *PDF4LHC recommendations for LHC Run II*, J. Phys. G **43** (2016) 023001 [arXiv:1510.03865] [INSPIRE].

[114] M. Czakon et al., *Top-pair production at the LHC through NNLO QCD and NLO EW*, JHEP **10** (2017) 186 [arXiv:1705.04105] [INSPIRE].

[115] E.P. Wigner, *Group Theory and its Application to the Quantum Mechanics of Atomic Spectra*, Proc. Edinb. Math. Soc. **12** (1960) 67.

[116] J.A. Aguilar-Saavedra, N.F. Castro and A. Onofre, *Constraints on the Wtb vertex from early LHC data*, Phys. Rev. D **83** (2011) 117301 [arXiv:1105.0117] [INSPIRE].

[117] M. Jacob and G.C. Wick, *On the General Theory of Collisions for Particles with Spin*, Annals Phys. **7** (1959) 404 [INSPIRE].

[118] I. Brivio et al., *O new physics, where art thou? A global search in the top sector*, JHEP **02** (2020) 131 [arXiv:1910.03606] [INSPIRE].

[119] ATLAS collaboration, *Measurement of differential t-channel single top (anti)quark production cross-sections at* 13 *TeV with the ATLAS detector*, JHEP **05** (2026) 174 [arXiv:2601.04938] [INSPIRE].

[120] G.A. González-Sprinberg and J. Vidal, *The top quark right coupling in the tbW-vertex*, Eur. Phys. J. C **75** (2015) 615 [arXiv:1510.02153] [INSPIRE].

[121] A. Arhrib and A. Jueid, *tbW Anomalous Couplings in the Two Higgs Doublet Model*, JHEP **08** (2016) 082 [arXiv:1606.05270] [INSPIRE].

[122] M. Fischer, S. Groote and J.G. Körner, *T-odd correlations in polarized top quark decays in the sequential decay $t(\uparrow) \to X_b + W^+(\to \ell^+ + \nu_\ell)$ and in the quasi-three-body decay $t(\uparrow) \to X_b + \ell^+ + \nu_\ell$*, Phys. Rev. D **97** (2018) 093001 [arXiv:1802.02492] [INSPIRE].

[123] M. Fischer, S. Groote, J.G. Körner and M.C. Mauser, *Complete angular analysis of polarized top quark decay at $O(\alpha_s)$*, Phys. Rev. D **65** (2002) 054036 [hep-ph/0101322] [INSPIRE].

[124] A. Czarnecki, J.G. Körner and J.H. Piclum, *Helicity fractions of W bosons from top quark decays at next-to-next-to-leading order in QCD*, Phys. Rev. D **81** (2010) 111503 [arXiv:1005.2625] [INSPIRE].

[125] ATLAS collaboration, *ATLAS Computing Acknowledgements*, ATL-SOFT-PUB-2026-001.

JHEP07(2026)107

The ATLAS collaboration

G. Aad[103], E. Aakvaag[17], B. Abbott[122], S. Abdelhameed[118a], K. Abeling[55], N.J. Abicht[49], S.H. Abidi[30], M. Aboelela[45], A. Aboulhorma[36e], H. Abramowicz[156], Y. Abulaiti[119], B.S. Acharya[69a,69b,a], A. Ackermann[63a], C. Adam Bourdarios[4], L. Adamczyk[86a], S.V. Addepalli[148], M. J. Addison[102], J. Adelman[117], A. Adiguzel[22c], T. Adye[136], A.A. Affolder[138], Y. Afik[40], M.N. Agaras[13], A. Aggarwal[101], C. Agheorghiesei[28c], F. Ahmadov[39,b], S. Ahuja[96], S. Ahuja[168], X. Ai[142b], G. Aielli[76a,76b], A. Aikot[168], M. Ait Tamlihat[36e], B. Aitbenchikh[36a], T.P.A. Åkesson[99], A.V. Akimov[150], D. Akiyama[173], N.N. Akolkar[25], S. Aktas[171], G.L. Alberghi[24b], J. Albert[170], U. Alberti[20], P. Albicocco[53], G.L. Albouy[60], S. Alderweireldt[52], Z.L. Alegria[123], M. Aleksa[37], I.N. Aleksandrov[39], C. Alexa[28b], T. Alexopoulos[10], F. Alfonsi[24b], M. Algren[56], M. Alhroob[172], B. Ali[134], H. M. J. Ali[92,c], S. Ali[32], S.W. Alibocus[93], M. Aliev[34c], G. Alimonti[71a], W. Alkakhi[55], C. Allaire[66], B.M.M. Allbrooke[151], D. R. Allen[123], J. S. Allen[102], J.F. Allen[52], P.P. Allport[21], A. Aloisio[72a,72b], F. Alonso[91], C. Alpigiani[141], Z.M.K. Alsolami[92], A. Alvarez Fernandez[101], M. Alves Cardoso[56], M.G. Alviggi[72a,72b], M. Aly[102], Y. Amaral Coutinho[82b], A. Ambler[105], C. Amelung[37], M. Amerl[102], C.G. Ames[110], T. Amezza[129], D. Amidei[107], B. Amini[54], K. Amirie[160], A. Amirkhanov[39], S.P. Amor Dos Santos[132a], K.R. Amos[168], D. Amperiadou[157], S. An[83], C. Anastopoulos[144], T. Andeen[11], J.K. Anders[93], A. C. Anderson[59], A. Andreazza[71a,71b], S. Angelidakis[9], A. Angerami[42], A.V. Anisenkov[39], A. Annovi[74a], C. Antel[37], E. Antipov[150], M. Antonelli[53], F. Anulli[75a], M. Aoki[83], T. Aoki[158], M.A. Aparo[151], L. Aperio Bella[48], M. Apicella[31], C. Appelt[156], A. Apyan[27], M. Arampatzi[10], S. J. Arbiol Val[87], C. Arcangeletti[53], A.T.H. Arce[51], J-F. Arguin[109], S. Argyropoulos[157], J.-H. Arling[48], O. Arnaez[4], H. Arnold[150], G. Artoni[75a,75b], H. Asada[112], K. Asai[120], S. Asatryan[178], N.A. Asbah[37], R. A. Ashby Pickering[172], A. M. Aslam[96], K. Assamagan[30], R. Astalos[29a], K. S. V. Astrand[99], S. Atashi[164], R.J. Atkin[34a], H. Atmani[36f], P.A. Atmasiddha[130], K. Augsten[134], A.D. Auriol[41], V.A. Austrup[102], A.S. Avad[95], G. Avolio[37], K. Axiotis[56], A. Azzam[13], D. Babal[29b], H. Bachacou[137], K. Bachas[157,d], A. Bachiu[35], E. Bachmann[50], M. J. Backes[63a], A. Badea[40], T.M. Baer[107], P. Bagnaia[75a,75b], M. Bahmani[19], D. Bahner[54], K. Bai[125], J.T. Baines[136], L. Baines[95], O.K. Baker[177], E. Bakos[16], D. Bakshi Gupta[8], L.E. Balabram Filho[82b], V. Balakrishnan[122], R. Balasubramanian[4], E.M. Baldin[38], P. Balek[86a], E. Ballabene[24b,24a], F. Balli[137], L.M. Baltes[63a], W.K. Balunas[33], J. Balz[101], I. Bamwidhi[118b], E. Banas[87], M. Bandieramonte[131], A. Bandyopadhyay[25], S. Bansal[25], L. Barak[156], M. Barakat[48], E.L. Barberio[106], D. Barberis[18b], M. Barbero[103], M. Z. Barel[116], T. Barillari[111], M-S. Barisits[37], T. Barklow[148], P. Baron[135], D.A. Baron Moreno[102], A. Baroncelli[62], A.J. Barr[128], J.D. Barr[97], F. Barreiro[100], J. Barreiro Guimarães da Costa[14], M.G. Barros Teixeira[132a], S. Barsov[38], F. Bartels[63a], R. Bartoldus[148], A.E. Barton[92], P. Bartos[29a], M. Baselga[49], S. Bashiri[87], A. Bassalat[66,e], M.J. Basso[161a], S. Bataju[45], R. Bate[169], R.L. Bates[59], S. Batlamous[100], M. Battaglia[138], D. Battulga[19], M. Bauce[75a,75b], M. Bauer[79], P. Bauer[25], L. T. Bayer[48], L.T. Bazzano Hurrell[31], J.B. Beacham[111], T. Beau[129], J.Y. Beaucamp[91], P.H. Beauchemin[163], P. Bechtle[25], H.P. Beck[20,f], K. Becker[172], A.J. Beddall[81], V.A. Bednyakov[39], C.P. Bee[150],

JHEP07(2026)107

L.J. Beemster[16], M. Begalli[82d], M. Begel[30], J.K. Behr[48], J.F. Beirer[37], F. Beisiegel[25], M. Belfkir[118b], G. Bella[156], L. Bellagamba[24b], A. Bellerive[35], C.D. Bellgraph[68], P. Bellos[21], K. Beloborodov[38], I. Benaoumeur[21], D. Benchekroun[36a], F. Bendebba[36a], Y. Benhammou[156], K.C. Benkendorfer[61], L. Beresford[48], M. Beretta[53], E. Bergeaas Kuutmann[166], N. Berger[4], B. Bergmann[134], J. Beringer[18a], G. Bernardi[5], C. Bernius[148], F.U. Bernlochner[25], A. Berrocal Guardia[13], T. Berry[96], P. Berta[135], A. Berti[132a], R. Bertrand[103], S. Bethke[111], A. Betti[75a,75b], A.J. Bevan[95], L. Bezio[56], N.K. Bhalla[54], S. Bharthuar[111], S. Bhatta[150], P. Bhattarai[148], Z.M. Bhatti[119], K. D. Bhide[54], V.S. Bhopatkar[123], R.M. Bianchi[131], G. Bianco[24b,24a], O. Biebel[110], M. Biglietti[77a], C. S. Billingsley[45], Y. Bimgdi[36f], M. Bindi[55], A. Bingham[176], A. Bingul[22b], C. Bini[75a,75b], G.A. Bird[33], M. Birman[174], M. Biros[135], S. Biryukov[151], T. Bisanz[49], E. Bisceglie[24b,24a], J.P. Biswal[136], D. Biswas[146], I. Bloch[48], A. Blue[59], U. Blumenschein[95], V.S. Bobrovnikov[39], L. Boccardo[57b,57a], M. Boehler[54], B. Boehm[171], D. Bogavac[13], A.G. Bogdanchikov[38], L. S. Boggia[129], V. Boisvert[96], P. Bokan[37], T. Bold[86a], M. Bomben[5], M. Bona[95], M. Boonekamp[137], A.G. Borbély[59], I.S. Bordulev[38], G. Borissov[92], D. Bortoletto[128], D. Boscherini[24b], M. Bosman[13], K. Bouaouda[36a], N. Bouchhar[168], L. Boudet[4], J. Boudreau[131], E.V. Bouhova-Thacker[92], D. Boumediene[41], R. Bouquet[57b,57a], A. Boveia[121], J. Boyd[37], D. Boye[30], I.R. Boyko[39], L. Bozianu[56], J. Bracinik[21], N. Brahimi[4], G. Brandt[176], O. Brandt[33], B. Brau[104], J.E. Brau[125], R. Brener[174], L. Brenner[116], R. Brenner[166], S. Bressler[174], G. Brianti[78a,78b], D. Britton[59], D. Britzger[111], I. Brock[25], R. Brock[108], G. Brooijmans[42], A.J. Brooks[68], E. M. Brooks[161b], E. Brost[30], L.M. Brown[170,161a], L.E. Bruce[61], T.L. Bruckler[128], P.A. Bruckman de Renstrom[87], B. Brüers[48], A. Bruni[24b], G. Bruni[24b], D. Brunner[47a,47b], M. Bruschi[24b], N. Bruscino[75a,75b], T. Buanes[17], Q. Buat[141], D. Buchin[111], A.G. Buckley[59], O. Bulekov[81], B.A. Bullard[148], S. Burdin[93], C.D. Burgard[49], A.M. Burger[90], B. Burghgrave[8], O. Burlayenko[54], J. Burleson[167], J.C. Burzynski[147], E.L. Busch[42], V. Büscher[101], P.J. Bussey[59], O. But[25], J.M. Butler[26], C.M. Buttar[59], J.M. Butterworth[97], P. Butti[37], W. Buttinger[136], C.J. Buxo Vazquez[108], A.R. Buzykaev[39], S. Cabrera Urbán[168], L. Cadamuro[66], H. Cai[37], Y. Cai[24b,113c,24a], Y. Cai[113a], V.M.M. Cairo[37], O. Cakir[3a], N. Calace[37], P. Calafiura[18a], G. Calderini[129], P. Calfayan[35], L. Calic[99], G. Callea[59], L.P. Caloba[82b], D. Calvet[41], S. Calvet[41], R. Camacho Toro[129], S. Camarda[37], D. Camarero Munoz[27], P. Camarri[76a,76b], C. Camincher[170], M. Campanelli[97], A. Camplani[43], V. Canale[72a,72b], A.C. Canbay[3a], E. Canonero[96], J. Cantero[168], Y. Cao[167], F. Capocasa[27], M. Capua[44b,44a], A. Carbone[71a,71b], R. Cardarelli[76a], J.C.J. Cardenas[8], M. P. Cardiff[27], G. Carducci[44b,44a], T. Carli[37], G. Carlino[72a], J.I. Carlotto[13], B.T. Carlson[131,g], E.M. Carlson[170], J. Carmignani[93], L. Carminati[71a,71b], A. Carnelli[4], M. Carnesale[37], S. Caron[115], E. Carquin[139g], I.B. Carr[106], S. Carrá[73a,73b], G. Carratta[24b,24a], C. Carrion Martinez[168], A.M. Carroll[125], M.P. Casado[13,h], P. Casolaro[72a,72b], M. Caspar[48], W.R. Castiglioni[40], F.L. Castillo[4], L. Castillo Garcia[13], V. Castillo Gimenez[168], N.F. Castro[132a,132e], A. Catinaccio[37], J.R. Catmore[127], T. Cavaliere[4], V. Cavaliere[30], L.J. Caviedes Betancourt[23b], E. Celebi[81], S. Cella[37], V. Cepaitis[56], K. Cerny[124], A.S. Cerqueira[82a], A. Cerri[74a,i], L. Cerrito[76a,76b], F. Cerutti[18a], B. Cervato[71a,71b],

A. Cervelli[24b], G. Cesarini[53], S.A. Cetin[81], P.M. Chabrillat[129], R. Chakkappai[66], S. Chakraborty[172], A. Chambers[61], J. Chan[18a], W.Y. Chan[158], J.D. Chapman[33], E. Chapon[137], B. Chargeishvili[154b], D.G. Charlton[21], C. Chauhan[135], Y. Che[113a], S. Chekanov[6], G.A. Chelkov[39,j], B. Chen[156], B. Chen[170], H. Chen[30], J. Chen[143a], J. Chen[147], M. Chen[128], S. Chen[88], S.J. Chen[113a], X. Chen[143a], X. Chen[15,k], Z. Chen[62], C.L. Cheng[175], H.C. Cheng[64a], S. Cheong[148], A. Cheplakov[39], E. Cherepanova[116], R. Cherkaoui El Moursli[36e], E. Cheu[7], K. Cheung[65], L. Chevalier[137], V. Chiarella[53], G. Chiarelli[74a], G. Chiodini[70a], A.S. Chisholm[21], A. Chitan[28b], M. Chitishvili[168], M.V. Chizhov[39,l], K. Choi[11], Y. Chou[141], E.Y.S. Chow[115], K.L. Chu[174], M.C. Chu[64a], X. Chu[14,113c], Z. Chubinidze[53], J. Chudoba[133], J.J. Chwastowski[87], D. Cieri[111], K.M. Ciesla[86a], V. Cindro[94], A. Ciocio[18a], F. Cirotto[72a,72b], Z.H. Citron[174], M. Citterio[71a], D.A. Ciubotaru[28b], A. Clark[56], P.J. Clark[52], N. Clarke Hall[97], C. Clarry[160], S.E. Clawson[48], C. Clement[47a,47b], L. Clissa[24b,24a], Y. Coadou[103], M. Cobal[69a,69c], A. Coccaro[57b], R.F. Coelho Barrue[132a], R. Coelho Lopes De Sa[104], S. Coelli[71a], M.M. Cohen[130], L. S. Colangeli[160], B. Cole[42], P. Collado Soto[100], J. Collot[60], M.R. Coluccia[70a], P. Conde Muiño[132a,132g], M.P. Connell[34c], S.H. Connell[34c], E.I. Conroy[128], M. Contreras Cossio[11], F. Conventi[72a,m], A.M. Cooper-Sarkar[128], L. Corazzina[75a,75b], F. A. Corchia[24b,24a], A. Cordeiro Oudot Choi[141], L.D. Corpe[41], M. Corradi[75a,75b], F. Corriveau[105,n], A. Cortes-Gonzalez[158], M.J. Costa[168], F. Costanza[4], D. Costanzo[144], J. Couthures[4], G. Cowan[96], K. Cranmer[175], L. Cremer[49], D. Cremonini[24b,24a], S. Crépé-Renaudin[60], F. Crescioli[129], T. Cresta[73a,73b], M. Cristinziani[146], M. Cristoforetti[78a,78b], E. Critelli[97], V. Croft[116], G. Crosetti[44b,44a], A. Cueto[100], H. Cui[97], Z. Cui[7], B.M. Cunnett[151], W.R. Cunningham[59], F. Curcio[168], J. R. Curran[52], G. D'amen[30], V. D'Amico[110], M. D'Andrea[57b,57a], G. D'anniballe[74a,74b], S. D'Auria[71a,71b], A. D'Avanzo[72a,72b], L. D'Eramo[41], A. D'Onofrio[72a,72b], M. D'Onofrio[93], M. D'uffizi[102], M.J. Da Cunha Sargedas De Sousa[57b,57a], J.V. Da Fonseca Pinto[82b], C. Da Via[102], W. Dabrowski[86a], T. Dado[37], S. Dahbi[153], T. Dai[107], D. Dal Santo[20], C. Dallapiccola[104], M. Dam[43], J.R. Dandoy[35], D. Dannheim[37], M. Danninger[147], V. Dao[150], G. Darbo[57b], S.J. Das[30], F. Dattola[48], T. Davidek[135], J. Davidson[172], I. Dawson[95], K. De[8], C. De Almeida Rossi[160], R. De Asmundis[72a], N. De Biase[48], S. De Castro[24b,24a], N. De Groot[115], P. de Jong[116], H. De la Torre[117], A. De Maria[113a], A. De Salvo[75a], U. De Sanctis[76a,76b], F. De Santis[70a,70b], A. De Santo[151], J.B. De Vivie De Regie[60], J. Debevc[94], D.V. Dedovich[39], J. Degens[93], A.M. Deiana[45], J. Del Peso[100], L. Delagrange[129], F. Deliot[137], C.M. Delitzsch[49], A. Dell'Acqua[37], L. Dell'Asta[71a,71b], M. Della Pietra[72a,72b], D. Della Volpe[56], M. Delmastro[4], C.C. Delogu[57b,57a], P.A. Delsart[60], S. Demers[177], M. Demichev[39], S.P. Denisov[38], H. Denizli[22a,o], M.G. Depala[93], D. Derendarz[87], F. Derue[129], P. Dervan[93,†], A. M. Desai[1], K. Desch[25], F.A. Di Bello[74a,74b], A. Di Ciaccio[76a,76b], L. Di Ciaccio[4], A. Di Domenico[75a,75b], C. Di Donato[72a,72b], A. Di Girolamo[37], G. Di Gregorio[66], A. Di Luca[78a,78b], B. Di Micco[77a,77b], R. Di Nardo[77a,77b], K.F. Di Petrillo[40], M. Diamantopoulou[35], F.A. Dias[116], M.A. Diaz[139a,139b], A. R. Didenko[39], M. Didenko[168], S.D. Diefenbacher[18a], E.B. Diehl[107], S. Díez Cornell[48], C. Diez Pardos[146], C. Dimitriadi[149], A. Dimitrievska[21], A. Dimri[150], Y. Ding[62], J. Dingfelder[25],

JHEP07(2026)107

T. Dingley[128], I-M. Dinu[28b], S.J. Dittmeier[63b], F. Dittus[37], M. Divisek[135], B. Dixit[93], F. Djama[103], T. Djobava[154b], C. Doglioni[102,99], A. Dohnalova[29a], Z. Dolezal[135], K. Domijan[86a], K.M. Dona[40], M. Donadelli[82d], B. Dong[108], J. Donini[41], J. Dopke[136], A. Doria[72a], N. Dos Santos Fernandes[132a], I.A. Dos Santos Luz[82e], P. Dougan[102], M.T. Dova[91], A.T. Doyle[59], M.P. Drescher[55], E. Dreyer[174], I. Drivas-koulouris[10], M. Drnevich[119], D. Du[62], T.A. du Pree[116], Z. Duan[113a], M. Dubau[4], F. Dubinin[39], M. Dubovsky[29a], E. Duchovni[174], G. Duckeck[110], P. K. Duckett[97], O.A. Ducu[28b], D. Duda[52], A. Dudarev[37], M.M. Dudek[87], E. R. Duden[27], L. Duflot[66], M. Dührssen[37], I. Duminica[28g], A.E. Dumitriu[28b], M. Dunford[63a], K. Dunne[47a,47b], A. Duperrin[103], H. Duran Yildiz[3a], A. Durglishvili[154b], G.I. Dyckes[18a], M. Dyndal[86a], B.S. Dziedzic[37], Z.O. Earnshaw[151], G.H. Eberwein[128], B. Eckerova[29a], S. Eggebrecht[55], E. Egidio Purcino De Souza[82e], G. Eigen[17], K. Einsweiler[18a], T. Ekelof[166], P.A. Ekman[99], S. El Farkh[36b], Y. El Ghazali[62], H. El Jarrari[105], A. El Moussaouy[36a], D. Elitez[37], M. Ellert[166], F. Ellinghaus[176], T.A. Elliot[96], N. Ellis[37], J. Elmsheuser[30], M. Elsawy[118a], M. Elsing[37], D. Emeliyanov[136], Y. Enari[83], S. Epari[109], D. Ernani Martins Neto[87], F. Ernst[37], M. Escalier[66], C. Escobar[168], E. Etzion[156], G. Evans[132a,132b], H. Evans[68], L.S. Evans[48], A. Ezhilov[38], S. Ezzarqtouni[36a], F. Fabbri[24b,24a], L. Fabbri[24b,24a], G. Facini[97], V. Fadeyev[138], R.M. Fakhrutdinov[38], D. Fakoudis[101], S. Falciano[75a], L.F. Falda Ulhoa Coelho[27], F. Fallavollita[111], G. Falsetti[44b,44a], J. Faltova[135], C. Fan[167], K. Y. Fan[64b], Y. Fan[14], Y. Fang[14,113c], M. Fanti[71a,71b], M. Faraj[69a,69b], Z. Farazpay[98], A. Farbin[8], A. Farilla[77a], K. Farman[153], T. Farooque[108], J. N. Farr[177], M. S. Farrington[61], S.M. Farrington[136,52], F. Fassi[36e], D. Fassouliotis[9], L. Fayard[66], P. Federic[135], P. Federicova[133], O.L. Fedin[38,j], M. Feickert[175], L. Feligioni[103], D.E. Fellers[18a], C. Feng[142a], Y. Feng[14], Z. Feng[116], M.J. Fenton[164], L. Ferencz[48], B. Fernandez Barbadillo[92], P. Fernandez Martinez[67], M.J.V. Fernoux[103], J. Ferrando[92], A. Ferrari[166], P. Ferrari[116,115], R. Ferrari[73a], D. Ferrere[56], C. Ferretti[107], M. P. Fewell[1], D. Fiacco[75a,75b], F. Fiedler[101], P. Fiedler[134], S. Filimonov[39], M.S. Filip[28b,p], A. Filipčič[94], E.K. Filmer[161a], F. Filthaut[115], M.C.N. Fiolhais[132a,132c,q], L. Fiorini[168], W.C. Fisher[108], T. Fitschen[102], P. M. Fitzhugh[137], I. Fleck[146], P. Fleischmann[107], T. Flick[176], M. Flores[34d,r], L.R. Flores Castillo[64a], M. Foll[127], F.M. Follega[78a,78b], N. Fomin[33], J.H. Foo[160], A. Formica[137], A.C. Forti[102], E. Fortin[37], A.W. Fortman[18a], L. Foster[18a], L. Fountas[9,s], D. Fournier[66], H. Fox[92], P. Francavilla[74a,74b], S. Francescato[61], S. Franchellucci[56], M. Franchini[24b,24a], S. Franchino[63a], D. Francis[37], L. Franco[48], L. Franconi[48], M. Franklin[61], G. Frattari[27], Y.Y. Frid[156], J. Friend[59], N. Fritzsche[37], A. Froch[56], D. Froidevaux[37], J.A. Frost[136], Y. Fu[108], S. Fuenzalida Garrido[139g], M. Fujimoto[150], K. Y. Fung[64a], E. Furtado De Simas Filho[82e], M. Furukawa[158], M. Fuste Costa[48], J. Fuster[168], A. Gaa[55], A. Gabrielli[24b,24a], A. Gabrielli[160], P. Gadow[37], G. Gagliardi[57b,57a], L.G. Gagnon[18a], S. Gaid[84b], S. Galantzan[156], J. Gallagher[1], E.J. Gallas[128], A.L. Gallen[166], B.J. Gallop[136], K.K. Gan[121], S. Ganguly[158], Y. Gao[52], A. Garabaglu[141], F.M. Garay Walls[139a,139b], C. García[168], A. Garcia Alonso[116], A.G. Garcia Caffaro[177], J.E. García Navarro[168], M. A. Garcia Ruiz[23b], M. Garcia-Sciveres[18a], G.L. Gardner[130], R.W. Gardner[40], N. Garelli[163], R.B. Garg[148], J.M. Gargan[33], C.A. Garner[160], C.M. Garvey[34a],

V. K. Gassmann[163], G. Gaudio[73a], V. Gautam[13], P. Gauzzi[75a,75b], J. Gavranovic[94], I.L. Gavrilenko[132a], A. Gavrilyuk[38], C. Gay[169], G. Gaycken[125], E.N. Gazis[10], A. Gekow[121], C. Gemme[57b], M.H. Genest[60], A. D. Gentry[114], S. George[96], T. Geralis[46], A. A. Gerwin[122], P. Gessinger-Befurt[37], M. Ghani[172], K. Ghorbanian[95], A. Ghosal[146], A. Ghosh[164], A. Ghosh[7], B. Giacobbe[24b], S. Giagu[75a,75b], T. Giani[116], A. Giannini[62], S.M. Gibson[96], M. Gignac[138], D.T. Gil[86b], A.K. Gilbert[86a], B.J. Gilbert[42], D. Gillberg[35], G. Gilles[116], D.M. Gingrich[2,t], M.P. Giordani[69a,69c], P.F. Giraud[137], G. Giugliarelli[69a,69c], D. Giugni[71a], F. Giuli[76a,76b], I. Gkialas[9,s], L.K. Gladilin[38], C. Glasman[100], M. Glazewska[20], R. M. Gleason[164], G. Glemža[48], M. Glisic[125], I. Gnesi[44b], Y. Go[30], M. Goblirsch-Kolb[37], B. Gocke[49], D. Godin[109], B. Gokturk[22a], S. Goldfarb[106], T. Golling[56], M.G.D. Gololo[34c], A. Golub[141], D. Golubkov[38], J.P. Gombas[108], A. Gomes[132a,132b], G. Gomes Da Silva[146], A.J. Gomez Delegido[37], R. Gonçalo[132a], L. Gonella[21], A. Gongadze[154c], F. Gonnella[21], J.L. Gonski[148], R.Y. González Andana[52], S. González de la Hoz[168], M. V. Gonzalez Rodrigues[48], R. Gonzalez Suarez[166], S. Gonzalez-Sevilla[56], L. Goossens[37], B. Gorini[37], E. Gorini[70a,70b], A. Gorišek[94], T.C. Gosart[130], A.T. Goshaw[51], M.I. Gostkin[39], S. Goswami[123], C.A. Gottardo[37], S. A. Gotz[110], M. Gouighri[36b], A.G. Goussiou[141], N. Govender[34c], R. P. Grabarczyk[128], I. Grabowska-Bold[86a], K. Graham[35], E. Gramstad[127], S. Grancagnolo[70a,70b], C.M. Grant[1], P.M. Gravila[28f], F.G. Gravili[70a,70b], H.M. Gray[18a], M. Greco[111], M. J. Green[1], C. Grefe[25], A. S. Grefsrud[17], I.M. Gregor[48], K.T. Greif[164], P. Grenier[148], S.G. Grewe[111], A.A. Grillo[138], K. Grimm[32], S. Grinstein[13,u], J.-F. Grivaz[66], E. Gross[174], J. Grosse-Knetter[55], L.H. Grossman[18b], L. Guan[107], G. Guerrieri[37], R. Guevara[127], R. Gugel[101], J.A.M. Guhit[107], A. Guida[19], E. Guilloton[172], S. Guindon[37], F. Guo[14,113c], J. Guo[143a], L. Guo[48], L. Guo[113b,v], Y. Guo[107], Y. Guo[42], A. Gupta[49], R. Gupta[131], S. Gupta[27], S. Gurbuz[25], S.S. Gurdasani[48], G. Gustavino[75a,75b], P. Gutierrez[122], L.F. Gutierrez Zagazeta[130], M. Gutsche[50], C. Gutschow[97], C. Gwenlan[128], C.B. Gwilliam[93], E.S. Haaland[127], A. Haas[119], M. Habedank[59], C. Haber[18a], H.K. Hadavand[8], A. Haddad[41], A. Hadef[50], A.I. Hagan[92], J. J. Hahn[146], E.H. Haines[97], M. Haleem[171], J. Haley[123], G.D. Hallewell[103], J.A. Hallford[48], K. Hamano[170], H. Hamdaoui[166], M. Hamer[25], S. E. D. Hammoud[66], E.J. Hampshire[96], J. Han[142a], L. Han[113a], L. Han[62], S. Han[14], K. Hanagaki[83], M. Hance[138], D.A. Hangal[42], H. Hanif[147], M.D. Hank[130], J.B. Hansen[43], P.H. Hansen[43], T. Harenberg[176], S. Harkusha[178], M.L. Harris[104], Y.T. Harris[25], J. Harrison[13], P.F. Harrison[172], M. L. E. Hart[97], N.M. Hartman[111], N.M. Hartmann[110], R. Z. Hasan[96,136], Y. Hasegawa[145], F. Haslbeck[128], S. Hassan[17], R. Hauser[108], M. Haviernik[135], C.M. Hawkes[21], R.J. Hawkings[37], Y. Hayashi[158], D. Hayden[108], C. Hayes[107], R.L. Hayes[116], C.P. Hays[128], J.M. Hays[95], H.S. Hayward[93], M. He[14,113c], Y. He[48], Y. He[97], N.B. Heatley[95], V. Hedberg[99], J. Heilman[35], S. Heim[48], T. Heim[18a], J.J. Heinrich[125], L. Heinrich[111], J. Hejbal[133], M. Helbig[50], A. Held[175], S. Hellesund[17], C.M. Helling[169], S. Hellman[47a,47b], A.M. Henriques Correia[37], H. Herde[99], Y. Hernández Jiménez[150], L.M. Herrmann[25], T. Herrmann[50], G. Herten[54], R. Hertenberger[110], L. Hervas[37], M.E. Hesping[101], N.P. Hessey[161a], J. Hessler[111], M. Hidaoui[36b], N. Hidic[135], E. Hill[160], T. S. Hillersoy[17], S.J. Hillier[21], J.R. Hinds[108], F. Hinterkeuser[25], M. Hirose[126],

JHEP07(2026)107

S. Hirose[162], D. Hirschbuehl[176], T.G. Hitchings[102], B. Hiti[94], J. Hobbs[150], R. Hobincu[28e], N. Hod[174], A.M. Hodges[167], M.C. Hodgkinson[144], B.H. Hodkinson[128], A. Hoecker[37], D. D. Hofer[107], J. Hofer[168], J. Hofner[101], M. Holzbock[37], L.B.A.H. Hommels[33], V. Homsak[128], J. J. Hong[68], T.M. Hong[131], B.H. Hooberman[167], W.H. Hopkins[6], M. C. Hoppesch[167], Y. Horii[112], M. E. Horstmann[111], S. Hou[153], M. R. Housenga[167], J. Howarth[59], J. Hoya[6], M. Hrabovsky[124], T. Hryn'ova[4], P.J. Hsu[65], S.-C. Hsu[141], T. Hsu[66], M. Hu[18a], Q. Hu[62], S. Huang[33], X. Huang[14,113c], Y. Huang[135], Y. Huang[113b], Y. Huang[14], Z. Huang[66], Z. Hubacek[134], F. Huegging[25], T.B. Huffman[128], M. Hufnagel Maranha De Faria[82a], C. A. Hugli[48], M. Huhtinen[37], S.K. Huiberts[127], R. Hulsken[105], C. E. Hultquist[18a], D.L. Humphreys[104], N. Huseynov[12], J. Huston[108], B. Huth[37], J. Huth[61], L. Huth[48], R. Hyneman[7], G. Iacobucci[56], G. Iakovidis[30], L. Iconomidou-Fayard[66], J. P. Iddon[37], P. Iengo[72a,72b], Y. Iiyama[158], T. Iizawa[158], Y. Ikegami[83], D. Iliadis[157], N. Ilic[160], H. Imam[36a], G. Inacio Goncalves[82d], S. A. Infante Cabanas[139c], T. Ingebretsen Carlson[47a,47b], J. M. Inglis[95], G. Introzzi[73a,73b], M. Iodice[77a], V. Ippolito[75a,75b], R. K. Irwin[93], M. Ishino[158], W. Islam[175], C. Issever[19], S. Istin[22a,w], K. Itabashi[126], H. Ito[173], R. Iuppa[78a,78b], A. Ivina[174], S. Izumiyama[112], V. Izzo[72a], P. Jacka[134], P. Jackson[1], P. Jain[48], K. Jakobs[54], T. Jakoubek[174], J. Jamieson[59], W. Jang[158], S. Jankovych[135], M. Javurkova[104], P. Jawahar[102], L. Jeanty[125], J. Jejelava[154a,x], P. Jenni[54,y], C.E. Jessiman[35], C. Jia[142a], H. Jia[169], J. Jia[150], X. Jia[111,113c], Z. Jia[113a], C. Jiang[52], Q. Jiang[64b], S. Jiggins[48], M. Jimenez Ortega[168], J. Jimenez Pena[13], S. Jin[113a], A. Jinaru[28b], O. Jinnouchi[140], P. Johansson[144], K.A. Johns[7], J.W. Johnson[138], F. A. Jolly[48], D.M. Jones[151], E. Jones[48], K.S. Jones[8], P. Jones[33], R.W.L. Jones[92], T.J. Jones[93], H.L. Joos[55], R. Joshi[121], J. Jovicevic[16], X. Ju[18a], J.J. Junggeburth[37], T. Junkermann[63a], A. Juste Rozas[13,u], M.K. Juzek[87], S. Kabana[139f], A. Kaczmarska[87], S. A. Kadir[148], M. Kado[111], H. Kagan[121], M. Kagan[148], A. Kahn[130], C. Kahra[101], T. Kaji[158], E. Kajomovitz[155], N. Kakati[174], N. Kakoty[13], I. Kalaitzidou[54], S. Kandel[8], N. Kanellos[10], N.J. Kang[138], D. Kar[34j,†], E. Karentzos[25], K. Karki[8], O. Karkout[116], S.N. Karpov[39], Z.M. Karpova[39], V. Kartvelishvili[92,154b], A.N. Karyukhin[38], E. Kasimi[157], J. Katzy[48], S. Kaur[35], K. Kawade[145], M.P. Kawale[122], C. Kawamoto[88], T. Kawamoto[62], E.F. Kay[37], S. Kazakos[108], V.F. Kazanin[38], J.M. Keaveney[34a], R. Keeler[170], G.V. Kehris[61], J.S. Keller[35], J. M. Kelly[170], J.J. Kempster[151], O. Kepka[133], J. Kerr[161b], B.P. Kerridge[136], B.P. Kerševan[94], L. Keszeghova[29a], R. A. Khan[131], A. Khanov[123], A.G. Kharlamov[38], T. Kharlamova[38], E.E. Khoda[141], M. Kholodenko[132a], T.J. Khoo[19], G. Khoriauli[171], Y. Khoulaki[36a], Y.A.R. Khwaira[129], B. Kibirige[34j], D. Kim[6], D.W. Kim[18b], Y.K. Kim[40], N. Kimura[97], M.K. Kingston[55], A. Kirchhoff[55], C. Kirfel[25], F. Kirfel[25], J. Kirk[136], A.E. Kiryunin[111], S. Kita[162], O. Kivernyk[25], M. Klassen[163], C. Klein[35], L. Klein[171], M.H. Klein[45], S.B. Klein[56], U. Klein[93], A. Klimentov[30], T. Klioutchnikova[37], P. Kluit[116], S. Kluth[111], E. Kneringer[79], T.M. Knight[160], A. Knue[49], M. Kobel[50], D. Kobylianskii[174], S.F. Koch[128], M. Kocian[148], P. Kodyš[135], D.M. Koeck[125], T. Koffas[35], O. Kolay[50], I. Koletsou[4], T. Komarek[87], K. Köneke[55], A.X.Y. Kong[1], T. Kono[120], N. Konstantinidis[97], P. Kontaxakis[56], B. Konya[99], R. Kopeliansky[42], S. Koperny[86a], R. Koppenhofer[54], K. Korcyl[87], K. Kordas[157,z],

A. Korn[97], S. Korn[55], I. Korolkov[13], N. Korotkova[38], B. Kortman[116], O. Kortner[111], S. Kortner[111], W.H. Kostecka[117], M. Kostov[29a], V.V. Kostyukhin[146], A. Kotsokechagia[37], A. Kotwal[51], A. Koulouris[37], A. Kourkoumeli-Charalampidi[73a,73b], C. Kourkoumelis[9], E. Kourlitis[111], O. Kovanda[125], R. Kowalewski[170], W. Kozanecki[125], A.S. Kozhin[38], V.A. Kramarenko[38], G. Kramberger[94], P. Kramer[25], M.W. Krasny[129], A. Krasznahorkay[104], A. C. Kraus[117], J.W. Kraus[176], J.A. Kremer[48], N. B. Krengel[146], T. Kresse[50], L. Kretschmann[176], J. Kretzschmar[93], P. Krieger[160], K. Krizka[21], K. Kroeninger[49], H. Kroha[111], J. Kroll[133], J. Kroll[130], K.S. Krowpman[108], U. Kruchonak[39], H. Krüger[25], N. Krumnack[80], M.C. Kruse[51], O. Kuchinskaia[39], S. Kuday[3a], S. Kuehn[37], R. Kuesters[54], T. Kuhl[48], V. Kukhtin[39], Y. Kulchitsky[39], S. Kuleshov[139d,139b], J. Kull[1], E. V. Kumar[110], M. Kumar[34j], N. Kumari[48], P. Kumari[161b], A. Kupco[133], A. Kupich[38], O. Kuprash[54], H. Kurashige[85], L.L. Kurchaninov[161a], O. Kurdysh[4], A. Kurova[38], M. Kuze[140], A.K. Kvam[104], J. Kvita[124], N.G. Kyriacou[141], M. Laassiri[30], C. Lacasta[168], F. Lacava[75a,75b], H. Lacker[19], D. Lacour[129], N.N. Lad[97], E. Ladygin[39], A. Lafarge[41], B. Laforge[129], T. Lagouri[177], F.Z. Lahbabi[36a], S. Lai[55,37], W. S. Lai[97], I.K. Lakomiec[55], J.E. Lambert[170], S. Lammers[68], W. Lampl[7], C. Lampoudis[157,z], G. Lamprinoudis[171], A.N. Lancaster[117], E. Lançon[30], U. Landgraf[54], M.P.J. Landon[95], V.S. Lang[54], A.J. Lankford[164], F. Lanni[37], C. S. Lantz[167], K. Lantzsch[25], A. Lanza[73a], M. Lanzac Berrocal[168], J.F. Laporte[137], T. Lari[71a], D. Larsen[17], L. Larson[11], F. Lasagni Manghi[24b], M. Lassnig[37], S.D. Lawlor[144], R. Lazaridou[164], M. Lazzaroni[71a,71b], E. T. T. Le[164], H. D. M. Le[108], E.M. Le Boulicaut[177], L.T. Le Pottier[18a], B. Leban[24b,24a], F. Ledroit-Guillon[60], T.F. Lee[161b], L.L. Leeuw[34c], M. Lefebvre[170], C. Leggett[18a], G. Lehmann Miotto[37], M. Leigh[56], W.A. Leight[104], W. Leinonen[115], A. Leisos[157,aa], M.A.L. Leite[82c], C.E. Leitgeb[19], R. Leitner[135], K.J.C. Leney[45], T. Lenz[25], S. Leone[74a], C. Leonidopoulos[52], A. Leopold[149], J. LePage-Bourbonnais[35], R. Les[108], C.G. Lester[33], M. Levchenko[38], J. Levêque[4], L.J. Levinson[174], G. Levrini[24b,24a], M.P. Lewicki[87], C. Lewis[141], D.J. Lewis[4], L. Lewitt[144], A. Li[30], B. Li[142a], C-Q. Li[111], C. Li[107], H. Li[142a], H. Li[102], H. Li[15], H. Li[62], H. Li[142a], J. Li[143a], K. Li[14], L. Li[143a], R. Li[177], S. Li[14,113c], S. Li[143b,143a], T. Li[5], X. Li[105], Y. Li[14], Z. Li[158], Z. Li[14,113c], Z. Li[62], S. Liang[14,113c], Z. Liang[14], M. Liberatore[137], B. Liberti[76a], G. B. Libotte[82d], K. Lie[64c], J. Lieber Marin[82e], H. Lien[68], H. Lin[107], S. F. Lin[150], L. Linden[110], R.E. Lindley[7], J.H. Lindon[37], J. Ling[61], E. Lipeles[130], A. Lipniacka[17], A. Lister[169], J.D. Little[68], B. Liu[14], B.X. Liu[113b], D. Liu[155], D. Liu[138], E. H. L. Liu[21], J.K.K. Liu[119], K. Liu[143b], K. Liu[143b,143a], M. Liu[62], M.Y. Liu[62], P. Liu[14], Q. Liu[148], S. Liu[150], X. Liu[142a], Y. Liu[113b,113c], Y. Liu[167], Y.L. Liu[142a], Y.W. Liu[62], Z. Liu[66,ab], S.L. Lloyd[95], E.M. Lobodzinska[48], P. Loch[7], E. Lodhi[160], K. Lohwasser[144], E. Loiacono[48], J. D. Lomas[21], J.D. Long[42], I. Longarini[164], R. Longo[167], A. Lopez Solis[13], N.A. Lopez-canelas[7], N. Lorenzo Martinez[4], A.M. Lory[110], M. Losada[118a], G. Löschcke Centeno[4], X. Lou[47a,47b], X. Lou[14,113c], A. Lounis[66], P.A. Love[92], M. Lu[66], S. Lu[130], Y.J. Lu[153], H.J. Lubatti[141], C. Luci[75a,75b], F.L. Lucio Alves[113a], F. Luehring[68], B. S. Lunday[130], O. Lundberg[149], J. Lunde[37], N.A. Luongo[6], M.S. Lutz[37], A.B. Lux[26], D. Lynn[30], R. Lysak[133], V. Lysenko[134], E. Lytken[99],

V. Lyubushkin[39], T. Lyubushkina[39], M.M. Lyukova[150], H. Ma[30], K. Ma[62], L.L. Ma[142a], W. Ma[62], Y. Ma[123], J.C. MacDonald[101], B. Maček[94], P.C. Machado De Abreu Farias[82e], D. Macina[37], R. Madar[41], T. Madula[97], J. Maeda[85], T. Maeno[30], P.T. Mafa[34c,ac], H. Maguire[144], M. Maheshwari[33], V. Maiboroda[66], A. Maio[132a,132b,132d], K. Maj[86a], O. Majersky[48], S. Majewski[125], R. Makhmanazarov[38], N. Makovec[66], V. Maksimovic[16], B. Malaescu[129], J. Malamant[127], Pa. Malecki[87], V.P. Maleev[38], F. Malek[60,ad], M. Mali[94], D. Malito[96], A. Maloizel[5], S. Maltezos[10], A. Malvezzi Lopes[82d], S. Malyukov[39], J. Mamuzic[94], G. Mancini[53], M. N. Mancini[27], G. Manco[73a,73b], J.P. Mandalia[95], S.S. Mandarry[151], I. Mandić[94], L. Manhaes de Andrade Filho[82a], I.M. Maniatis[174], J. Manjarres Ramos[90], D.C. Mankad[174], A. Mann[110], T. Manoussos[37], M.N. Mantinan[40], S. Manzoni[37], L. Mao[143a], X. Mapekula[34c], A. Marantis[157], R.R. Marcelo Gregorio[95], G. Marchiori[5], C. Marcon[71a], E. Maricic[16], M. Marinescu[48], S. Marium[48], M. Marjanovic[122], A. Markhoos[54], M. Markovitch[66], M. K. Maroun[104], M. C. Marr[147], G. T. Marsden[102], E.J. Marshall[92], Z. Marshall[18a], S. Marti-Garcia[168], J. Martin[97], T.A. Martin[136], V.J. Martin[52], B. Martin dit Latour[17], S. Martin-Haugh[136], L. Martinelli[75a,75b], M. Martinez[13,u], P. Martinez Agullo[168], V.I. Martinez Outschoorn[104], P. Martinez Suarez[37], G. Martinovicova[135], V.S. Martoiu[28b], A.C. Martyniuk[97], A. Marzin[37], D. Mascione[78a,78b], L. Masetti[101], J. Masik[102], A.L. Maslennikov[39], S.L. Mason[42], P. Massarotti[72a,72b], P. Mastrandrea[74a,74b], A. Mastroberardino[44b,44a], T. Masubuchi[126], T.T. Mathew[125], J. Matousek[135], D.M. Mattern[49], K. Mauer[48], J. Maurer[28b], T. Maurin[59], A.J. Maury[66], C. Mavungu Tsava[103], D.A. Maximov[38], A. E. May[102], E. Mayer[41], R. Mazini[34j], I. Maznas[117], S.M. Mazza[138], E. Mazzeo[37], J.P. Mc Gowan[170], S.P. Mc Kee[107], C.A. Mc Lean[6], C.C. McCracken[169], E.F. McDonald[106], A.E. McDougall[116], L. F. Mcelhinney[92], J.A. Mcfayden[151], R.P. McGovern[130], R.P. Mckenzie[34j], T.C. Mclachlan[48], D.J. Mclaughlin[97], S.J. McMahon[136], C.M. Mcpartland[93], R.A. McPherson[170,n], S. Mehlhase[110], A. Mehta[93], D. Melini[168], B.R. Mellado Garcia[34j], A.H. Melo[55], F. Meloni[48], A.M. Mendes Jacques Da Costa[102], L. Meng[92], S. Menke[111], M. Mentink[37], E. Meoni[44b,44a], G. Mercado[117], S. Merianos[157], C. Merlassino[69a,69c], C. Meroni[71a,71b], J. Metcalfe[6], A.S. Mete[6], E. Meuser[101], C. Meyer[68], J-P. Meyer[137], Y. Miao[113a], R.P. Middleton[136], M. Mihovilovic[66], L. Mijović[52], G. Mikenberg[174], M. Mikestikova[133], M. Mikuž[94], H. Mildner[101], A. Milic[37], D.W. Miller[40], E. H. Miller[148], A. Milov[174], D.A. Milstead[47a,47b], T. Min[113a], A.A. Minaenko[38], I.A. Minashvili[154b], A.I. Mincer[119], B. Mindur[86a], M. Mineev[39], Y. Mino[88], L.M. Mir[13], M. Miralles Lopez[59], M. Mironova[18a], M. Missio[41], A. Mitra[172], V.A. Mitsou[168], Y. Mitsumori[112], O. Miu[160], P.S. Miyagawa[95], T. Mkrtchyan[37], M. Mlinarevic[97], T. Mlinarevic[97], M. Mlynarikova[135], L. Mlynarska[86a], C. Mo[143a], S. Mobius[20], M. H. Mohamed Farook[114], S. Mohapatra[42], M.F. Mohd Soberi[52], S. Mohiuddin[123], G. Mokgatitswane[34j], L. Moleri[174], U. Molinatti[128], L.G. Mollier[20], B. Mondal[133], S. Mondal[134], K. Mönig[48], E. Monnier[103], L. Monsonis Romero[168], J. Montejo Berlingen[13], A. Montella[47a,47b], M. Montella[121], F. Montereali[77a,77b], F. Monticelli[91], S. Monzani[69a,69c], A. Morancho Tarda[43], N. Morange[66], A.L. Moreira De Carvalho[48], M. Moreno Llácer[168], C. Moreno Martinez[56], J.M. Moreno Perez[23b], P. Morettini[57b], S. Morgenstern[37], M. Morii[61], M. Morinaga[158],

M. Moritsu[89], F. Morodei[75a,75b], P. Moschovakos[37], B. Moser[54], M. Mosidze[154b], T. Moskalets[45], P. Moskvitina[115], J. Moss[32], P. Moszkowicz[86a], T. Motta Quirino[82d], A. Moussa[36d], Y. Moyal[174], H. Moyano Gomez[13], E.J.W. Moyse[104], T.G. Mroz[87], S. Muanza[103], M. Mucha[25], J. Mueller[131], G.A. Mullier[166], A.J. Mullin[33], J.J. Mullin[51], A.C. Mullins[45], A.E. Mulski[61], D.P. Mungo[160], D. Munoz Perez[168], F.J. Munoz Sanchez[102], W.J. Murray[172,136], M. Muškinja[94], C. Mwewa[48], A.G. Myagkov[38,j], A.J. Myers[8], G. Myers[107], M. Myska[134], B.P. Nachman[148], K. Nagai[128], K. Nagano[83], R. Nagasaka[158], J.L. Nagle[30,ae], E. Nagy[103], A.M. Nairz[37], Y. Nakahama[83], K. Nakamura[83], K. Nakkalil[5], A. Nandi[63b], H. Nanjo[126], E.A. Narayanan[45], Y. Narukawa[158], I. Naryshkin[38], L. Nasella[71a,71b], S. Nasri[118b], C. Nass[25], G. Navarro[23a], A. Nayaz[19], P.Y. Nechaeva[38], S. Nechaeva[24b,24a], F. Nechansky[133], L. Nedic[128], T.J. Neep[21], A. Negri[73a,73b], M. Negrini[24b], C. Nellist[116], C. Nelson[105], K. Nelson[107], S. Nemecek[133], M. Nessi[37,af], M.S. Neubauer[167], J. Newell[93], P.R. Newman[21], C.W. Ng[131], Y.W.Y. Ng[167], B. Ngair[118a], H.D.N. Nguyen[109], J.D. Nichols[122], R.B. Nickerson[128], R. Nicolaidou[137], J. Nielsen[138], M. Niemeyer[55], J. Niermann[37], N. Nikiforou[37], V. Nikolaenko[38,j], I. Nikolic-Audit[129], P. Nilsson[30], I. Ninca[48], G. Ninio[156], A. Nisati[75a], R. Nisius[111], N. Nitika[174], E.K. Nkadimeng[34b], T. Nobe[158], D. Noll[148], T. Nommensen[152], M.B. Norfolk[144], B.J. Norman[35], L.C. Nosler[18a], M. Noury[36a], J. Novak[94], T. Novak[94], P. Novotny[174], R. Novotny[134], L. Nozka[124], K. Ntekas[164], D. Ntounis[148], N.M.J. Nunes De Moura Junior[82b], A.P. O'Neill[20], J. Ocariz[129], I. Ochoa[132a], A. Odella Rodriguez[13], S. Oerdek[48], J.T. Offermann[40], A. Ogrodnik[87], A. Oh[102], C.C. Ohm[149], H. Oide[83], M.L. Ojeda[37], Y. Okumura[158], L.F. Oleiro Seabra[132a], I. Oleksiyuk[56], G. Oliveira Correa[13], D. Oliveira Damazio[30], J.L. Oliver[1], R. Omar[68], Ö.O. Öncel[54], Y. Onoda[140], A. Onofre[132a,132e,ag], P.U.E. Onyisi[11], M.J. Oreglia[40], D. Orestano[77a,77b], R. Orlandini[77a,77b], R.S. Orr[160], L.M. Osojnak[42], Y. Osumi[112], G. Otero y Garzón[31], H. Otono[89], M. Ouchrif[36d], F. Ould-Saada[127], T. Ovsiannikova[141], M. Owen[59], R.E. Owen[136], V.E. Ozcan[22a], F. Ozturk[87], N. Ozturk[8], S. Ozturk[81], H.A. Pacey[128], K. Pachal[161a], A. Pacheco Pages[13], C. Padilla Aranda[13], G. Padovano[75a,75b], S. Pagan Griso[18a], J. Pampel[25], J. Pan[177], D.K. Panchal[11], C.E. Pandini[60], J.G. Panduro Vazquez[136], H.D. Pandya[1], H. Pang[137], P. Pani[48], G. Panizzo[69a,69c], L. Panwar[129], L. Paolozzi[56], S. Parajuli[167], A. Paramonov[6], C. Paraskevopoulos[53], D. Paredes Hernandez[64b], S.R. Paredes Saenz[52], A. Pareti[73a,73b], K.R. Park[42], T.H. Park[111], F. Parodi[57b,57a], J.A. Parsons[42], U. Parzefall[54], B. Pascual Dias[41], L. Pascual Dominguez[100], E. Pasqualucci[75a], S. Passaggio[57b], F. Pastore[96], P. Patel[87], U.M. Patel[51], J.R. Pater[102], T. Pauly[37], F. Pauwels[135], C.I. Pazos[163], M. Pedersen[127], R. Pedro[132a], S.V. Peleganchuk[38], O. Penc[133], S. Peng[15], G. D. Penn[177], K.E. Penski[110], M. Penzin[38], B.S. Peralva[82d], A.P. Pereira Peixoto[141], L. Pereira Sanchez[148], D.V. Perepelitsa[30,ae], G. Perera[104], E. Perez Codina[37], M. Perganti[10], H. Pernegger[37], S. Perrella[75a,75b], K. Peters[48], R.F.Y. Peters[102], B.A. Petersen[37], T.C. Petersen[43], E. Petit[103], V. Petousis[134], A. R. Petri[71a,71b], C. Petridou[157,z], T. Petru[135], M. Pettee[18a], A. Petukhov[81], K. Petukhova[37], R. Pezoa[139g], L. Pezzotti[24b,24a], G. Pezzullo[177], L. Pfaffenbichler[37], A. J. Pfleger[79], T. Pham[106], T.M. Pham[175], P.W. Phillips[136],

G. Piacquadio[150], E. Pianori[18a], F. Piazza[125], R. Piegaia[31], D. Pietreanu[28b], A.D. Pilkington[102], M. Pinamonti[69a,69c], J.L. Pinfold[2], G. Pinheiro Matos[42], B.C. Pinheiro Pereira[132a], J. Pinol Bel[13], A. E. Pinto Pinoargote[129], L. Pintucci[69a,69c], K. M. Piper[151], A. Pirttikoski[56], D.A. Pizzi[35], L. Pizzimento[64b], A. Plebani[33], M.-A. Pleier[30], V. Pleskot[135], E. Plotnikova[39], G. Poddar[95], R. Poettgen[99], L. Poggioli[129], S. Polacek[135], G. Polesello[73a], A. Poley[147], A. Polini[24b], C.S. Pollard[172], Z.B. Pollock[121], E. Pompa Pacchi[122], N. I. Pond[97], D. Ponomarenko[68], L. Pontecorvo[37], S. Popa[28a], G.A. Popeneciu[28d], A. Poreba[37], D.M. Portillo Quintero[161a], S. Pospisil[134], M. A. Postill[144], P. Postolache[28c], K. Potamianos[172], P.A. Potepa[86a], I.N. Potrap[39], C.J. Potter[33], H. Potti[152], J. Poveda[168], M.E. Pozo Astigarraga[37], R. Pozzi[37], A. Prades Ibanez[76a,76b], S.R. Pradhan[144], J. Pretel[170], D. Price[102], M. Primavera[70a], L. Primomo[69a,69c], M.A. Principe Martin[100], R. Privara[124], T. Procter[86b], M.L. Proffitt[141], N. Proklova[130], K. Prokofiev[64c], G. Proto[111], J. Proudfoot[6], M. Przybycien[86a], W.W. Przygoda[86b], A. Psallidas[46], J.E. Puddefoot[144], D. Pudzha[53], H. I. Purnell[1], D. Pyatiizbyantseva[115], J. Qian[107], R. Qian[108], D. Qichen[128], Y. Qin[13], T. Qiu[52], A. Quadt[55], M. Queitsch-Maitland[102], G. Quetant[56], R.P. Quinn[169], G. Rabanal Bolanos[61], D. Rafanoharana[111], F. Raffaeli[76a,76b], F. Ragusa[71a,71b], J.L. Rainbolt[40], S. Rajagopalan[30], E. Ramakoti[39], L. Rambelli[57b,57a], I.A. Ramirez-Berend[35], K. Ran[107,113c], D. S. Rankin[130], N.P. Rapheeha[34j], H. Rasheed[28b], A. Rastogi[18a], S. Rave[101], S. Ravera[57b,57a], B. Ravina[37], I. Ravinovich[174], M. Raymond[37], A.L. Read[127], N.P. Readioff[144], D.M. Rebuzzi[73a,73b], A. S. Reed[59], K. Reeves[27], D. Reikher[37], A. Rej[49], C. Rembser[37], H. Ren[62], M. Renda[28b], F. Renner[48], A.G. Rennie[59], M. Repik[56], A.L. Rescia[57b,57a], S. Resconi[71a], M. Ressegotti[57b], S. Rettie[116], W.F. Rettie[35], M. M. Revering[33], E. Reynolds[18a], O.L. Rezanova[39], P. Reznicek[135], H. Riani[36d], N. Ribaric[51], B. Ricci[69a,69c], E. Ricci[78a,78b], R. Richter[111], S. Richter[47a,47b], E. Richter-Was[86b], M. Ridel[129], S. Ridouani[36d], P. Rieck[119], P. Riedler[37], E.M. Riefel[47a,47b], J. O. Rieger[116], M. Rijssenbeek[150], M. Rimoldi[34c], L. Rinaldi[24b,24a], P. Rincke[166,55], G. Ripellino[166], I. Riu[13], J.C. Rivera Vergara[170], F. Rizatdinova[123], E. Rizvi[95], B.R. Roberts[40], S.S. Roberts[138], D. Robinson[33], A. Robson[59], A. Rocchi[76a,76b], C. Roda[74a,74b], F.A. Rodriguez[117], S. Rodriguez Bosca[37], Y. Rodriguez Garcia[23a], A.M. Rodríguez Vera[117], S. Roe[37], J.T. Roemer[37], O. Røhne[127], R.A. Rojas[37], C.P.A. Roland[129], A. Romaniouk[79], E. Romano[73a,73b], M. Romano[24b], A.C. Romero Hernandez[167], N. Rompotis[93], L. Roos[129], S. Rosati[75a], B.J. Rosser[40], E. Rossi[128], E. Rossi[72a,72b], L.P. Rossi[61], L. Rossini[54], R. Rosten[121], M. Rotaru[28b], R. Roth[37], D. Rousseau[66], D. Rousso[48], S. Roy-Garand[160], A. Rozanov[103], Z. M. A. Rozario[59], Y. Rozen[155], A. Rubio Jimenez[168], V.H. Ruelas Rivera[19], T.A. Ruggeri[1], A. Ruggiero[128], A. Ruiz-Martinez[168], A. Rummler[37], G.B. Rupnik Boero[37], Z. Rurikova[54], N.A. Rusakovich[39], S. Ruscelli[49], H.L. Russell[170], G. Russo[75a,75b], J.P. Rutherfoord[7], S. Rutherford Colmenares[33], M. Rybar[135], P. Rybczynski[86a], A. Ryzhov[45], H.F-W. Sadrozinski[138], F. Safai Tehrani[75a], S. Saha[1], M. Sahinsoy[81], B. Sahoo[174], A. Saibel[168], B. T. Saifuddin[122], M. Saimpert[137], G.T. Saito[82c], M. Saito[158], T. Saito[158], A. Sala[71a,71b], A. Salnikov[148], J. Salt[168], A. Salvador Salas[156], F. Salvatore[151], A. Salzburger[37], D. Sammel[54], E. Sampson[92],

D. Sampsonidis[157,z], D. Sampsonidou[125], M.A.A. Samy[59], J. Sánchez[168], V. Sanchez Sebastian[168], H. Sandaker[127], C.O. Sander[48], J.A. Sandesara[175], M. Sandhoff[176], C. Sandoval[23b], L. Sanfilippo[63a], D.P.C. Sankey[136], T. Sano[88], A. Sansoni[53], M. Santana Queiroz[18b], L. Santi[37], C. Santoni[41], H. Santos[132a,132b], A. Santra[174], E. Sanzani[24b,24a], K.A. Saoucha[84b], J.G. Saraiva[132a,132d], J. Sardain[7], O. Sasaki[83], K. Sato[162], C. Sauer[37], E. Sauvan[4], P. Savard[160,t], R. Sawada[158], C. Sawyer[136], L. Sawyer[98], A. M. Sayed[27], C. Sbarra[24b], A. Sbrizzi[24b,24a], T. Scanlon[97], J. Schaarschmidt[141], U. Schäfer[101], A.C. Schaffer[66,45], D. Schaile[110], R.D. Schamberger[150], C. Scharf[19], M.M. Schefer[20], V.A. Schegelsky[38], D. Scheirich[135], M. Schernau[139f], C. Scheulen[56], C. Schiavi[57b,57a], M. Schioppa[44b,44a], B. Schlag[148], S. Schlenker[37], J. Schmeing[176], E. Schmidt[111], M. A. Schmidt[176], K. Schmieden[25], C. Schmitt[101], N. Schmitt[101], S. Schmitt[48], N.A. Schneider[110], L. Schoeffel[137], A. Schoening[63b], P.G. Scholer[35], E. Schopf[146], M. Schott[25], S. Schramm[56], T. Schroer[56], H-C. Schultz-Coulon[63a], M. Schumacher[54], B.A. Schumm[138], Ph. Schune[137], H.R. Schwartz[7], A. Schwartzman[148], T.A. Schwarz[107], Ph. Schwemling[137], R. Schwienhorst[108], F.G. Sciacca[20], A. Sciandra[30], G. Sciolla[27], F. Scuri[74a], C.D. Sebastiani[37], K. Sedlaczek[117], S.C. Seidel[114], A. Seiden[138], B.D. Seidlitz[42], C. Seitz[48], J.M. Seixas[82b], G. Sekhniaidze[72a], L. Selem[60], N. Semprini-Cesari[24b,24a], A. Semushin[178], D. Sengupta[56], V. Senthilkumar[168], L. Serin[66], M. Sessa[72a,72b], H. Severini[122], F. Sforza[57b,57a], A. Sfyrla[56], Q. Sha[14], H. Shaddix[117], A.H. Shah[33], R. Shaheen[149], J.D. Shahinian[130], M. Shamim[37], L.Y. Shan[14], M. Shapiro[18a], A. Sharma[37], A.S. Sharma[169], P. Sharma[30], P.B. Shatalov[38], K. Shaw[151], S.M. Shaw[102], Q. Shen[14], D.J. Sheppard[147], P. Sherwood[97], L. Shi[97], X. Shi[14], S. Shimizu[83], I.P.J. Shipsey[128,†], S. Shirabe[89], M. Shiyakova[39,ah], M.J. Shochet[40], D.R. Shope[127], B. Shrestha[122], S. Shrestha[121,ai], I. Shreyber[39], M.J. Shroff[170], P. Sicho[133], A.M. Sickles[167], E. Sideras Haddad[34j,165], A. C. Sidley[116], A. Sidoti[24b], F. Siegert[50], Dj. Sijacki[16], F. Sili[62], J.M. Silva[52], I. Silva Ferreira[82b], M.V. Silva Oliveira[30], S.B. Silverstein[47a], S. Simion[66], R. Simoniello[37], E.L. Simpson[102], H. Simpson[151], L.R. Simpson[6], S. Simsek[81], S. Sindhu[55], P. Sinervo[160], S. Singh[30], S. N. Singh[27], S. Sinha[48], S. Sinha[102], M. Sioli[24b,24a], K. Sioulas[9], I. Siral[37], E. Sitnikova[48], J. Sjölin[47a,47b], A. Skaf[55], E. Skorda[21], P. Skubic[122], M. Slawinska[87], I. Slazyk[17], I. Sliusar[127], V. Smakhtin[174], B.H. Smart[136], S.Yu. Smirnov[139b], Y. Smirnov[34c], L.N. Smirnova[38,j], O. Smirnova[99], A.C. Smith[42], D.R. Smith[164], J.L. Smith[102], M. B. Smith[35], R. Smith[148], H. Smitmanns[101], M. Smizanska[92], K. Smolek[134], P. Smolyanskiy[134], A.A. Snesarev[39], H.L. Snoek[116], R. M. Snyder[51], S. Snyder[30], R. Sobie[170,n], A. Soffer[156], C.A. Solans Sanchez[37], E.Yu. Soldatov[39], U. Soldevila[168], A.A. Solodkov[34j], S. Solomon[27], A. Soloshenko[39], K. Solovieva[54], O.V. Solovyanov[41], P. Sommer[50], A. Sonay[13], A. Sopczak[134], A.L. Sopio[52], F. Sopkova[29b], J. D. Sorenson[114], I.R. Sotarriva Alvarez[140], V. Sothilingam[63a], O. J. Soto Sandoval[139c,139b], S. Sottocornola[68], R. Soualah[84a], Z. Soumaimi[36e], D. South[48], N. Soybelman[174], S. Spagnolo[70a,70b], D. Sperlich[54], B. Spisso[72a,72b], D.P. Spiteri[59], L. Splendori[103], M. Spousta[135], E.J. Staats[35], R. Stamen[63a], E. Stanecka[87], W. Stanek-Maslouska[48], M.V. Stange[50], B. Stanislaus[18a], M.M. Stanitzki[48], E.A. Starchenko[38], G.H. Stark[138],

J. Stark[90], P. Staroba[133], P. Starovoitov[84b], R. Staszewski[87], C. Stauch[110], G. Stavropoulos[46], A. Stefl[37], A. Stein[101], P. Steinberg[30], B. Stelzer[147,161a], H.J. Stelzer[131], O. Stelzer[161a], H. Stenzel[58], T.J. Stevenson[151], G.A. Stewart[37], J.R. Stewart[123], G. Stoicea[28b], M. Stolarski[132a], S. Stonjek[111], A. Straessner[50], J. Strandberg[149], S. Strandberg[47a,47b], M. Stratmann[176], M. Strauss[122], T. Strebler[103], P. Strizenec[29b], R. Ströhmer[171], D.M. Strom[125], R. Stroynowski[45], A. Strubig[47a,47b], S.A. Stucci[30], B. Stugu[17], J. Stupak[122], N.A. Styles[48], D. Su[148], S. Su[62], X. Su[62], D. Suchy[29a], A. D. Sudhakar Ponnu[55], L. Sudit[174], K. Sugizaki[130], V.V. Sulin[38], D.M.S. Sultan[128], L. Sultanaliyeva[25], S. Sultansoy[3b], S. Sun[175], W. Sun[14], N. Sur[99], N. Suri Jr[177], M.R. Sutton[151], M. Svatos[133], P. N. Swallow[33], M. Swiatlowski[161a], A. Swoboda[37], I. Sykora[29a], M. Sykora[135], T. Sykora[135], D. Ta[101], K. Tackmann[48,aj], A. Taffard[164], R. Tafirout[161a], Y. Takubo[83], M. Talby[103], A.A. Talyshev[38], K.C. Tam[64b], N.M. Tamir[156], A. Tanaka[158], J. Tanaka[158], R. Tanaka[66], M. Tanasini[150], Z. Tao[169], S. Tapia Araya[139g], S. Tapprogge[101], A. Tarek Abouelfadl Mohamed[37], S. Tarem[155], K. Tariq[14], G. Tarna[37], G.F. Tartarelli[71a], M. J. Tartarin[90], P. Tas[135], M. Tasevsky[133], E. Tassi[44b,44a], A.C. Tate[167], Y. Tayalati[36e,ak], G.N. Taylor[106], W. Taylor[161b], R.J. Taylor Vara[168], A.S. Tegetmeier[90], P. Teixeira-Dias[96], J.J. Teoh[160], K. Terashi[158], J. Terron[100], S. Terzo[13], M. Testa[53], R.J. Teuscher[160,n], A. Thaler[79], O. Theiner[56], T. Theveneaux-Pelzer[103], D.W. Thomas[96], J.P. Thomas[21], E.A. Thompson[18a], P.D. Thompson[21], E. Thomson[130], R. E. Thornberry[45], C. Tian[62], Y. Tian[56], V. Tikhomirov[81], Yu.A. Tikhonov[39], S. Timoshenko[38], D. Timoshyn[135], E.X.L. Ting[1], P. Tipton[177], A. Tishelman-Charny[30], K. Todome[140], S. Todorova-Nova[135], L. Toffolin[69a,69c], M. Togawa[83], J. Tojo[89], S. Tokár[29a], O. Toldaiev[68], G. Tolkachev[103], M. Tomoto[83], L. Tompkins[148,al], E. Torrence[125], H. Torres[90], D. I. Torres Arza[139g], E. Torró Pastor[168], M. Toscani[31], C. Tosciri[40], M. Tost[11], D.R. Tovey[144], T. Trefzger[171], P.M. Tricarico[13], A. Tricoli[30], I.M. Trigger[161a], S. Trincaz-Duvoid[129], D.A. Trischuk[170], A. Tropina[39], D. Truncali[76a,76b], L. Truong[34c], M. Trzebinski[87], A. Trzupek[87], F. Tsai[150], M. Tsai[107], A. Tsiamis[157], P.V. Tsiareshka[39], S. Tsigaridas[161a], A. Tsirigotis[157,aa], V. Tsiskaridze[154a], E.G. Tskhadadze[154a], Y. Tsujikawa[88], I.I. Tsukerman[38], V. Tsulaia[18a], S. Tsuno[83], K. Tsuri[120], D. Tsybychev[150], Y. Tu[64b], A. Tudorache[28b], V. Tudorache[28b], S. B. Tuncay[128], S. Turchikhin[57b,57a], I. Turk Cakir[3a], R. Turra[71a], T. Turtuvshin[39,am], P.M. Tuts[42], S. Tzamarias[157,z], Y. Uematsu[83], F. Ukegawa[162], P.A. Ulloa Poblete[139c,139b], E.N. Umaka[30], G. Unal[37], A. Undrus[30], G. Unel[164], J. Urban[29b], P. Urrejola[139e], G. Usai[8], R. Ushioda[159], M. Usman[109], F. Ustuner[52], Z. Uysal[81], V. Vacek[134], B. Vachon[105], T. Vafeiadis[37], A. Vaitkus[97], C. Valderanis[110], E. Valdes Santurio[47a,47b], M. Valente[37], S. Valentinetti[24b,24a], A. Valero[168], E. Valiente Moreno[168], A. Vallier[90], J.A. Valls Ferrer[168], D. R. Van Arneman[116], A. Van Der Graaf[49], H. Z. Van Der Schyf[34j], P. Van Gemmeren[6], M. Van Rijnbach[37], S. Van Stroud[97], I. Van Vulpen[116], P. Vana[135], M. Vanadia[76a,76b], U. M. Vande Voorde[149], W. Vandelli[37], E.R. Vandewall[148], D. Vannicola[156], L. Vannoli[53], R. Vari[75a], M. Varma[177], E.W. Varnes[7], C. Varni[79], D. Varouchas[66], L. Varriale[168], K.E. Varvell[152], M.E. Vasile[28b], L. Vaslin[83], M. D. Vassilev[148], A. Vasyukov[39], L. M. Vaughan[123], R. Vavricka[135], T. Vazquez Schroeder[13], J. Veatch[32], V. Vecchio[102], M.J. Veen[104], I. Veliscek[30],

I. Velkovska[94], L.M. Veloce[160], F. Veloso[132a,132c], A.G. Veltman[52], S.H. Venetianer[163], S. Veneziano[75a], A. Ventura[70a,70b], A. Verbytskyi[111], M. Verducci[74a,74b], C. Vergis[95], M. Verissimo De Araujo[82b], W. Verkerke[116], J.C. Vermeulen[116], C. Vernieri[148], M. Vessella[164], M.C. Vetterli[147,t], A. Vgenopoulos[101], N. Viaux Maira[139g,an], T. Vickey[144], O.E. Vickey Boeriu[144], G.H.A. Viehhauser[128], L. Vigani[63b], M. Vigl[111], M. Villa[24b,24a], M. Villaplana Perez[168], E.M. Villhauer[40], E. Vilucchi[53], M. Vincent[168], M.G. Vincter[35], A. Visibile[116], A. Visive[116], C. Vittori[37], I. Vivarelli[24b,24a], M.I. Vivas Albornoz[48], E. Voevodina[111], F. Vogel[110], J.C. Voigt[50], P. Vokac[134], Yu. Volkotrub[86b], L. Vomberg[25], E. Von Toerne[25], B. Vormwald[37], K. Vorobev[51], M. Vos[168], K. Voss[146], M. Vozak[37], L. Vozdecky[122], N. Vranjes[16], M. Vranjes Milosavljevic[16], M. Vreeswijk[116], N.K. Vu[143b,143a], R. Vuillermet[37], O. Vujinovic[101], I. Vukotic[40], I. K. Vyas[35], J.F. Wack[33], S. Wada[162], C. Wagner[148], J.M. Wagner[18a], W. Wagner[176], S. Wahdan[176], H. Wahlberg[91], C. H. Waits[122], J. Walder[136], R. Walker[110], K. Walkingshaw Pass[59], W. Walkowiak[146], A. Wall[130], E.J. Wallin[99], T. Wamorkar[18a], K. Wandall-Christensen[168], A. Wang[62], A.Z. Wang[138], C. Wang[48], C. Wang[11], H. Wang[18a], J. Wang[64c], P. Wang[102], P. Wang[97], R. Wang[61], R. Wang[6], S. Wang[14], S.M. Wang[153], T. Wang[115], T. Wang[62], W. Wang[14], W.T. Wang[128], X. Wang[167], X. Wang[143a], X. Wang[48], Y. Wang[150], Y. Wang[62], Z. Wang[107], Z. Wang[143b], Z. Wang[107], C. Wanotayaroj[83], A. Warburton[105], A.L. Warnerbring[146], S. Waterhouse[96], A.T. Watson[21], H. Watson[52], M.F. Watson[21], E. Watton[37], G. Watts[141], B.M. Waugh[97], J. M. Webb[54], C. Weber[30], M.S. Weber[20], S.M. Weber[63a], C. Wei[62], Y. Wei[54], A.R. Weidberg[128], E.J. Weik[119], J. Weingarten[49], C. Weiser[54], C.J. Wells[48], T. Wenaus[30], T. Wengler[37], N.S. Wenke[111], N. Wermes[25], M. Wessels[63a], A.M. Wharton[92], A. White[8], A.S. White[61], M.J. White[1], D. Whiteson[164], L. Wickremasinghe[126], W. Wiedenmann[175], M. Wielers[136], R. Wierda[149], C. Wiglesworth[43], H.G. Wilkens[37], J. J. H. Wilkinson[33], D.M. Williams[42], H.H. Williams[130], S. Williams[33], S. Willocq[104], B.J. Wilson[102], D.J. Wilson[102], P.J. Windischhofer[40], F.I. Winkel[31], F. Winklmeier[125], B.T. Winter[54], M. Wittgen[148], M. Wobisch[98], T. Wojtkowski[60], Z. Wolffs[116], J. Wollrath[37], M.W. Wolter[87], H. Wolters[132a,132c], M.C. Wong[138], E.L. Woodward[42], S.D. Worm[48], B.K. Wosiek[87], K.W. Woźniak[87], S. Wozniewski[55], K. Wraight[59], C. Wu[160], C. Wu[21], J. Wu[158], M. Wu[113b], M. Wu[115], S. Wu[14,ao], S.L. Wu[175], X. Wu[62], Y. Wu[62], Y.Q. Wu[160], Z. Wu[4], Z. Wu[113a], J. Wuerzinger[111], T.R. Wyatt[102], B.M. Wynne[52], S. Xella[43], L. Xia[113a], M. Xie[62], A. Xiong[125], D. Xu[14], H. Xu[62], L. Xu[62], R. Xu[130], T. Xu[107], W. Xu[113a], Y. Xu[141], Z. Xu[52], R. Xue[131], B. Yabsley[152], S. Yacoob[34a], Y. Yamaguchi[83], E. Yamashita[158], H. Yamauchi[162], T. Yamazaki[18a], Y. Yamazaki[85], S. Yan[59], Z. Yan[104], H.J. Yang[143a,143b], H.T. Yang[62], S. Yang[62], T. Yang[64c], X. Yang[37], X. Yang[14], Y. Yang[158], Y. Yang[62], W-M. Yao[18a], C. L. Yardley[151], J. Ye[14], S. Ye[30], X. Ye[62], Y. Yeh[97], I. Yeletskikh[39], B. Yeo[18b], M.R. Yexley[97], T. P. Yildirim[128], K. Yorita[173], C. Young[148], C.J.S. Young[37], I.N.L. Young[59], N.D. Young[125], Y. Yu[62], J. Yuan[14,113c,ao], M. Yuan[107], R. Yuan[143b], L. Yue[97], M. Zaazoua[62], B. Zabinski[87], I. Zahir[36a], A. Zaio[57b,57a], Z.K. Zak[87], T. Zakareishvili[168], S. Zambito[56], J.A. Zamora Saa[139d], J. Zang[158], R. Zanzottera[71a,71b], O. Zaplatilek[134], C. Zeitnitz[176], H. Zeng[14], D.T. Zenger Jr[27], O. Zenin[38], T. Ženiš[29a], S. Zenz[95], D. Zerwas[66], D.F. Zhang[144],

JHEP07(2026)107

G. Zhang[14,ao], J. Zhang[142a], J. Zhang[6], L. Zhang[62], L. Zhang[113a], P. Zhang[14,113c], R. Zhang[113a], S. Zhang[90], T. Zhang[158], Y. Zhang[141], Y. Zhang[97], Y. Zhang[62], Y. Zhang[113a], Z. Zhang[18a], Z. Zhang[142a], Z. Zhang[66], H. Zhao[141], T. Zhao[142a], Y. Zhao[35], Z. Zhao[62], Z. Zhao[62], A. Zhemchugov[39], J. Zheng[113a], K. Zheng[167], X. Zheng[62], Z. Zheng[148], D. Zhong[167], B. Zhou[107], B. Zhou[143b,143a], H. Zhou[7], N. Zhou[143a], Y. Zhou[15], Y. Zhou[113a], Y. Zhou[7], J. Zhu[107], X. Zhu[143b], Y. Zhu[143a], Y. Zhu[62], X. Zhuang[14], K. Zhukov[68], N.I. Zimine[39], J. Zinsser[63b], M. Ziolkowski[146], L. Živković[16], A. Zoccoli[24b,24a], K. Zoch[61], A. Zografos[37], T.G. Zorbas[144], O. Zormpa[46], L. Zwalinski[37]

[1] *Department of Physics, University of Adelaide, Adelaide, Australia*
[2] *Department of Physics, University of Alberta, Edmonton AB, Canada*
[3a] *Department of Physics, Ankara University, Ankara, Türkiye*
[3b] *Division of Physics, TOBB University of Economics and Technology, Ankara, Türkiye*
[4] *LAPP, Université Savoie Mont Blanc, CNRS/IN2P3, Annecy, France*
[5] *APC, Université Paris Cité, CNRS/IN2P3, Paris, France*
[6] *High Energy Physics Division, Argonne National Laboratory, Argonne IL, U.S.A.*
[7] *Department of Physics, University of Arizona, Tucson AZ, U.S.A.*
[8] *Department of Physics, University of Texas at Arlington, Arlington TX, U.S.A.*
[9] *Physics Department, National and Kapodistrian University of Athens, Athens, Greece*
[10] *Physics Department, National Technical University of Athens, Zografou, Greece*
[11] *Department of Physics, University of Texas at Austin, Austin TX, U.S.A.*
[12] *Institute of Physics, Azerbaijan Academy of Sciences, Baku, Azerbaijan*
[13] *Institut de Física d'Altes Energies (IFAE), Barcelona Institute of Science and Technology, Barcelona, Spain*
[14] *Institute of High Energy Physics, Chinese Academy of Sciences, Beijing, China*
[15] *Physics Department, Tsinghua University, Beijing, China*
[16] *Institute of Physics, University of Belgrade, Belgrade, Serbia*
[17] *Department for Physics and Technology, University of Bergen, Bergen, Norway*
[18a] *Physics Division, Lawrence Berkeley National Laboratory, Berkeley CA, U.S.A.*
[18b] *University of California, Berkeley CA, U.S.A.*
[19] *Institut für Physik, Humboldt Universität zu Berlin, Berlin, Germany*
[20] *Albert Einstein Center for Fundamental Physics and Laboratory for High Energy Physics, University of Bern, Bern, Switzerland*
[21] *School of Physics and Astronomy, University of Birmingham, Birmingham, U.K.*
[22a] *Department of Physics, Bogazici University, Istanbul, Türkiye*
[22b] *Department of Physics Engineering, Gaziantep University, Gaziantep, Türkiye*
[22c] *Department of Physics, Istanbul University, Istanbul, Türkiye*
[23a] *Facultad de Ciencias y Centro de Investigaciónes, Universidad Antonio Nariño, Bogotá, Colombia*
[23b] *Departamento de Física, Universidad Nacional de Colombia, Bogotá, Colombia*
[24a] *Dipartimento di Fisica e Astronomia A. Righi, Università di Bologna, Bologna, Italy*
[24b] *INFN Sezione di Bologna, Italy*
[25] *Physikalisches Institut, Universität Bonn, Bonn, Germany*
[26] *Department of Physics, Boston University, Boston MA, U.S.A.*
[27] *Department of Physics, Brandeis University, Waltham MA, U.S.A.*
[28a] *Transilvania University of Brasov, Brasov, Romania*
[28b] *Horia Hulubei National Institute of Physics and Nuclear Engineering, Bucharest, Romania*
[28c] *Department of Physics, Alexandru Ioan Cuza University of Iasi, Iasi, Romania*
[28d] *National Institute for Research and Development of Isotopic and Molecular Technologies, Physics Department, Cluj-Napoca, Romania*
[28e] *National University of Science and Technology Politechnica, Bucharest, Romania*

[28f] West University in Timisoara, Timisoara, Romania
[28g] Faculty of Physics, University of Bucharest, Bucharest, Romania
[29a] Faculty of Mathematics, Physics and Informatics, Comenius University, Bratislava, Slovak Republic
[29b] Department of Subnuclear Physics, Institute of Experimental Physics of the Slovak Academy of Sciences, Kosice, Slovak Republic
[30] Physics Department, Brookhaven National Laboratory, Upton NY, U.S.A.
[31] Universidad de Buenos Aires, Facultad de Ciencias Exactas y Naturales, Departamento de Física, y CONICET, Instituto de Física de Buenos Aires (IFIBA), Buenos Aires, Argentina
[32] California State University, CA, U.S.A.
[33] Cavendish Laboratory, University of Cambridge, Cambridge, U.K.
[34a] Department of Physics, University of Cape Town, Cape Town, South Africa
[34b] iThemba Labs, Western Cape, South Africa
[34c] Department of Mechanical Engineering Science, University of Johannesburg, Johannesburg, South Africa
[34d] National Institute of Physics, University of the Philippines Diliman (Philippines), Philippines
[34e] Department of Physics, Stellenbosch University, Matieland, South Africa
[34f] University of KwaZulu-Natal, School of Agriculture and Science, Mathematics, Westville, South Africa
[34g] University of South Africa, Department of Physics, Pretoria, South Africa
[34h] University of Pretoria, Department of Mechanical and Aeronautical Engineering, Pretoria, South Africa
[34i] University of Zululand, KwaDlangezwa, South Africa
[34j] School of Physics, University of the Witwatersrand, Johannesburg, South Africa
[35] Department of Physics, Carleton University, Ottawa ON, Canada
[36a] Faculté des Sciences Ain Chock, Université Hassan II de Casablanca, Morocco
[36b] Faculté des Sciences, Université Ibn-Tofail, Kénitra, Morocco
[36c] Faculté des Sciences Semlalia, Université Cadi Ayyad, LPHEA-Marrakech, Morocco
[36d] LPMR, Faculté des Sciences, Université Mohamed Premier, Oujda, Morocco
[36e] Faculté des sciences, Université Mohammed V, Rabat, Morocco
[36f] Institute of Applied Physics, Mohammed VI Polytechnic University, Ben Guerir, Morocco
[37] CERN, Geneva, Switzerland
[38] Affiliated with an institute formerly covered by a cooperation agreement with CERN
[39] Affiliated with an international laboratory covered by a cooperation agreement with CERN
[40] Enrico Fermi Institute, University of Chicago, Chicago IL, U.S.A.
[41] LPC, Université Clermont Auvergne, CNRS/IN2P3, Clermont-Ferrand, France
[42] Nevis Laboratory, Columbia University, Irvington NY, U.S.A.
[43] Niels Bohr Institute, University of Copenhagen, Copenhagen, Denmark
[44a] Dipartimento di Fisica, Università della Calabria, Rende, Italy
[44b] INFN Gruppo Collegato di Cosenza, Laboratori Nazionali di Frascati, Italy
[45] Physics Department, Southern Methodist University, Dallas TX, U.S.A.
[46] National Centre for Scientific Research "Demokritos", Agia Paraskevi, Greece
[47a] Department of Physics, Stockholm University, Sweden
[47b] Oskar Klein Centre, Stockholm, Sweden
[48] Deutsches Elektronen-Synchrotron DESY, Hamburg and Zeuthen, Germany
[49] Fakultät Physik, Technische Universität Dortmund, Dortmund, Germany
[50] Institut für Kern- und Teilchenphysik, Technische Universität Dresden, Dresden, Germany
[51] Department of Physics, Duke University, Durham NC, U.S.A.
[52] SUPA – School of Physics and Astronomy, University of Edinburgh, Edinburgh, U.K.
[53] INFN e Laboratori Nazionali di Frascati, Frascati, Italy
[54] Physikalisches Institut, Albert-Ludwigs-Universität Freiburg, Freiburg, Germany
[55] II. Physikalisches Institut, Georg-August-Universität Göttingen, Göttingen, Germany
[56] Département de Physique Nucléaire et Corpusculaire, Université de Genève, Genève, Switzerland
[57a] Dipartimento di Fisica, Università di Genova, Genova, Italy
[57b] INFN Sezione di Genova, Italy
[58] II. Physikalisches Institut, Justus-Liebig-Universität Giessen, Giessen, Germany
[59] SUPA – School of Physics and Astronomy, University of Glasgow, Glasgow, U.K.

JHEP07(2026)107

[60] LPSC, Université Grenoble Alpes, CNRS/IN2P3, Grenoble INP, Grenoble, France
[61] Laboratory for Particle Physics and Cosmology, Harvard University, Cambridge MA, U.S.A.
[62] Department of Modern Physics and State Key Laboratory of Particle Detection and Electronics, University of Science and Technology of China, Hefei, China
[63a] Kirchhoff-Institut für Physik, Ruprecht-Karls-Universität Heidelberg, Heidelberg, Germany
[63b] Physikalisches Institut, Ruprecht-Karls-Universität Heidelberg, Heidelberg, Germany
[64a] Department of Physics, Chinese University of Hong Kong, Shatin, N.T., Hong Kong, China
[64b] Department of Physics, University of Hong Kong, Hong Kong, China
[64c] Department of Physics and Institute for Advanced Study, Hong Kong University of Science and Technology, Clear Water Bay, Kowloon, Hong Kong, China
[65] Department of Physics, National Tsing Hua University, Hsinchu, Taiwan
[66] IJCLab, Université Paris-Saclay, CNRS/IN2P3, 91405, Orsay, France
[67] Centro Nacional de Microelectrónica (IMB-CNM-CSIC), Barcelona, Spain
[68] Department of Physics, Indiana University, Bloomington IN, U.S.A.
[69a] INFN Gruppo Collegato di Udine, Sezione di Trieste, Udine, Italy
[69b] ICTP, Trieste, Italy
[69c] Dipartimento Politecnico di Ingegneria e Architettura, Università di Udine, Udine, Italy
[70a] INFN Sezione di Lecce, Italy
[70b] Dipartimento di Matematica e Fisica, Università del Salento, Lecce, Italy
[71a] INFN Sezione di Milano, Italy
[71b] Dipartimento di Fisica, Università di Milano, Milano, Italy
[72a] INFN Sezione di Napoli, Italy
[72b] Dipartimento di Fisica, Università di Napoli, Napoli, Italy
[73a] INFN Sezione di Pavia, Italy
[73b] Dipartimento di Fisica, Università di Pavia, Pavia, Italy
[74a] INFN Sezione di Pisa, Italy
[74b] Dipartimento di Fisica E. Fermi, Università di Pisa, Pisa, Italy
[75a] INFN Sezione di Roma, Italy
[75b] Dipartimento di Fisica, Sapienza Università di Roma, Roma, Italy
[76a] INFN Sezione di Roma Tor Vergata, Italy
[76b] Dipartimento di Fisica, Università di Roma Tor Vergata, Roma, Italy
[77a] INFN Sezione di Roma Tre, Italy
[77b] Dipartimento di Matematica e Fisica, Università Roma Tre, Roma, Italy
[78a] INFN-TIFPA, Italy
[78b] Università degli Studi di Trento, Trento, Italy
[79] Universität Innsbruck, Department of Astro and Particle Physics, Innsbruck, Austria
[80] Department of Physics and Astronomy, Iowa State University, Ames IA, U.S.A.
[81] Istinye University, Sariyer, Istanbul, Türkiye
[82a] Departamento de Engenharia Elétrica, Universidade Federal de Juiz de Fora (UFJF), Juiz de Fora, Brazil
[82b] Universidade Federal do Rio De Janeiro COPPE/EE/IF, Rio de Janeiro, Brazil
[82c] Instituto de Física, Universidade de São Paulo, São Paulo, Brazil
[82d] Rio de Janeiro State University, Rio de Janeiro, Brazil
[82e] Federal University of Bahia, Bahia, Brazil
[83] KEK, High Energy Accelerator Research Organization, Tsukuba, Japan
[84a] Khalifa University of Science and Technology, Abu Dhabi, United Arab Emirates
[84b] University of Sharjah, Sharjah, United Arab Emirates
[85] Graduate School of Science, Kobe University, Kobe, Japan
[86a] AGH University of Krakow, Faculty of Physics and Applied Computer Science, Krakow, Poland
[86b] Marian Smoluchowski Institute of Physics, Jagiellonian University, Krakow, Poland
[87] Institute of Nuclear Physics Polish Academy of Sciences, Krakow, Poland
[88] Faculty of Science, Kyoto University, Kyoto, Japan
[89] Research Center for Advanced Particle Physics and Department of Physics, Kyushu University, Fukuoka, Japan

[90] L2IT, Université de Toulouse, CNRS/IN2P3, UPS, Toulouse, France
[91] Instituto de Física La Plata, Universidad Nacional de La Plata and CONICET, La Plata, Argentina
[92] Physics Department, Lancaster University, Lancaster, U.K.
[93] Oliver Lodge Laboratory, University of Liverpool, Liverpool, U.K.
[94] Department of Experimental Particle Physics, Jožef Stefan Institute and Department of Physics, University of Ljubljana, Ljubljana, Slovenia
[95] Department of Physics and Astronomy, Queen Mary University of London, London, U.K.
[96] Department of Physics, Royal Holloway University of London, Egham, U.K.
[97] Department of Physics and Astronomy, University College London, London, U.K.
[98] Louisiana Tech University, Ruston LA, U.S.A.
[99] Fysiska institutionen, Lunds universitet, Lund, Sweden
[100] Departamento de Física Teorica C-15 and CIAFF, Universidad Autónoma de Madrid, Madrid, Spain
[101] Institut für Physik, Universität Mainz, Mainz, Germany
[102] School of Physics and Astronomy, University of Manchester, Manchester, U.K.
[103] CPPM, Aix-Marseille Université, CNRS/IN2P3, Marseille, France
[104] Department of Physics, University of Massachusetts, Amherst MA, U.S.A.
[105] Department of Physics, McGill University, Montreal QC, Canada
[106] School of Physics, University of Melbourne, Victoria, Australia
[107] Department of Physics, University of Michigan, Ann Arbor MI, U.S.A.
[108] Department of Physics and Astronomy, Michigan State University, East Lansing MI, U.S.A.
[109] Group of Particle Physics, University of Montreal, Montreal QC, Canada
[110] Fakultät für Physik, Ludwig-Maximilians-Universität München, München, Germany
[111] Max-Planck-Institut für Physik (Werner-Heisenberg-Institut), München, Germany
[112] Graduate School of Science and Kobayashi-Maskawa Institute, Nagoya University, Nagoya, Japan
[113a] Department of Physics, Nanjing University, Nanjing, China
[113b] School of Science, Shenzhen Campus of Sun Yat-sen University, China
[113c] University of Chinese Academy of Science (UCAS), Beijing, China
[114] Department of Physics and Astronomy, University of New Mexico, Albuquerque NM, U.S.A.
[115] Institute for Mathematics, Astrophysics and Particle Physics, Radboud University/Nikhef, Nijmegen, Netherlands
[116] Nikhef National Institute for Subatomic Physics and University of Amsterdam, Amsterdam, Netherlands
[117] Department of Physics, Northern Illinois University, DeKalb IL, U.S.A.
[118a] New York University Abu Dhabi, Abu Dhabi, United Arab Emirates
[118b] United Arab Emirates University, Al Ain, United Arab Emirates
[119] Department of Physics, New York University, New York NY, U.S.A.
[120] Ochanomizu University, Otsuka, Bunkyo-ku, Tokyo, Japan
[121] Ohio State University, Columbus OH, U.S.A.
[122] Homer L. Dodge Department of Physics and Astronomy, University of Oklahoma, Norman OK, U.S.A.
[123] Department of Physics, Oklahoma State University, Stillwater OK, U.S.A.
[124] Palacký University, Joint Laboratory of Optics, Olomouc, Czech Republic
[125] Institute for Fundamental Science, University of Oregon, Eugene, OR, U.S.A.
[126] Graduate School of Science, University of Osaka, Osaka, Japan
[127] Department of Physics, University of Oslo, Oslo, Norway
[128] Department of Physics, Oxford University, Oxford, U.K.
[129] LPNHE, Sorbonne Université, Université Paris Cité, CNRS/IN2P3, Paris, France
[130] Department of Physics, University of Pennsylvania, Philadelphia PA, U.S.A.
[131] Department of Physics and Astronomy, University of Pittsburgh, Pittsburgh PA, U.S.A.
[132a] Laboratório de Instrumentação e Física Experimental de Partículas – LIP, Lisboa, Portugal
[132b] Departamento de Física, Faculdade de Ciências, Universidade de Lisboa, Lisboa, Portugal
[132c] Departamento de Física, Universidade de Coimbra, Coimbra, Portugal
[132d] Centro de Física Nuclear da Universidade de Lisboa, Lisboa, Portugal
[132e] Departamento de Física, Escola de Ciências, Universidade do Minho, Braga, Portugal
[132f] Departamento de Física Teórica y del Cosmos, Universidad de Granada, Granada (Spain), Spain

JHEP07(2026)107

[132g] Departamento de Física, Instituto Superior Técnico, Universidade de Lisboa, Lisboa, Portugal
[133] Institute of Physics of the Czech Academy of Sciences, Prague, Czech Republic
[134] Czech Technical University in Prague, Prague, Czech Republic
[135] Charles University, Faculty of Mathematics and Physics, Prague, Czech Republic
[136] Particle Physics Department, Rutherford Appleton Laboratory, Didcot, U.K.
[137] IRFU, CEA, Université Paris-Saclay, Gif-sur-Yvette, France
[138] Santa Cruz Institute for Particle Physics, University of California Santa Cruz, Santa Cruz CA, U.S.A.
[139a] Departamento de Física, Pontificia Universidad Católica de Chile, Santiago, Chile
[139b] Millennium Institute for Subatomic physics at high energy frontier (SAPHIR), Santiago, Chile
[139c] Instituto de Investigación Multidisciplinario en Ciencia y Tecnología, y Departamento de Física, Universidad de La Serena, Chile
[139d] Universidad Andres Bello, Department of Physics, Santiago, Chile
[139e] Universidad San Sebastian, Recoleta, Chile
[139f] Instituto de Alta Investigación, Universidad de Tarapacá, Arica, Chile
[139g] Departamento de Física, Universidad Técnica Federico Santa María, Valparaíso, Chile
[140] Department of Physics, Institute of Science, Tokyo, Japan
[141] Department of Physics, University of Washington, Seattle WA, U.S.A.
[142a] Institute of Frontier and Interdisciplinary Science and Key Laboratory of Particle Physics and Particle Irradiation (MOE), Shandong University, Qingdao, China
[142b] School of Physics, Zhengzhou University, China
[143a] State Key Laboratory of Dark Matter Physics, School of Physics and Astronomy, Shanghai Jiao Tong University, Key Laboratory for Particle Astrophysics and Cosmology (MOE), SKLPPC, Shanghai, China
[143b] State Key Laboratory of Dark Matter Physics, Tsung-Dao Lee Institute, Shanghai Jiao Tong University, Shanghai, China
[144] Department of Physics and Astronomy, University of Sheffield, Sheffield, U.K.
[145] Department of Physics, Shinshu University, Nagano, Japan
[146] Department Physik, Universität Siegen, Siegen, Germany
[147] Department of Physics, Simon Fraser University, Burnaby BC, Canada
[148] SLAC National Accelerator Laboratory, Stanford CA, U.S.A.
[149] Department of Physics, Royal Institute of Technology, Stockholm, Sweden
[150] Departments of Physics and Astronomy, Stony Brook University, Stony Brook NY, U.S.A.
[151] Department of Physics and Astronomy, University of Sussex, Brighton, U.K.
[152] School of Physics, University of Sydney, Sydney, Australia
[153] Institute of Physics, Academia Sinica, Taipei, Taiwan
[154a] E. Andronikashvili Institute of Physics, Iv. Javakhishvili Tbilisi State University, Tbilisi, Georgia
[154b] High Energy Physics Institute, Tbilisi State University, Tbilisi, Georgia
[154c] University of Georgia, Tbilisi, Georgia
[155] Department of Physics, Technion, Israel Institute of Technology, Haifa, Israel
[156] Raymond and Beverly Sackler School of Physics and Astronomy, Tel Aviv University, Tel Aviv, Israel
[157] Department of Physics, Aristotle University of Thessaloniki, Thessaloniki, Greece
[158] International Center for Elementary Particle Physics and Department of Physics, University of Tokyo, Tokyo, Japan
[159] Graduate School of Science and Technology, Tokyo Metropolitan University, Tokyo, Japan
[160] Department of Physics, University of Toronto, Toronto ON, Canada
[161a] TRIUMF, Vancouver BC, Canada
[161b] Department of Physics and Astronomy, York University, Toronto ON, Canada
[162] Division of Physics and Tomonaga Center for the History of the Universe, Faculty of Pure and Applied Sciences, University of Tsukuba, Tsukuba, Japan
[163] Department of Physics and Astronomy, Tufts University, Medford MA, U.S.A.
[164] Department of Physics and Astronomy, University of California Irvine, Irvine CA, U.S.A.
[165] University of West Attica, Athens, Greece
[166] Department of Physics and Astronomy, University of Uppsala, Uppsala, Sweden
[167] Department of Physics, University of Illinois, Urbana IL, U.S.A.

[168] Instituto de Física Corpuscular (IFIC), Centro Mixto Universidad de Valencia – CSIC, Valencia, Spain
[169] Department of Physics, University of British Columbia, Vancouver BC, Canada
[170] Department of Physics and Astronomy, University of Victoria, Victoria BC, Canada
[171] Fakultät für Physik und Astronomie, Julius-Maximilians-Universität Würzburg, Würzburg, Germany
[172] Department of Physics, University of Warwick, Coventry, U.K.
[173] Waseda University, Tokyo, Japan
[174] Department of Particle Physics and Astrophysics, Weizmann Institute of Science, Rehovot, Israel
[175] Department of Physics, University of Wisconsin, Madison WI, U.S.A.
[176] Fakultät für Mathematik und Naturwissenschaften, Fachgruppe Physik, Bergische Universität Wuppertal, Wuppertal, Germany
[177] Department of Physics, Yale University, New Haven CT, U.S.A.
[178] Yerevan Physics Institute, Yerevan, Armenia

[a] Also at Department of Physics, King's College London, London, U.K.
[b] Also at Institute of Physics, Azerbaijan Academy of Sciences, Baku, Azerbaijan
[c] Also at Imam Mohammad Ibn Saud Islamic University, Saudi Arabia
[d] Also at Department of Physics, University of Thessaly, Greece
[e] Also at An-Najah National University, Nablus, Palestine
[f] Also at Department of Physics, University of Fribourg, Fribourg, Switzerland
[g] Also at Department of Physics, Westmont College, Santa Barbara, U.S.A.
[h] Also at Departament de Fisica de la Universitat Autonoma de Barcelona, Barcelona, Spain
[i] Also at University of Siena, Italy
[j] Also at Affiliated with an institute formerly covered by a cooperation agreement with CERN
[k] Also at The Collaborative Innovation Center of Quantum Matter (CICQM), Beijing, China
[l] Also at Faculty of Physics, Sofia University, 'St. Kliment Ohridski', Sofia, Bulgaria
[m] Also at Università di Napoli Parthenope, Napoli, Italy
[n] Also at Institute of Particle Physics (IPP), Canada
[o] Also at Department of Physics, Bolu Abant Izzet Baysal University, Bolu, Türkiye
[p] Also at Faculty of Physics, University of Bucharest, Romania
[q] Also at Borough of Manhattan Community College, City University of New York, New York NY, U.S.A.
[r] Also at National Institute of Physics, University of the Philippines Diliman (Philippines), Philippines
[s] Also at Department of Financial and Management Engineering, University of the Aegean, Chios, Greece
[t] Also at TRIUMF, Vancouver BC, Canada
[u] Also at Institucio Catalana de Recerca i Estudis Avancats, ICREA, Barcelona, Spain
[v] Also at Henan University, China
[w] Also at Yeditepe University, Physics Department, Istanbul, Türkiye
[x] Also at Institute of Theoretical Physics, Ilia State University, Tbilisi, Georgia
[y] Also at CERN, Geneva, Switzerland
[z] Also at Center for Interdisciplinary Research and Innovation (CIRI-AUTH), Thessaloniki, Greece
[aa] Also at Hellenic Open University, Patras, Greece
[ab] Also at Department of Modern Physics and State Key Laboratory of Particle Detection and Electronics, University of Science and Technology of China, Hefei, China
[ac] Also at Department of Mathematical Sciences, University of South Africa, Johannesburg, South Africa
[ad] Also at Department of Physics, Stellenbosch University, South Africa
[ae] Also at University of Colorado Boulder, Department of Physics, Colorado, U.S.A.
[af] Also at Département de Physique Nucléaire et Corpusculaire, Université de Genève, Genève, Switzerland
[ag] Also at Centre of Physics of the Universities of Minho and Porto (CF-UM-UP), Portugal
[ah] Also at Institute for Nuclear Research and Nuclear Energy (INRNE) of the Bulgarian Academy of Sciences, Sofia, Bulgaria
[ai] Also at Washington College, Chestertown, MD, U.S.A.
[aj] Also at Institut für Experimentalphysik, Universität Hamburg, Hamburg, Germany
[ak] Also at Institute of Applied Physics, Mohammed VI Polytechnic University, Ben Guerir, Morocco
[al] Also at Department of Physics, Stanford University, Stanford CA, U.S.A.

JHEP07(2026)107

[am] *Also at Institute of Physics and Technology, Mongolian Academy of Sciences, Ulaanbaatar, Mongolia*
[an] *Also at Millennium Institute for Subatomic physics at high energy frontier (SAPHIR), Santiago, Chile*
[ao] *Also at University of Chinese Academy of Sciences (UCAS), Beijing, China*
[†] *Deceased*

JHEP07(2026)107